5-2012

POPULATION CODING IN LAMINAR CORTICAL CIRCUITS

Bryan J. Hansen

POPULATION CODING IN LAMINAR CORTICAL CIRCUITS

By

Bryan Joseph Hansen, B.S.

APPROVED:

_____
Valentin Dragoi, Ph.D.
Supervisory Professor

_____
Daniel J. Felleman, Ph.D.

_____
Anne Sereno, Ph.D.

_____
Harel Shouval, Ph.D.

_____
Kevin Morano, Ph.D.

APPROVED:

_____
Dean, The University of Texas
Health Science Center at Houston
Graduate School of Biomedical Sciences

POPULATION CODING IN LAMINAR CORTICAL CIRCUITS

A DISSERTATION

Presented to the Faculty of
The University of Texas
Health Science Center at Houston
and
The University of Texas
M. D. Anderson Cancer Center
Graduate School of Biomedical Sciences

in Partial Fulfillment

of the Requirements
for the Degree of
DOCTOR OF PHILOSOPHY

By

Bryan Joseph Hansen, B.S.
Houston, Texas
May 2012

DEDICATION

This thesis is dedicated to my daughter, Addison Jean Hansen- never stop exploring the world around you and never settle, always challenge yourself and your abilities.

ACKNOWLEDGEMENTS

I would like to extend my sincerest gratitude to my supervisor, Valentin Dragoi. His continued guidance and motivation throughout my graduate school career has been an inspiration to strive for the best and never accept anything less. While it was not always easy, he taught me to take each success and failure as new challenges. In the end, his dedication to science and to my training have forever shaped my views as a scientist. Behind every great advisor, is a great lab conducting experiments every day and making the lab a fun and creative place to work. I would like to thank all the members of the Dragoi lab past and present for their continued support. One of the most important things we did as a lab was our weekly lab meeting where we discussed recent papers in the field and presented our research; this time was instrumental in my development through graduate school.

To my committee members past and present, I have gained so much knowledge from each one of you about how to approach scientific questions, formulate hypotheses, and draw conclusions from my experimental results. Specifically, Dan Felleman, who taught me a valuable lesson -when to say, “I don’t know”, because if you do not, they can always tell. I would like to thank my funding sources, the Houston Area Vision Training Grant (5-T32 EY0007024) and the Training in Neurosciences fellowships (5-T32 NS007467) for financial support as well as for guidance with professional development. I would also like to thank all the members of Neurobiology and Anatomy staff for their continued support and help in making our research possible. To the CLAMC staff, your commitment to and care of our research animals has been incredible.

I have been fortunate to meet some truly exceptional people, which now I call my close friends, throughout my graduate career. We have all started on this incredibly challenging journey together and these people are the only individuals who know exactly what each other is going through. Over the years, they have been a constant outlet to complain about reviewer's comments or failed experiments, but they are also an immeasurable source of fun. If our hard work was not matched with an equal amount of fun we would never survive. Personally, I would like to thank Katelyn Weymouth for our marathon lunches and for being a great friend.

To my mom, Kori Hansen, whether I was writing a book report on *Crime and Punishment*, studying for my EMT exam, or stage manager for *Oklahoma*, she has always been there motivating and supporting me in my endeavors. When times were tough, and they have been, she was there making a joke or just wanting to talk about music. I would not be the man I am today if it was not for my mom's continued positive influence in my life. To my sister, Danielle Hansen, thank you for all your support, I am very proud you. To my mother-in-law, Verda Rossnagel, and brothers-in-law, Mark and Chief, thank you for your loving support.

To my wife, Kristin Hansen, words will never convey how much you have inspired and motivated me along this journey. Seeing you continue to challenge yourself as a teacher, as a graduate student (while pregnant), and now as a Child Life Specialist has been infectious in motivating me to continue to strive for the best. Seeing how you approached each new challenge with such unwavering drive always challenged me to do more. Thank you for everything you have done for me but most importantly thank you for being you. Finally, to my daughter, Addison Hansen, who I hope someday will value learning and recognize knowledge is the key to open all the doors in your life.

POPULATION CODING IN LAMINAR CORTICAL CIRCUITS

Publication No. _____
Bryan Joseph Hansen, B.S.
Supervisory Professor: Valentin Dragoi, Ph.D.

One of the fundamental questions in neuroscience is to understand how encoding of sensory inputs is distributed across neuronal networks in cerebral cortex to influence sensory processing and behavioral performance. The fact that the structure of neuronal networks is organized according to cortical layers raises the possibility that sensory information could be processed differently in distinct layers. The goal of my thesis research is to understand how laminar circuits encode information in their population activity, how the properties of the population code adapt to changes in visual input, and how population coding influences behavioral performance. To this end, we performed a series of novel experiments to investigate how sensory information in the primary visual cortex (V1) emerges across laminar cortical circuits. First, it is commonly known that the amount of information encoded by cortical circuits depends critically on whether or not nearby neurons exhibit correlations. We examined correlated variability in V1 circuits from a laminar-specific perspective and observed that cells in the input layer, which have only local projections, encode incoming stimuli optimally by exhibiting low correlated variability. In contrast, output layers, which send projections to other cortical and subcortical areas, encode information suboptimally by exhibiting large correlations. These results argue that neuronal populations in different cortical layers play different roles in network computations. Secondly, a fundamental feature of cortical neurons is their ability to adapt to changes in incoming stimuli. Understanding how adaptation emerges across cortical layers to influence information processing is vital for understanding efficient sensory coding. We examined the effects of adaptation, on the time-scale of a visual fixation,

on network synchronization across laminar circuits. Specific to the superficial layers, we observed an increase in gamma-band (30-80 Hz) synchronization after adaptation that was correlated with an improvement in neuronal orientation discrimination performance. Thus, synchronization enhances sensory coding to optimize network processing across laminar circuits. Finally, we tested the hypothesis that individual neurons and local populations synchronize their activity in real-time to communicate information about incoming stimuli, and that the degree of synchronization influences behavioral performance. These analyses assessed for the first time the relationship between changes in laminar cortical networks involved in stimulus processing and behavioral performance.

TABLE OF CONTENTS

LIST OF FIGURES

LIST OF TABLE

LIST OF ABBREVIATIONS

Primary visual cortex	V1
Spike-count correlation (noise correlation)	r_{sc}
Local-field potential	LFP
Spike-field coherence	SFC
d-prime (discrimination performance)	*d'*
Coefficient of variation	CV
Supragranular	SG
Granular	G
Infragranular	IG
Evoked-response potential	ERP
Current-source density	CSD
Cycles per degree	cpd
Standard error of the mean	SEM
Interspike-interval	ISI

1. GENERAL INTRODUCTION

One of the fundamental questions in neuroscience is to understand how the encoding of sensory inputs is distributed across neuronal networks to influence sensory processing and behavioral performance. Sensory processing is a phenomenon that requires network interactions. The fact that the structure of local cortical networks is organized according to unique cortical layers raises the possibility that sensory information could be processed differently in distinct layers. In the visual system, information is transmitted from the retina through the thalamus and analyzed by the visual cortex at distinct hierarchical levels to construct an internal representation of the environment. As is true across all neocortical regions, the primary visual cortex (V1) is composed of six unique layers that work in concert to process and communicate information about our sensory environment. Much of what we know about cortical layers has relied on anatomical approaches studying specific connections. Recent advances in electrode technology now allow us access to functional connections within and between cortical layers using sophisticated laminar electrodes. This work is clinically relevant if you consider there is growing clinical research suggesting that brain injury and neurological disorders (Coplan and Lydiard, 1998), such as epilepsy (Swann et al., 2001), result from impaired connections within and between neuronal networks (i.e. temporal and frontal). These faulty connections may lead to poor network communication and a potential loss of vital information. Therefore, identifying how 'normal' networks synchronize information could help develop better diagnostic tools or even therapies targeted at improving network communication and ultimately restoring proper communication (Bohland et al., 2009). The experiments outlined in this thesis could offer a

new perspective for the diagnosis and treatment of neurological disorders related to known defects in the wiring of brain circuitry.

In this thesis, I first studied how laminar circuits in V1 encode information in their population activity by measuring the structure of noise correlations within cortical layers. This research represents the first level in understanding how pairs of neurons in different cortical layers modulate their activity in response to a flashed grating stimulus. The amount of information encoded by cortical circuits depends critically on whether or not pairs of nearby neurons exhibit correlated responses. Despite the fact that strong trial-by-trial correlated variability (or noise correlation) in response strength has been reported in many cortical areas (Bair et al., 2001; de la Rocha et al., 2007; Gutnisky and Dragoi, 2008; Kohn and Smith, 2005; Nauhaus et al., 2009; Smith and Kohn, 2008), recent evidence suggests that neuronal correlations are much lower than previously thought (Ecker et al., 2010; Renart et al., 2010). Estimation of correlated neuronal firing is fundamental for understanding how populations of neurons encode sensory inputs. The structure of correlations in a network has been shown to influence the available information in the responses of a population of cells (Abbott and Dayan, 1999) and possibly limit behavioral performance (Chen et al., 2008). In addition, many groups have proposed that a decorrelated state of the cortex would be advantageous for information processing by reducing the number of neurons necessary to achieve accurate network performance; importantly this is proposed to occur when two neurons share similar features (Abbott and Dayan, 1999; Averbeck and Lee, 2004; Ecker et al., 2010; Shadlen and Newsome, 1998). Clearly, elucidating whether cortical networks operate in a correlated or decorrelated state is fundamental for understanding how neuronal populations encode information.

We reasoned that since responses of cortical neurons are significantly influenced by the inputs from other neurons in their local network, correlations may depend on the network environment (i.e. cortical layers) in which neurons are embedded. Indeed, cortical layers are ubiquitous structures throughout neocortex (Nassi and Callaway, 2009) consisting of highly recurrent networks (Gilbert and Wiesel, 1983) characterized by distinct connection patterns. By measuring responses from pairs of neurons, correlation analysis provides significant information about the connectivity of neuronal networks, and has been apllied to study the connectivity in the retina, between the thalamus and visual cortex, and between other cortical neurons (Alonso and Martinez, 1998; Greschner et al., 2011; Reid and Alonso, 1995). Not only does the distribution of cortical connectivity influence the correlation structure and amount of information, but the distribution of synaptic conductances is also important. For example, in a network modeling the heterogeneity of orientation tuning curves in V1 (Ringach et al., 2002), noise correlations were significantly lower, resulting in better orientation discrimination performance as opposed to a network with non–heterogenous tuning curves (Chelaru and Dragoi, 2008).

In chapter 5, I will revisit the issue of correlated variability, utilizing a newly developed technique - multi-contact laminar electrodes that allow us to characterize responses across cortical layers. We found that correlations between neurons depend strongly on the local network context – neurons in the input (granular) layer of V1 showed virtually no correlated variability, while neurons in the output layers (supragranular and infragranular) exhibited strong response correlations. Contrary to expectation that the output layers would encode stimulus information most accurately, our results are consistent with the fact that the input

network encodes more information and offers superior discrimination performance because of lower correlated variability.

Our study of population coding in laminar circuits continues in chapter 6 by investigating how the population code adapts to changes in visual information. Adaptation occurs along many stimulus dimensions such as luminance, contrast, orientation, spatial frequency, direction of motion, color, and shape. The effects of pattern adaptation have been extensively explored in psychophysical and electrophysiological experiments. We explored this issue in the context of rapid, adaptation-induced plasticity in V1 of awake-behaving monkeys. Neurons in V1 have been shown to exhibit plasticity of feature coding even after brief exposure (at the time scale of visual fixation) to a stimulus of fixed structure (Muller et al., 1999; Yao and Dan, 2001; Dragoi et al., 2002; Felsen et al., 2002; Gutnisky and Dragoi, 2008). Specifically, adaptation to oriented gratings induces a repulsive shift in the preferred orientation of individual V1 neurons and changes orientation selectivity when the adapting grating is similar to the cell's optimal orientation (Dragoi et al., 2002; Felsen et al., 2002). Examining rapid adaptation in the visual cortex is important for understanding how individual neurons and local circuits change their coding properties in real-time. We focused on rapid adaptation because this phenomenon has been previously demonstrated to depend on the local network context in which neurons are embedded (Dragoi et al., 2000; Dragoi et al., 2001), thus raising the possibility that the adaptive capacity of individual neurons may exhibit layer dependency.

Surprisingly, adaptation has never been directly investigated in relation to neuronal oscillatory activity, particularly in the gamma frequency range. Indeed, gamma synchronization is involved in a variety of experimental conditions ranging from working memory to reaction time (Gray et al., 1989; Engel et al., 1991a; Fries et al., 2001; Taylor et al., 2005; Womelsdorf et al., 2006; Cardin et al., 2009; Gregoriou et al., 2009; Chalk et al., 2010). However, whether the capacity of individual neurons to exhibit adaptive changes or plasticity is influenced by synchrony in the gamma frequency band remains unclear. Adaptation can be viewed as a form of associative learning, which allows us to study how network processing is shaped dynamically to alter stimulus representations relevant for visual behavior. While studies measuring electroencephalographs (EEGs) in humans have shown that certain forms of associative learning may be accompanied by gamma synchronization (Miltner et al., 1999), whether and how synchrony between individual neurons and local population activity is altered when neurons undergo adaptation remains unclear. Recently, several studies have addressed the relationship between neuronal synchronization and adaptive cortical changes during learning and memory (van Wingerden et al.; Masquelier et al., 2009; Rutishauser et al., 2010). However, these studies have focused on longer forms of plasticity while ignoring plastic changes occurring at more rapid time scales.

To elucidate these issues, we report that brief exposure (300 ms) to a stimulus of fixed orientation modulates the strength of synchronization between individual neurons and local population activity in the gamma-band frequency (30-80 Hz) in macaque primary visual cortex, and influences the ability of individual neurons to encode stimulus orientation. Using laminar probes, we found that although stimulus presentation elicits a large increase in the gamma

synchronization of rhythmic neuronal activity in the input (granular) layers of V1, adaptation caused a pronounced increase in synchronization in the cortical output (supragranular) layers. Surprisingly, the increase in gamma synchronization after adaptation was significantly correlated with an improvement in neuronal orientation discrimination performance only in the supragranular layers. Thus, synchronization between the spiking activity of individual neurons and their local population may enhance sensory coding to optimize network processing across laminar circuits.

The final experiments addressed in this thesis are to study the effects of population coding and synchronization as it relates to behavioral performance. In congruence with the goal of systems neuroscience to understand the relationship of brain activity to cognitive behavior, chapter 7 will explore the relationship between sensory coding in laminar circuits and behavioral performance. One way in which networks of cells can efficiently process information about incoming stimuli is either through changes in local oscillatory activity (i.e. measured as the power spectrum of the LFPs) or synchronization (i.e. measured as the phase-locking between spiking activity and LFPs). Examining whether and how neuronal synchronization influences stimulus processing among populations and behavioral performance is important for understanding the fundamental principles of efficient information coding. We devised a set of experiments to examine how neuronal synchronization influences network processing in V1 and how synchronization influences behavioral performance in an orientation discrimination task. We tested the hypothesis that individual neurons and local populations synchronize their activity in real-time to communicate information about incoming stimuli, and that the degree of synchronization is related to behavioral performance. These analyses will

allow us to assess for the first time the relationship between changes in laminar cortical networks involved in stimulus processing and behavioral performance in awake-behaving monkeys.

The focus of these projects was to gain more information about how the laminar network circuits influence population coding (i.e. correlations and coherence) and behavioral performance. Despite the considerable amount of progress over the last few decades, we still know very little about how information is processed across cortical layers. Particularly, this lack of understanding is because such advances in electrode technology were not available until recently. Currently, there appears to be a wave of studies exploring laminar-dependent population coding and it is fortunate that we are able to address such questions (Buffalo et al., 2011; Hansen and Dragoi, 2011; Lakatos et al., 2009; Maier et al., 2010; Maier et al., 2011). One of the goals of this thesis is to address the importance of laminar circuits in understanding how individual neurons and populations process visual information. We focused on the correlation structure between pairs of neurons across cortical layers and network synchronization between neurons and LFPs.

Overall, this thesis contributes to the study of population coding, specifically how information is processed within and between cortical layers (Hansen, et al., 2011). Each one of these projects builds on the other by studying how laminar circuits encode information in their population activity (chapter 5), how the properties of the population code adapt to changes in visual input (Hansen and Dragoi, 2011), and how population coding influences behavioral performance (chapter 7). In the correlation study, we hypothesized that the spatial spread of

intracortical connections, particularly in the supragranular and infragranular, may underlie the mechanism by which there is an increase in the common input driving a pair of neurons, which results in higher noise correlations. In our adaptation and synchronization study, the key laminar feature was the unique distribution of GABAb receptors (known to be involved in gamma oscillations) in the supragranular and granular layers of V1 (Fitzpatrick et al., 1987; Whittington et al., 1995; Eickhoff et al., 2007). Relating these well-characterized laminar structures to behavior is the challenge of the final part of the thesis, which focuses on behavioral performance during an orientation discrimination task. The results obtained in this thesis provide only one side of the story as to what is going on within V1, while the real goal is to explore communication between visual and other cortical regions. Current work in the Dragoi laboratory is focusing on this very problem by carrying-out dual recordings in area V1 and V4 using laminar probes while monkeys perform an orientation discrimination task.

The thesis is organized as follows: in chapters 2, 3, and 4, I will provide background information on cortical layers, population coding, and network synchronization respectively. Chapter 5 begins with a detailed description of the laminar recording technique and our method for identifying cortical layers, which is used throughout the thesis. In this chapter, I will also describe our method for computing noise correlations and summarize our results from the laminar noise correlation work. In chapter 6, we explored how local populations synchronize their activity in V1 during a rapid adaptation task. In addition, a detailed description of the methods used to compute synchronization is emphasized in chapter 6. Chapter 7 builds on the results from chapters 5 and 6, but focuses on network synchronization and its relationship to behavioral performance during an orientation discrimination task. In chapter 8, I will conclude

the thesis by discussing general conclusions and the significance of our research. I will also address some of the important questions raised by this research and suggest future experiments that extend the present findings.

“It's not about how to achieve your dreams. It's about how to lead your life. If you lead your life the right way, the karma will take care of itself. The dreams will come to you.”

― Randy Pausch

2. LAMINAR CORTICAL CIRCUITS

2.1 Introduction

In 1840, Jules Baillarger, a French neurologist, discovered arguably the most impressive anatomical feature of the cortex – its unique laminar organization. He accurately observed that the cerebral cortex was divided into six layers that alternated between white and grey laminae. About 60 years later with the advent of both Golgi and Nissl staining techniques, Santiago Ramon y Cajal provided a detailed account of the cellular morphologies throughout the cortex (**Figure 2.1**). This work allowed Ramon y Cajal to identify specific neuronal pathways and circuits and even hypothesize about their functional significance. Much of the research that continued over the next 50 years relied heavily on anatomy and the identification of various cell types, which led to further division of the six cortical laminae into sublaminae (Broadmann, 1909). In the late 1950s microelectrodes were first used to study the function of the visual cortex and its pathways. One of the greatest discoveries in neuroscience came from the work of David Hubel and Torston Wiesel who performed numerous experiments utilizing the single-unit recording technique to study the visual cortex in cats and monkeys. They discovered the principles by which information is processed in the visual cortex – through a unique columnar structure. This forever changed how we think about the cortex and ultimately led Hubel and Wiesel to receive the Nobel Prize in 1982.

In this chapter, I will describe the laminar structure of the striate or primary visual cortex (V1) as well as the feedforward and feedback projections that makeup its circuitry (**2.2**

Cortical circuits in primary visual cortex). Next, I will explain how the circuitry across cortical layers influences information processing. In the third section, I will describe research that has explored functional laminar organization and processing in the visual cortex (**2.3 Laminar processing of visual information**). Finally, I will discuss the advantages of recording across cortical layers and why other techniques are unsuitable to answer questions of laminar processing proposed in this thesis (**2.4 Importance of laminar recordings**).

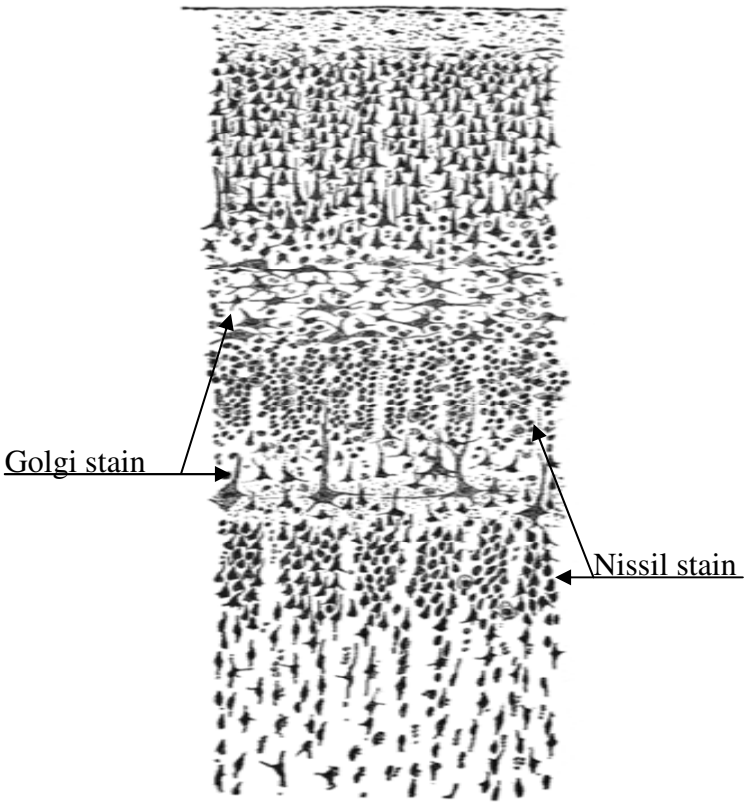

Figure 2.1. Drawing of cortical lamination by Santiago Ramon y Cajal
Nissl-stained visual cortex of a human adult showing a vertical cross-section, with the surface of the cortex at the top. The Nissl stain shows the cell bodies of neurons; the Golgi stain shows the dendrites and axons of a random subset of neurons (adapted from Ramon y Cajal, 1899).

2.2 Cortical circuits in primary visual cortex

The examination of cortical circuits has rarely focused on how information is encoded in different cortical layers (topic of chapters 5-7). It is widely accepted that different cortical layers each contain a characteristic pattern of connections. One the best examples of this laminar structure is the primary visual cortex (V1) of macaque monkeys which is divided into six main layers composed of various sub layer divisions (Billings-Gagliardi et al., 1974). Each layer is defined by a distinct combination of cell types and a unique pattern of connectivity. Layer 1 is made up of predominantly dendrites and axonal connections (O'Kusky and Colonnier, 1982; Fitzpatrick et al., 1987; Nassi and Callaway, 2009). The major thalamorecpient layer of V1, layer 4C (referred to as layer 4 in other cortical areas), or the granular (G) layer, occupies roughly the middle third of the cortical thickness and is rich in stellate neurons that receive the bulk of thalamic afferents. Layer 4C has been further subdivided into 4Cα (upper layer 4C) and 4Cβ (lower layer 4C), based largely on their differential thalamic connections. Superficial to layer 4C are the supragranular (SG) layers, which includes layers 2, 3A, 3B, 4A, and 4B (Casagrande and Kaas, 1994). Below layer 4C are the infragranular (IG) layers 5 and 6. In contrast to layer 4C, collectively the SG and IG layers contain primarily pyramidal neurons that project to diverse cortical and subcortical targets. To avoid confusion of layer terminology in chapters 5-7, I will refer to cortical layers as supragranular, granular, and infragranular. In order to appreciate the richness of visual processing in V1, we must first understand the distinct afferents that target V1 from the lateral geniculate nucleus (LGN) of the thalamus (**Figure 2.2**).

Cortical information processing begins in V1, which receives feedforward projections from three major parallel pathways arising from the LGN: parvocellular (P), magnocellular (M), and koniocellular (K). The parvocellular pathway is characterized by small receptive fields, low contrast sensitivity, and red-green color-opponency. In the macaque neurons in the four most dorsal layers of the LGN (P layers), send axons which synapse primarily in layer 4Cβ of V1, while weaker projections synapse on neurons in layers 6 and 4A (Hubel and Wiesel, 1972; Blasdel and Lund, 1983). A very important feature of P cells is their small receptive size (high resolution) and their color opponent receptive field organization, which enables them to detect red-green chromatic contrast. P cells are also identified by their unique axonal configuration, which results in slower conduction velocities, and previous research has suggested that this pathway is less well suited for rapid detection (Casagrande and Norton, 1991). The magnocellular pathway is characterized by large receptive fields, high contrast sensitivity and achromatic signals. Neurons in the two most ventral layers of the LGN (M layers) send axons which synapse primarily in layer 4Cα of V1, while weaker projections synapse on a subset of layer 6 neurons (Blasdel and Lund, 1983). In contrast to P cells, M cells have large receptive fields, higher contrast sensitive and faster axonal conduction velocities allowing them to signal changes in luminance contrast (Shapley and Lennie, 1985). These properties make M cells ideal at detecting subtle changes in light intensity making them perfect at identifying rapidly moving stimuli (Callaway, 1998). In the macaque monkey, the LGN koniocellular pathway arises from cells primarily located in the intercalated layers (i.e. inserted between pairs of M and P layers as well as in interlaminar regions; Conley and Fitzpatrick, 1989). These cells, also identifiable by their CaMKII reactivity (Calkins et al. 2004), have been shown to receive input from blue/yellow bistratified ganglion cells of the retina (Dacey and

Lee, 1994). The LGN K cells send axonal projections to V1, which terminate in layer 1 and within the cytoxidase-dense (CO) blob regions of layers 2 and 3 (Hendry and Yoshioka, 1994).

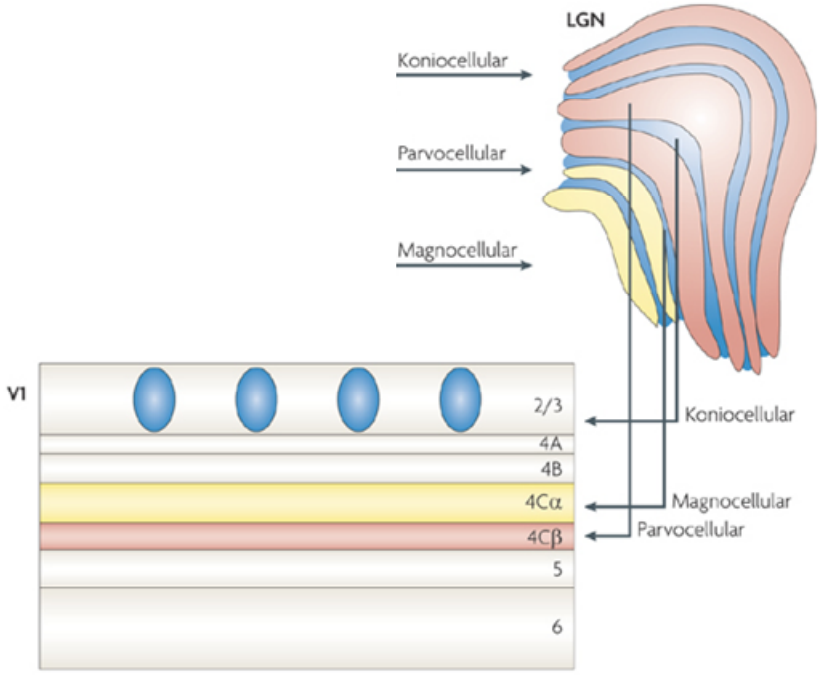

Figure 2.2. Parallel pathways from LGN to the cortex
Parvocellular layers of the LGN send projections on to layer 4Cβ of V1 (red). Magnocellular layers of the LGN send projections on to layer 4Cα of V1 (yellow). Koniocellular layers of the LGN send projections on to the cytochrome oxidase-expressing patches (or blobs) of layers 2 and 3 (blue). To summarize layer 4Cα and 4Cβ receive M and P input, respectively. Layers 2 and 3 blobs and layer 1 receive K input (provided by Nassi and Callaway, 2009; reprinted with permission).

While pioneering work on interlaminar circuits began with intracellular recordings (Ling and Gerard, 1949) and anatomical reconstructions in vivo (Gilbert and Wiesel, 1983), the most significant progress in understanding V1 interlaminar circuits came from more recent in vitro slice recordings as well as photoactivation studies (Callaway and Katz, 1993). Given the unique layer identification and sub layer distinctions of V1 in the macaque monkey, I will now describe the major interlaminar circuits (summarized in **Figure 2.3**). Understanding the precise lamination of V1 is vital for understanding visual processing and provides us with an unique

insight into our analysis and interpretation of results described in chapters 5, (noise correlations) 6 and 7 (synchronization).

The major thalamorecipient layer of V1 is 4C, which is composed of spiny stellate neurons, that project mostly to layers 2-4B with weaker projections to layers 5 and 6 (Callaway, 1998). The parvocellular-recipient layer 4Cβ first sends axonal projections to 4A, which send evenly distributed connections to layer 3B, which target both blob and interblob regions. The magnocellular-recipient layer 4Cα sends axons that synapse evenly onto neurons in layer 4B. There are two types of neurons in layer 4B: (i) the spiny stellates local axons are confined to layers 4B and 4Cα and (ii) the pyramidal neurons that while extending projections into layer 1 also preferentially targeting blobs in layers 2, 3A and 3B (Yabuta and Callaway, 1998; Nassi and Callaway, 2009).

Neurons in cortical layers 2, 3 and 4B provide the majority of feedforward projections from V1 to higher cortical areas such as V2, V3 and MT. In addition, a subset of supragranular neurons send intrinsic projections to neurons in layer 5. Neurons in layer 5 send extrinsic projections to superior colliculus, pulvinar, pons, and send intrinsic feedback projections that synapse onto neurons in layers 2-4B (Wiser and Callaway, 1996). The precise role of the feedback connections from layer 5 to 2-4B is not well understood. Given that these dense connections lack any specificity for blob or interblob regions suggests that they may play a modulatory role.

Layer 6 contains neurons that provide extrinsic projections to the calaustrum and LGN as well as two types of intrinsic V1 projections. There are two classes of pyramidal cells in layer 6, with the first class receiving input from neurons in layers 2-4B which synapse on their basal dendrites which ramify in layer 5. These cells subsequently provide reciprocal feedback to cells in layers 2-4B. The second class of layer 6 neurons has only few dendritic branches within layer 5 and provides strong feedback to layer 4C (Wiser and Callaway, 1996). Layer 6 is also important because it receives similar input from the M and P projection from LGN to 4C, although to a much lesser extent (Usrey and Fitzpatrick, 1994). While layer 6 is not capable of driving neurons in layer 4C, it is thought to play a vital modulatory role in V1 circuits (Wiser and Callaway, 1996).

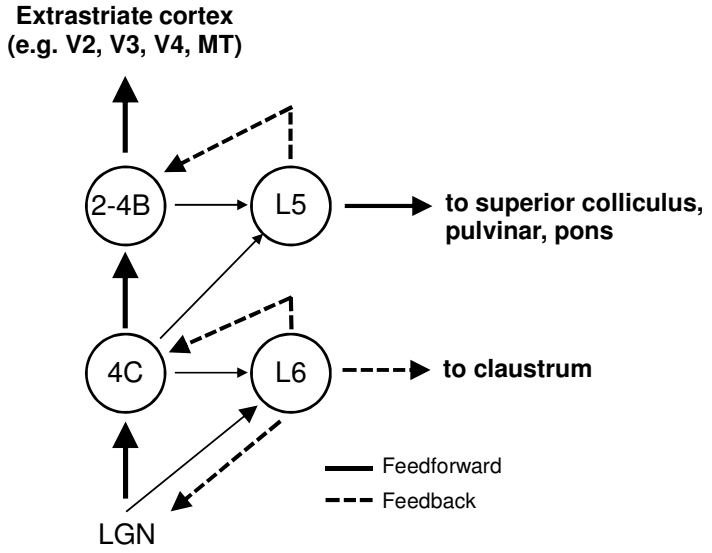

Figure 2.3. The interlaminar circuit of V1
Schematic diagram of the local cortical circuitry. The most direct pathway for information flow (thick arrows) is from LGN to layer 4C, to layers 2-4B to layer 4 of extrastriate cortex. Layers 5 and 6 make up the feedback modules, which receive weak input from lower feedforward modules (thin arrows). At the same level, heavy feedback is also sent to feedforward modules (dashed arrows). Feedback modules also provide a major output of V1, targeting subcortical structures (adapted from Callaway, 1998).

One important distinction between cortical networks in the granular and supra and infragranular layers is the spatial spread of inter and intra-laminar connections. All cortical layers contain short-range connection patterns. Particularly in layer 4C, where neurons receive the majority of geniculate input, the spatial spread of intra-laminar axonal arbors of connections is small (Gilbert and Wiesel, 1983; Feldmeyer et al., 2002; Briggs and Callaway, 2005). In contrast, the spatial spread of intra-laminar axonal arbors originating within layers 2, 3, and 5 may extend several millimeters (Gilbert and Wiesel, 1983; Ts'o et al., 1986; Malach et al., 1993; Bosking et al., 1997; Angelucci et al., 2002; Shmuel et al., 2005). Similar long-range horizontal connections have been observed in a number of primate extrastriate cortical areas as well as other sensory cortices (Schwark and Jones, 1989; Yoshioka et al., 1992; Levitt et al., 1994; Read et al., 2001). This ubiquity suggests that such connections play an important role in cortical processing independent of the particular species or sensory system.

Despite these differences, the excitatory and inhibitory inputs in all cortical layers are believed to be strongest at the preferred orientation of the postsynaptic neuron (Blakemore and Tobin, 1972; Nelson and Frost, 1978; Gilbert and Wiesel, 1983; Ferster, 1986). Very recent evidence has suggested that this behavior may emerge from the interaction of lateral inhibition (via the surround pathways), which is tuned to the preferred orientation of the receptive field (Shushruth et al., 2012). Since long-range horizontal connections preferentially target iso-oriented cells, they are likely to sharpen the orientation tuning of excitatory and inhibitory intracortical inputs to neurons in supragranular and infragranular layers. Little work has investigated whether and how long-range excitatory projections target excitatory and/or inhibitory interneurons. Based on our current understanding of long-range horizontal

connectivity, we hypothesize that there is a larger percentage of common input associated with similarly oriented cells and because of the overrepresentation of iso-oriented information, the tuning profile in supragranular and infragranular layers is narrow (see chapter 5 section 3.4 which discusses our conceptual model approach for understanding intracortical connections).

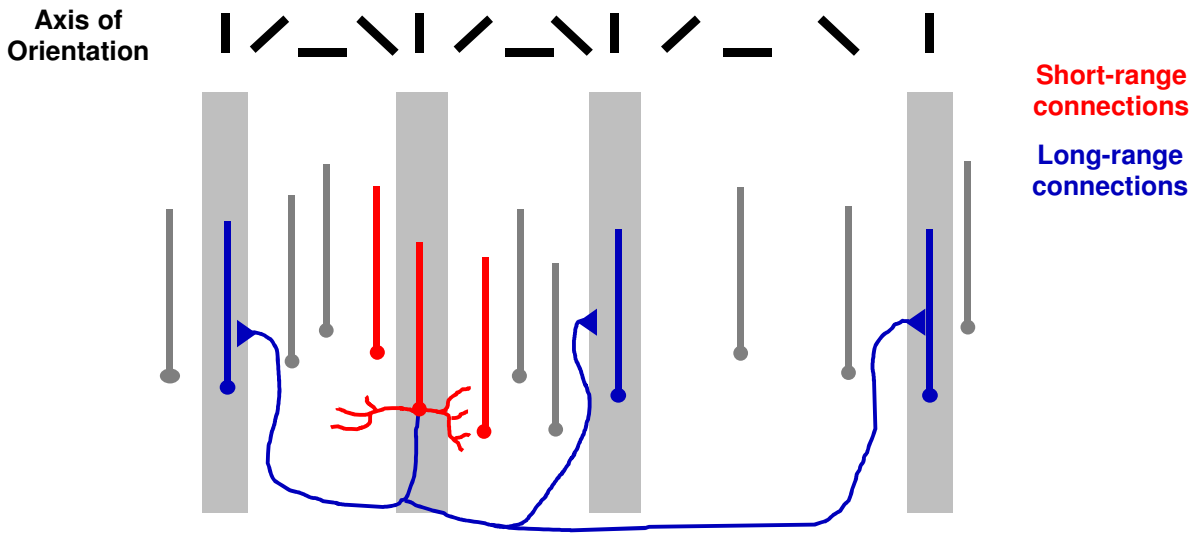

Figure 2.4. The spatial spread of intracortical connections
In the granular layers, where neurons receive geniculate input, the spatial spread of connections is small (red connections). Intrinsic horizontal connections, spreading several millimeters and originating from and terminating in layers 2/3 and layer 5/6, are well characterized (blue connections; adapted from Ts'o et al., 1986).

Each layer, with the exception of layer 4C, has a unique pattern of output projections suggesting that specific processing maybe localized to particular layers. The two most well characterized extrastriate pathways include layers 2 and 3 and 4B. The major feedforward projections of V1 to higher cortical areas originate from neurons located in layers 2 and 3. In layers 2 and 3, the two most important features that influence extrastriate projections are the depth (i.e. the bottom third versus the upper two thirds) and the relative position to CO blobs. Considering the depth of layers 2 and 3, it has been suggested through studies of retrograde

labeling, that neurons in blob and interblobs of layers 2 and 3A (upper two-thirds) send projections to thin and pale stripes respectively (Kennedy and Bullier, 1985). This issue is further complicated by the fact that other studies report labeling of 3B (bottom one-third), 4A, and 4B after injections into V2 (Van Essen et al., 1986). Extensive work identifying the extrastriate projections of layers 2 and 3 has also focused on understanding the differential targets originating from blob and interblob regions. It has been suggested that the particular V1 to V2 target region may vary depending on the distance from the center of a blob (Livingstone and Hubel, 1984). Two models have been proposed to explain the extrastriate connectivity between V1 and V2 and the degree to which new parallel pathways remain segregated remains controversial. The tripartite scheme proposed by Livingstone and Hubel (1984) in which layers 2 and 3 CO blobs project to thin stripes, layer 2/3 interblobs project to pale stripes, and cells in layer 4B project to thick stripes (Van Essen and DeYoe, 1985; Shipp and Zeki, 1985). The bipartite scheme proposed by Sincich and Horton (2002) in which cells in layers 2, 3, 4A, 4B, and 5/6 within CO blobs project to thin stripes, and cells in layers 2, 3, 4A, 4B, and 5/6 in the interblobs project to both pale and thick stripes.

Layer 4B contains both spiny stellate and pyramidal neurons with both types sending the majority of projections to extrastriate areas (Callaway and Wiser, 1996). Pyramidal neurons in 4B are located underneath interblob regions and send parvocellular-dominated input to V2 thick stripes. Layer 4B projections to V2 have been the topic of controversy (as described in the above section) with two groups suggesting different projection pathways based upon the distribution of CO blob and interblob columns (Federer et al., 2009; Sinchich and Horton, 2005). Stellate neurons in 4B provide a unique and direct input to MT neurons, which is useful

for relaying a quick magnocellular-dominated signal (Shipp and Zeki, 1989a; Maunsell et al., 1990). Other 4B extrastriate targets include V3 and MST, but the neuronal types projecting to these areas are not clearly identified (Callaway, 1998). Other feedforward projections from V1 have also been identified originating from layer 4A. Even though 4A is a particularly narrow layer with respect to the other layers its neurons make similar projections to regions of V2 also targeted by cells from 3B and 4B (Van Essen et al., 1986; Levitt et al., 1994).

2.3 Laminar processing of visual information

Single-unit electrophysiological recordings from V1 have revealed systematic differences in the visual responses of neurons in different layers (Dow, 1974; Nowak et al., 1995; Ringach et al., 1997). Recent studies have identified unique laminar differences in receptive field properties across cortical layers in V1 related to changes in orientation selectivity (Martinez et al., 2005; **Figure 2.3**). Indeed, there is evidence that receptive field structure (e.g. simple or complex), identified based on activation of an optimal stimulus, is important for information processing. For example, a bright bar of light aligned horizontally with the ON subregion of a given receptive field would produce a robust response. Any deviation in this configuration such as rotating the bar vertically or occupying a large part of the OFF subregion would considerably reduce the effectiveness of the stimulus (Martinez et al., 2002; Martinez et al., 2005; Hirsch and Martinez, 2006). Numerous groups have extended their analysis of receptive properties to laminar recordings and have identified in cat visual cortex laminar-specific properties (Martinez and Alonso, 2001; Martinez et al., 2002; Sun and Dan, 2009). It was observed that superficial layers contain on average more complex cells, while the majority of simple cells are

restricted to those layers receiving direct connections from the LGN (granular layer 4). A recent study on spatial receptive fields across cortical layers observed that for neurons in output layers the concept of a classical receptive field might no longer be appropriate (Yeh et al., 2009). The authors observed that in output or superficial layers spatial receptive field maps vary a lot depending on the type of stimulus used. Therefore, greater emphasis should be placed on mapping receptive fields according to laminar origin using both sparse noise stimuli as well flashing spots. All of these studies offer compelling evidence in favor of the idea that specific cortical layers are involved in analyzing different aspects of visual information.

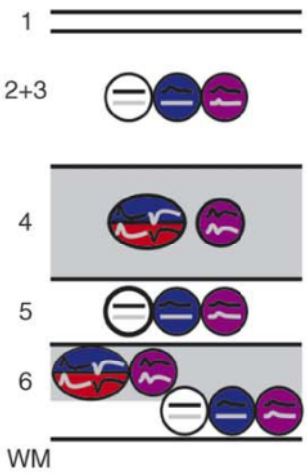

Figure 2.5. Laminar organization of receptive field structure
Distribution of simple and complex cells through the cortical depth, gray bands chart input from the primary layers of the lateral geniculate nucleus. Simple receptive fields are indicated by the ovals filled with red (ON) and blue (OFF) subregions. Complex cells are drawn as circles that are shaded purple (to denote spatially overlapping ON and OFF responses) or blue (to indicate cells that strongly or exclusively prefer one stimulus contrast) or that are unfilled (to indicate a lack of response to simple static patterns). Stylized time courses of responses to bright and dark flashed stimuli are superimposed on the symbols for the receptive fields (provided by Hirsch and Martinez, 2006; reprinted with permission).

Given that receptive field properties in V1 depend on cortical layers, are other fundamental properties such as orientation selectivity, arranged in a layer-specific manner? It

has been shown that cells in supragranular and infragranular layers are more sharply tuned for orientation and that the spontaneous activity of layer 4 cells is higher than that of cells outside the granular layer (Hirsch and Martinez, 2006; **Figure 2.5**). Whereas cells in the lowest subregion of the granular layer (4C) are not orientation selective and have receptive fields similar to those found in the LGN. However, Ringach et al. (2002) have shown that there is significant diversity in orientation selectivity across all V1 layers. Indeed, they observed cells with high and low orientation selectivity across all cortical layers.

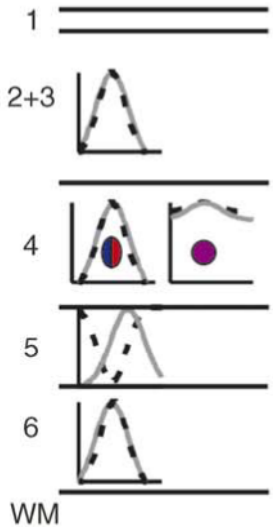

Figure 2.6. Laminar organization of orientation tuning
Each inset shows representative tuning curves for excitatory (solid line) and inhibitory (dashed line) inputs. In layer 4, excitatory and inhibitory inputs to simple cells are tuned and share the same orientation preference, whereas both types of input to complex cells are untuned. Excitatory and inhibitory inputs to complex cells in layers 2/3 also share the same orientation preference, but in layer 5 the tuning curves for the two types of inputs diverge and can be orthogonal (provided by Hirsch and Martinez, 2006; reprinted with permission).

2.4 Importance of laminar recordings

Given recent advances in optogenetics, we now have the ability to activate and deactivate specific cell types through cutting-edge viral-transfection of light-driven ion channels and pumps (e.g. channelrodopsin and halorhodopsin). This has given the researcher unprecedented ability to selectively stimulate or deactivate neurons with particular wavelengths of light. This technique, which is widely used in mouse, given the immense genetic flexibility, is beginning to be applied to recordings with awake-behaving monkeys (Boyden et al., 2005; Zhang et al., 2007). One way we could take advantage of this technique in studying laminar cortical circuitry would be to test to what extent horizontal connectivity influences laminar processing. Additionally, new methods are being developed that utilize state-of-the-art approaches for developing viral tracing (Nassi and Callaway, 2006; Nassi et al., 2006; Nassi and Callaway, 2007). These genetically modified viruses allow us access to both mono– and multisynaptic connections across the brain, which has never been studied until now. It should be noted, that while tracer injection techniques rely solely on anatomical localization and not functional aspects they are still invaluable in identifying complex circuitry within and between visual areas.

While all of the above techniques have various advantages and disadvantages in studying sensory processing, it is my opinion that to study population coding and the relationship to behavioral performance, multi-electrode recordings, given their precise millisecond time scale, is the best available technique. It can be argued that the foundation of systems neuroscience has relied on multi-electrode recordings and this has forever changed

how we understand the function of neurons and brain circuits. Although existing multi-electrode arrays are informative for measuring responses across many millimeters of cortical space along the cortical surface, they lack the ability to measure cortical depth and are unsuitable to approach the issue of laminar cortical circuits.

Multi-electrode recordings have become the standard for analyzing how neuronal networks in the cortex encode stimulus information. Recent advancements in electrode technology have emphasized the implementation of multi-contact laminar electrodes. These tools enable us unprecedented characterization of local cortical circuits. Although multi-electrode recordings offer useful information about neuronal population coding, laminar electrodes enable greater resolution and more information about the specific location of neurons. Since the cortex is organized into layers with anatomically different inputs and outputs, this raises the question of how sensory information is processed differently in these layers.

While the resolution of this technique still lacks the ability to assess the contribution of different sub layers (e.g. 4Cα and 4Cβ to cortical processing), this technology will continue to flourish as more laboratories utilize laminar recordings. Additionally, the design and implementation of chronically implantable arrays is currently underway and will likely replace multi-electrode recordings. In the future, arrays containing electrodes with multiple contacts along their shafts (essentially multiple laminar electrodes) are being developed in parallel. In chapter 5, I will present our method for recording individual neurons and LFPs across cortical layers of V1 utilizing multi-contact laminar electrodes (Plextrode® U-Probe, Plexon Inc.).

Throughout this thesis, I will argue the point that since responses of cortical neurons as well as local field potentials are significantly influenced by the inputs from other neurons and local populations in their network, information processing may depend on the network environment in which neurons are embedded. In this chapter, I have presented previous research that clearly acknowledges that the structure of local networks must be dependent on cortical layer. Examining how networks in different layers of the cerebral cortex encode information is fundamental for understanding how brain circuits process sensory inputs in real time. Indeed, cortical layers are ubiquitous structures (Nassi and Callaway, 2009) consisting of highly recurrent networks (Gilbert and Wiesel, 1983) characterized by distinct connection patterns.

In recent years, significant progress has been made in our understanding of the differences in response properties of neurons across cortical layers (Buffalo et al., 2011; Lakatos et al., 2008; Sun and Dan, 2009; Maier et al., 2010; Hansen and Dragoi, 2011). However, there is still a great deal to learn about whether and how individual neurons and populations of neurons encode information in a layer-specific manner. In chapter 5, I will describe our work exploring spike count correlations between pairs of neurons and how the correlation structure changes as a function of layer. Then in chapters 6 and 7, I will explain our findings in terms of local population coding including synchronization and communication of information across cortical layers in response to rapid adaptation and behavioral performance in orientation discrimination task.

"By always thinking unto them [his discoveries]. *I keep the subject constantly before me and wait till the first dawnings open little by little into the full light."*

— Isaac Newton

3. POPULATION CODING

3.1 Introduction

It has long been reported that nearby cells in many cortical areas exhibit correlated trial-to-trial response variability, (Zohary et al., 1994; Shadlen and Newsome, 1998; Bair et al., 2001; Kohn and Smith, 2005; Cohen and Newsome, 2008; Gutnisky and Dragoi, 2008; Smith and Kohn, 2008) possibly originating from common synaptic input. Furthermore, these correlations can have a significant impact on coding efficiency (Averbeck and Romanski, 2006; de la Rocha et al., 2007; Gutnisky and Dragoi, 2008) and information transmission (Salinas and Sejnowski, 2000). Estimation of correlated neuronal firing is fundamental for understanding how populations of neurons encode sensory inputs. Recent evidence suggests that the structure of correlations across a network influences the amount of available information in the responses of a population of cells (Abbott and Dayan, 1999; Sompolinsky et al., 2001; Cohen and Kohn, 2011), possibly limiting behavioral performance (Abbott and Dayan, 1999; Palmer et al., 2007; Chen et al., 2008). In addition, correlations between neurons can serve to constrain the possible coding strategies employed by the cortex to process sensory stimuli (Zohary et al., 1994; Shadlen and Newsome, 1998; Bair et al., 2001; Kohn and Smith, 2005; Cohen and Newsome, 2008; Gutnisky and Dragoi, 2008; Smith and Kohn, 2008).

The goal of this chapter is to introduce the background and principles regarding neuronal coding between pairs of cells and how this information underlies the correlation structure of cortical networks. This is an instrumental first step in understanding how individual neurons respond to incoming stimuli. While a great deal of work has focused on understanding

the importance of signal correlations across cortical networks, there is an increasing emphasis on identifying the importance of spike count or 'noise' correlations. In Section 3.2, I will define the term correlation and explain the differences between signal and noise correlations (**3.2 Noise v. signal correlation**). In order to understand the importance of correlations, I will provide examples of functional connectivity (**3.3.1**) and an experimental framework for their interruption and mechanisms underlying correlations (**3.3.2**). Finally, I will discuss some recent results suggesting that correlations are an order of magnitude lower than previously thought (**3.4 Reconciling correlation values**).

3.2 Noise vs. signal correlation

One of most important functions of the nervous system is to translate accurately the real world characteristics (e.g. visual environment) from neuronal responses. In the visual system, the information transmitted from the retina is analyzed and transformed by the visual cortex at multiple stages to construct an internal representation of the environment. This is a rather daunting task considering the fact that at any given point in time neuronal responses are ever changing even under identical stimulus conditions. This problem is further compounded by the fact that in most cases the vital information is distributed across hundreds of neurons. It has long been suggested that the visual cortex functions as a type of passive filter that creates a static, spatial, representation of the visual scene via hierarchical processing. According to this view, variations in neuronal responses to identical stimuli are thought to reflect independent fluctuations, or 'noise'.

Currently, one of the major goals in systems neuroscience is to understand how information is represented and processed by the brain. Individual neurons have restricted information processing capabilities and limited access to all the needed information to perform common brain computations. In addition, neuronal responses are inherently noisy representations of the external world and as a result represent information much worse than the nervous system as a whole (e.g. Georgopoulos et al., 1986; Paradiso, 1988; Averbeck and Romanski, 2006). Therefore, to obtain better estimates of the nature of sensory information the brain has to collect information from several different neurons thus pooling information from across many sources. An emerging field has developed in order to study the various mechanisms by which the brain averages together responses from multiple neurons known as population coding. The goal of this field is to study population coding in a probabilistic way given the inherent problems associated with the study of neurons that are noisy by nature. The main questions that this field addresses are: (i) to what degree of accuracy does a neuronal population represent sensory information and (ii) how does the presence of noise affect such representations.

A careful understanding of the structure of the noise is required not only to answer these questions, but also to do so in a quantitative manner. Specifically, the goal of the population coding field is first to determine whether the noise measured between two neurons is correlated. It is increasingly being realized that neurons have substantial noise correlations (Zohary et al., 1994; Bair et al., 2001; Romo et al., 2003; Kohn and Smith, 2005; Puchalla et al., 2005; Averbeck and Romanski, 2006; Schneidman et al., 2006; Cohen and Newsome, 2008; Gutnisky and Dragoi, 2008; Smith and Kohn, 2008; Poort and Roelfsema, 2009).

However, we must be cautious when computing noise correlation values as it is not acceptable to obtain a simple average correlation value to infer the population coding efficiency (Zohary et al., 1994). Population coding and measures of how accurate the population encodes stimulus information depends on two factors: (i) the relationship between the correlated noise between a pair of neurons and (ii) the degree of selectivity of the neurons to given set of stimuli (Abbott and Dayan, 1999; Sompolinsky et al., 2001).

In the following example, I will illustrate the importance in understanding the distribution of noise with respect to the neurons' tuning curves (Averbeck and Lee, 2004). There are two types of correlations commonly used throughout systems neuroscience literature. The 'signal correlation' is a similarity measure of the tuning function curve between a pair of neurons (**Figure 3.1**). Signal correlation is often used to quantify the extent to which a pair of neurons has similar functional properties (e.g. orientation selectivity or orientation tuning). For example in the case of orientation selectivity, if two neurons have a signal correlation close to 1 they will have a similar preferred orientation and if their signal correlation is close to -1, the two neurons have opposite preferred orientations (e.g. 90º apart). It has been proposed that a decrease in the signal correlation for example through adaptation (Barlow and Foldiak, 1989) might underlie a sparsening of responses at the population level. While I have mentioned that neurons are inherently noisy, 'noise correlation' represents Pearson's correlation coefficient of the trial-to-trial responses of the spike count between a pair of neurons for multiple presentations of an identical stimulus (**Figure 3.2**). Spike counts are typically measured over a brief timescale such as the stimulus presentation, which can range from a few hundred milliseconds to several seconds. In **Figure 3.3**, I plot hypothetical responses of two neurons for

different signal and noise correlation configurations. Each ellipse indicates a certain fixed confidence interval (i.e. 95%). The joint neuronal responses to two stimuli are plotted (blue and red) for three different cases. The black dots represent the mean response of each neuron to the stimulus.

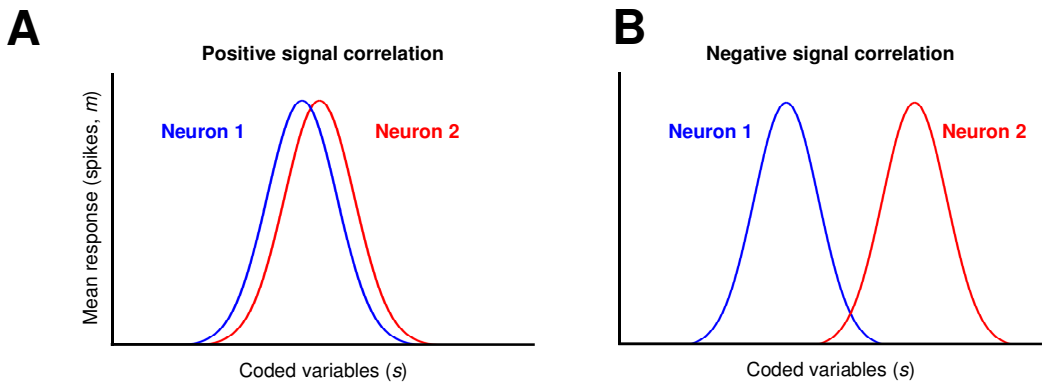

Figure 3.1. Signal correlations (r_{signal})
Signal correlation is a measure of the similarity of tuning between neurons. The figure shows the mean response (m) as function of given set of coded variables (e.g. orientations). Each figure is an example of neuronal response distributions that would produce either positive (**A**) or negative (**B**) signal correlations (adapted from Averbeck and Lee, 2004).

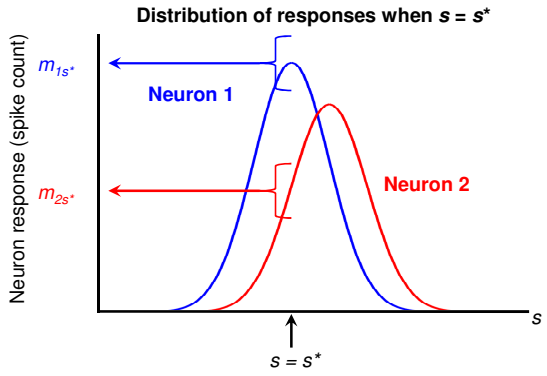

Figure 3.2. Noise correlations (r_{sc})
A measure of the correlation in the variability of trial-to-trial spike counts between neurons, after the mean responses are removed. This is an example of the distribution of responses for neuron 1 and 2 for a particular value of coded stimuli s. That is $s = s^*$ is a particular visual stimulus (e.g. orientation). When a pair of neurons has a positive noise correlation, both neurons respond above or below the mean responses (adapted from Averbeck and Lee, 2004).

One of the most widely studied aspects of correlations and population coding is the impact on information processing. **Figure 3.3** shows the hypothetical distributions between two neurons for different signal and noise correlation configurations. The joint neuronal responses for two stimuli are plotted (blue and red) for three different cases. The black dots represent the mean response to each of the stimuli. Each ellipse indicates a certain confidence interval (i.e. 95%), while the degree of overlap between the two ellipses is related with the difficulty of discriminating two stimuli on a given trial. The first condition in **Figure 3.3** A shows what might happen when the noise correlation is positive but the signal correlation is negative. It is also noteworthy that in **Figure 3.3** B where the neurons are uncorrelated, there is a higher degree of overlap. This means that for a given pair of neurons they have an opposite signal and noise correlation they will carry more information than if they were uncorrelated. Moreover, arguably the worst-case scenario for stimulus coding in this schematic example is plotted in **Figure 3.3** C. The neuronal pair has both positive signal and noise correlations and consequently the separation between the two distributions is reduced resulting in poorer discrimination. The previous examples allow us to emphasize two key aspects. First, to determine how much information about the stimulus is represented we need to know the correlation structure between neurons; individual neuronal responses fail to capture the full picture of the population. Second, we are not able to conclude whether this information is efficiently represented by knowing only the 'noise correlation'; we have to know its relationship to the signal correlations. With this established working definition of both signal and noise correlations, we can now discuss why noise correlations are particularly important.

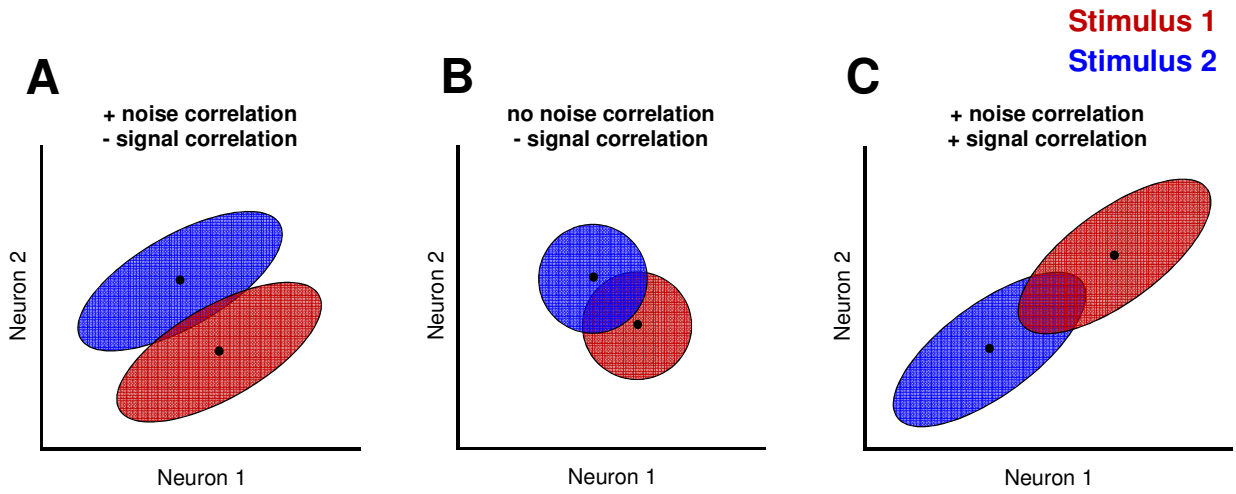

Figure 3.3. Impact of noise correlations on information coding
The ellipses represent the strength and sign of the noise correlations. The black point represents the mean responses to the two stimuli (blue and red). (**A**) Positive noise correlations and negative signal correlations. (**B**) The noise is uncorrelated but the signal correlation is negative. (**C**) Positive signal and noise correlations (adapted from Averbeck and Lee, 2006).

3.3 Importance of correlations

3.3.1 Benefits and uses

Throughout this section, I will use the terms 'correlation' and 'noise correlation' interchangeably. To reiterate, noise correlations are a measure of the correlated variability in trial-to-trial spike counts between a pair of neurons. Previous literature has suggested that correlations have a significant effect on the amount of information encoded by neuronal populations (Zohary et al., 1994; Shadlen and Newsome, 1998; Abbott and Dayan, 1999; Averbeck and Romanski, 2006). Many groups have observed, in a variety of cortical areas that in a population of neurons correlations are beneficial by reducing the signal-to-noise ratio of averaged response (Zohary et al., 1994). This led others to investigate the importance of correlations in population coding. Correlations are also useful in providing information about

the functional architecture of neuronal networks and populations of neurons. While much of the work on connectivity has been anatomical in nature, correlations have been used to study functional connectivity in the retina (Greschner et al., 2011), between the thalamus and visual cortex (Reid and Alonso, 1995), and between neurons in the cortex (Aertsen et al., 1989; Alonso and Martinez, 1998). Correlations allow one to observe changes in a given circuit under multiple stimulus condition or behavioral responses. As a result, analysis of correlations between neurons can provide a detailed picture of the network function or computations that are not accessible by simply studying the firing rate activity from two neurons independently (Ahissar et al., 1992; Vaadia et al., 1995; Kohn and Smith, 2005; Cohen and Newsome, 2008).

While it would appear that there is extensive research on correlations in a variety of brain regions, behavioral and stimulus conditions, and timescales (**Table 3.1**) there is still little known about how neurons process information across cortical layers. All of these studies have reported a range of correlations values, but overall values tend to be small and positive. Because it was observed that correlations tend to be highest when pairs are nearby (Lee et al., 1998; Constantinidis and Goldman-Rakic, 2002; Smith and Kohn, 2008), it has been suggested that correlations may reflect fluctuations in responses. Consistent with this view, correlations were significantly low in pairs of neurons recorded in different hemispheres (Cohen and Maunsell, 2009). It is noteworthy that correlations measured in motor areas appear to be overall lower compared to recordings in sensory cortices. Other factors like distance, tuning similarity, and architecture may reconcile some of the variability across studies. However, recent evidence suggests that differences associated with spike-sorting techniques, the time window in which spikes are counted, and the response strength can all bias estimates of correlations (Cohen and

Kohn, 2011). Furthermore, the responses of cortical neurons depend on their local network environment, which is known to change as a function of cortical layer. Our contribution to the field is a detailed investigation of the laminar dependency of noise correlation in V1, which will be, discussed in chapter 5.

Area	Firing rate (spikes per s)	Duration (ms)	State (task, anesthesia, etc.)	r_{SC}
V1	~25	2,560	Anesthetized	0.2
V1	~8	1,280	Anesthetized	0.16
V1		1,894	Anesthetized	0.25
V1			Anesthetized	0.26
V1	~50	1,860	Fixation	0.25
V1	~3	500	Fixation	0.01
V1		400	Tracing	0.18
V1	30	1,000	Discrimination	0.1
V2	5	1,000	Anesthetized	0.11
V4	5.2	1,000	Fixation	0.05
V4	21	200	Attention/detection task	0.04
V4	>5, ~20	800	Attention/tracking task	0.05
MT	~10	300	Anesthetized	0.09
MT	~20	500	Fixation	0.1
MT	28.5	500	Discrimination	0.13
MT	~20	1,000	Discrimination	0.15

Table 3.1. Summary of studies measuring spike count correlations
All of these studies have reported a range of correlations values, but overall values tend to be small and positive (provided by Cohen and Kohn, 2011; reprinted with permission). References for each study: **V1**: Kohn & Smith, 2005; Smith & Kohn, 2008; Reich et al., 2001; Rasch et al., 2011; Gutnisky & Dragoi, 2008; Ecker et al., 2010; Poort & Roelfsema, 2009; Salmonds et al., 2009. **V2**: Zandvakili & Kohn, unpublished. **V4**: Smith and Sommer, personal communication; Cohen & Maunsell, 2009; Mitchell et al., 2009. **MT**: Graf personal communication; Huang & Lisberger, 2009; Cohen & Newsome, 2008; Zoharay et al., 1994 and Bair et al., 2001.

3.3.2 Underlying mechanisms of noise correlations

Correlations are plastic – and as a result are often influenced by a variety of factors that also have control over the general responsivity of the neurons themselves. Some factors include the strength of the stimulus or sensory environment, as well as various internal states that govern our attention and arousal. Previous work from the Dragoi laboratory has also shown that adaptation can affect the correlation structure (Gutnisky and Dragoi, 2008). This issue becomes increasingly important when one considers that even small changes in correlations can have far reaching consequences on population coding (Averbeck and Romanski, 2006), which as a result can have a dramatic effect on sensory processing. Even with an overwhelming amount of evidence describing the precise spatial and temporal scales at which correlations are influenced, little is known about the mechanisms responsible for the modulation of correlations. One prevailing theory is that correlations in the trial-to-trial variability of spike-counts between two neurons arise from the firing of a common presynaptic neuron or pool of neurons (Shadlen and Newsome, 1998). We can hypothesize that each stimulus drives a particular subset of cells within a given network and that the common input is modulated by the unique stimulus properties. Indeed this is what has been observed in V1 where correlations are high in response to a stimulus grating whose orientation is between the preferred orientation of the two cells (Kohn and Smith, 2005). However, in the medial temporal (MT) cortical region, which is involved in visual motion processing, correlations are strongest for the speed at which the visual stimulus is presented (Huang and Lisberger, 2009). At timescales of around 100 ms, there is a clear stimulus-dependent influence on the structure of correlations. Yet at longer timescales, hundreds of milliseconds, other factors are influencing correlations.

At longer timescales, the spike-count correlation (r_{sc}) is independent of the stimulus (Zohary et al., 1994; Bair et al., 2001) thereby suggesting that correlations arise from variations in the state of the cortical network not related to the input. These variations are widespread and affect cortical responsivity. One study suggests that these fluctuations are responsible for the large depolarizations identified in intracellular recordings, involved in up/down states (Destexhe and Contreras, 2006) and the modulation of excitatory and inhibitory inputs at frequencies between 6-10 Hz (Poulet and Petersen, 2008). When a visual stimulus is presented, these fluctuations are reduced during sensory stimulation (Nauhaus et al., 2009) and behavioral control (Crochet and Petersen, 2006). Previous research in visual areas V4 and MT has shown that attention as well as arousal can influence neuronal responsivity, leading to an overall reduction in correlations at slow timescales (Cohen and Newsome, 2008). Likewise in V1, correlations are reduced during stimulus drive and are affected more by strong stimuli (e.g. high contrast) than by weaker stimuli (Kohn and Smith, 2005; Huang and Lisberger, 2009). Taken together, the results from fluctuations in the cortical network are entirely consistent with results that claim a reduction in correlations during stimulus presentation and active behavioral states. To conclude, at brief timescales correlations are stimulus-dependent and most likely arise from common synaptic inputs. As the timescale increases, there is an enhancement of correlations by widespread low frequency variations in the cortical network. Finally, either the internal state (e.g. high or low spontaneous activity) or the external stimulus presentation are suggested as possible mechanisms by which one can modulate the strength of correlations.

3.4 Reconciling correlation values

The issue of correlated neuronal activity has been challenged by recent evidence describing spike count correlations in sensory cortex on the order of 10^{-2} (Cohen and Kohn, 2011). As described previously, many labs have reported high noise correlations values, in a variety of visual areas, in the range of 0.1-0.3 (see **Table 3.1**). However a recent study by Ecker et al. (2010), using tetrode recordings, measured noise correlations in V1 of awake-behaving macaques and reported values in the range of 0.01-0.03 (**Figure 3.4**). Two key points which need to be addressed: (i) the authors binned their data in long spike-time windows (500 ms) and such long timescales should bias correlations toward higher values (ii) there is evidence that stimulus size, while not mentioned, is also an important issue in exciting center vs. surround receptive field locations. Chapter 5 will describe our results suggesting that stimulus size is very important and related to the spatial scale of intracortical connections. Theoretical and experimental research from Renart et al. (2010) in somatosensory and auditory cortices of anaesthetized rodents also reported extremely low correlations and claimed that such extreme average correlation values are strongly dependent on the internal state of the cortex. Again, they observed extremely low correlations during activated states (**Figure 3.5**), which surprisingly are known to be devoid of up-down fluctuations (Anderson et al., 2000; Haider et al., 2006).

One possible mechanism to explain these extremely low noise correlations is that neurons originated from a balanced network. The idea of a balanced network postulates that connections between and within two pools of excitatory and inhibitory cells follow a reciprocal

path (van Vreeswijk and Sompolinsky, 1996; Sompolinsky et al., 2001) with recurrent inhibition closely following excitation. Therefore, excitatory and inhibitory synaptic currents will cancel each other out decorrelating neurons; leading to what Renart et al. (2010) define as an asynchronous, or uncorrelated state. It can be argued that a decorrelated state of the cortex would be advantageous for information processing by reducing the number of neurons necessary to achieve highly accurate network performance (Shadlen and Newsome, 1998; Abbott and Dayan, 1999; Averbeck and Romanski, 2006; Ecker et al., 2010).

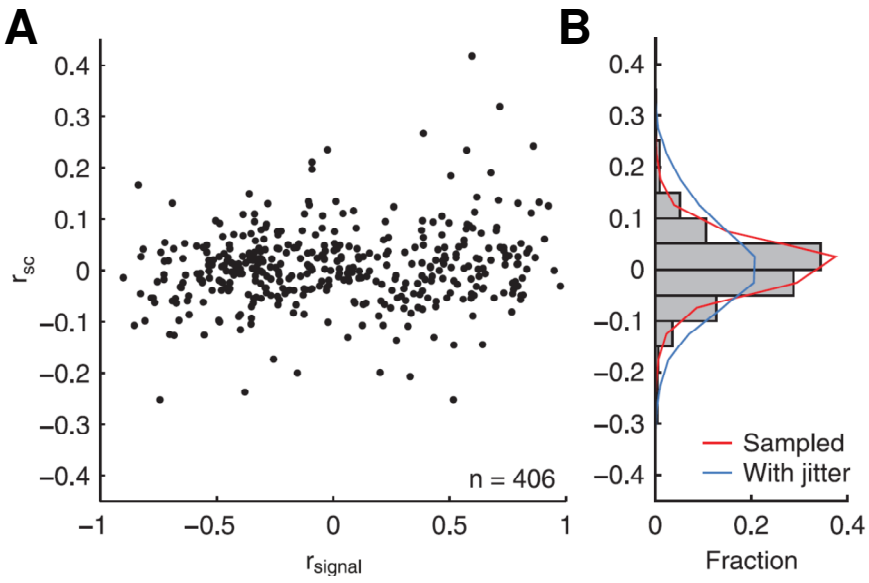

Figure 3.4. Spike count correlations of pairs of neurons recorded by the same tetrode
(**A**) Relation between r_{signal} and r_{sc} for all pairs of nearby neurons (both neurons recorded by the same tetrode). (**B**) Distribution of r_{sc} (mean ± SEM = 0.005 ± 0.004). Colored lines are distributions obtained by generating artificial data with the same number of trials as in the experiments (red, fixed r_{sc} = 0.01; blue, average r_{sc} = 0.01 and S.D. 0.1), which indicate that most of the scatter in the empirical distribution is due to estimating correlations from finite data (provided by Ecker et al., 2010; reprinted with permission).

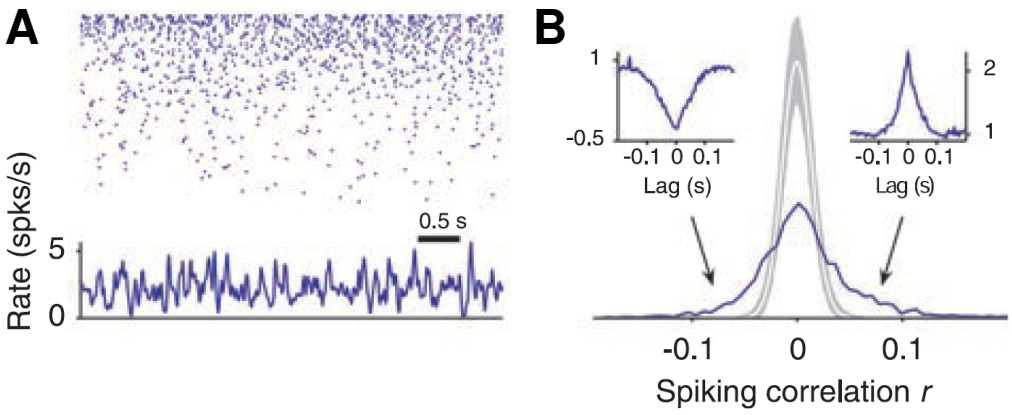

Figure 3.5. Distribution of correlations in rat neocortex
(**A**) Raster (top) and instantaneous population activity (bottom) for a population of 100 simultaneously recorded neurons (sorted by rate) during a period of cortical activation (ACT). (**B**) Histogram of spike count correlations of the population in (**A**) is wide ($\sigma_r >> \bar{r}$). The white curve is the mean histogram of the jittered spike trains [jitter ± 200 ms, gray shade 95% confidence interval; count window 50 ms]. Insets show average raw cross-correlograms of all negatively (left) and positively (right) significantly correlated pairs ($P < 0.01$) (provided by Renart et al., 2010; reprinted with permission).

Current experimental and theoretical research (including our own) has offered various explanations as to why low correlation values were observed in sensory cortex. Cohen and Kohn (2011) provide a detailed review as well as network simulations in which they attempt to explain why Ecker et al. (2010) observed such low correlations. One aspect they consider was difference in spike-sorting techniques; the fact that small errors in sorting can have a dramatic influence on the measure of noise correlations needs to be investigated further. Errors that add independent variability to the responses of one neuron will bias estimates of correlations to zero, whereas errors that involve combining of responses of multiple cells will increase the magnitude of the noise correlation measure. Implementing various simulation and computation techniques, Cohen and Kohn (2011) observed that combining several units effectively averages out any variability that should be independent of each cell; therefore, any measure of spike-

count correlation between clusters of multi-unit activity will exceed that if the measure was between constituent neurons. On the other hand, being overly restrictive in spike sorting can underestimate correlation measures. The main problem is that results obtained from overly strict spike sorting wrongly divide waveforms belonging to a single neuron in to multiple neurons (Rinberg et al., 2003). Computer simulations of this scenario reduced the measure of noise correlations by 30%. Relating these observations to the results of Ecker et al. (2010) in which they utilized tetrode recordings and made the claim that such a technique offers superior single-unit isolation is important. Chapter 5 will provide experimental evidence that suggests an additional possibility to reconcile these results, with previous research on correlations- that the local network circuitry gives rise to laminar dependent changes in the correlation structure.

“Science is not about control. It is about cultivating a perpetual condition of wonder in the face of something that forever grows one step richer and subtler than our latest theory about it. It is about reverence, not mastery.”

— Richard Powers

4. NETWORK SYNCHRONIZATION

4.1 Introduction

A review article entitled the 'Cerebral and cerebellar potentials' by Frédéric Bremer in 1958 provided the first "theoretical and experimental data pertaining to the nature, origin, synchrony and functional significance of brain waves". Fifty years later, the study of cortical rhythms is one of the most popular areas of brain science and has emerged as an area of converging interests across many scientific disciplines (e.g. physics, computer science, engineering and biology). Today, rhythmic modulation and synchronization of neuronal activity are two widely observed phenomena found in all major brain systems studied (Buzsaki, 2006; Tiesinga et al., 2008; Fries, 2009). Synchronized neuronal activity is a ubiquitous phenomenon observed at all levels of neuroscience from cellular membranes, to the firing pattern of single neurons, and the joint firing among two and more neurons. However, synchronization is most widely studied and accessible as a network phenomenon measured as small fluctuations in local field potentials. Analysis at the network level has accurately identified that periods of rhythmic neuronal synchronization emerge during specific functional states, that have a clear relationship between cognitive functioning and behavior (Womelsdorf et al., 2010; Donner and Siegel, 2011; Fell and Axmacher, 2011). Synchronization is measured as the coherence between two signals (x and y) recorded at different sites, which represents a complex quantity whose magnitude is a measure of the phase synchrony for a given frequency. Coherence, either field-field or spike-field, is an absolute value that varies between 0 and 1 (e.g., in spike-field

coherence a value of 1 indicates a perfect phase relationship between the firing of the spikes to the fluctuations of the LFP).

It is true that neuronal synchronization is a very well studied phenomenon such that multiple frequencies must work in concert in a variety of cognitive tasks to communicate efficient and accurate information. For example, selective attention enhances neuronal synchronization, processing is said to arise first in the gamma-band (30-80 Hz) during stimulus processing (Fries, 2009). Similar modulation has also been observed in the alpha-band (8-14 Hz) during periods of activity from the same neuronal groups involved in processing information about distracting stimuli (Kelly et al., 2006; Thut et al., 2006; Womelsdorf and Fries, 2007; Fries et al., 2008; Siegel et al., 2008; Jensen and Mazaheri, 2010). Furthermore, decision-making and sensory-motor integration is predicted by beta-band (15-30 Hz) coherence of parietal and prefrontal areas (Pesaran et al., 2008; Siegel et al., 2011), and inter-areal theta-band (4-8 Hz) synchronization among hippocampus, striatum, parietal, and prefrontal cortices (Womelsdorf et al., 2010; Benchenane et al., 2011). Of particular importance, top-down control of attention, memory formation and recall is associated with synchronization across cortical networks involving prefrontal, hippocampal, and temporal subdivisions (Buschman and Miller, 2007, 2009; Gregoriou et al., 2009; Duzel et al., 2010; Arnal et al., 2011; Benchenane et al., 2011; Fell and Axmacher, 2011). Finally, research has shown that motor planning and action selection can occur from either rhythmic beta– and gamma– band synchronization in pre-motor and motor cortices (Baker, 2007; Siegel et al., 2011).

Oscillatory synchronization in visual cortex has been found to be critically involved in sensory processing (Gray et al., 1989; Engel et al., 1991a; Cardin et al., 2009), grouping (Gray et al., 1989; Engel et al., 1991a; but see Thiele and Stoner, 2003; Roelfsema et al., 2004; Palanca and DeAngelis, 2005; Dong et al., 2008; Lima et al., 2008), attention (Fries et al., 2001; Taylor et al., 2005; Womelsdorf et al., 2006; Gregoriou et al., 2009; Chalk et al., 2010), working memory (Pesaran et al., 2002), and behavioral reaction times (Womelsdorf et al., 2006). While occurring at varying temporal scales, neuronal groups in V1 and V4 exhibit strong oscillatory responses in the gamma-band frequency (Gray et al., 1989; Engel et al., 1991a; Fries et al., 2001), and single neurons synchronize their responses with the local population activity (Freiwald et al., 1995; Tsodyks et al., 1999). Previous work on synchronization in the visual cortex has focused on higher frequency oscillations, while recent studies have emphasized lower frequency synchronization, particularly alpha (Bollimunta et al., 2011) and beta oscillations (Engel and Fries, 2011; Wang, 2010). The reason for such an increase in interest in lower frequencies is due in part to better tools capable of analyzing spectral differences as well as a clearer framework associated with cognitive function.

This chapter will describe the neuronal signal by which we measure synchronization and its importance in processing information in the visual cortex (**4.2 Local field potentials in the visual cortex**). Section 4.3 (**Frequency-dependent synchronization**) will define the three major signals of interest in network communication (alpha, beta, and gamma) and provide a theoretical and experimental framework for their importance and role in cognition. Given the added importance of behavior at the network level, this section will emphasize previous work in the field exploring the relationship between synchronization and behavioral performance

associated with processing visual information. The chapter will conclude by briefly mentioning some recent work exploring the laminar dependence of synchronization and a possible underlying mechanism for the observed findings.

4.2 Local field potentials in the visual cortex

Placing an electrode in the brain that is capable of measuring extracellular activity yields two distinct signals: (i) discrete, high frequency (in the range of 0.6 to 3 kHz) spiking activity from neurons near the electrode shaft and (ii) low frequency voltage fluctuations (less than 200 Hz) that consist of the mean extracellular field potential comprised of the aggregate electrical activity (**Figure 4.1**). The latter is a measure of local activity of a network of neurons (Pesaran et al., 2002) and is referred to as a local field potential (LFP) signal. LFPs consist of low-frequency extracellular voltage fluctuations that are believed to reflect the input to a given cortical area (within 250 to 500 μm of the recording electrode, Kruse and Eckhorn, 1996; Katzner et al., 2009), including both local excitatory and inhibitory intracortical inputs (Logothetis, 2003). LFPs are also thought to reflect the collective dendritic processing of a local population. Previous research has explored the spatial spread of LFPs across cortical layers in V1 and observed a unique layer-specific pattern (Xing et al., 2009; i.e. spatial spread was only 120μm in layer 4B). Section 4.4 will discuss in detail the importance of LFPs across cortical layers. Given the fact that most neuronal connections are local, the frequency of oscillations is constrained by both the size of the local network and the energy that is required to elicit and maintain high oscillations. Thus, high frequency oscillations are confined to a

small neuronal space, whereas larger networks are recruited during slow oscillations (Steriade, 2001; Csicsvari et al., 2003).

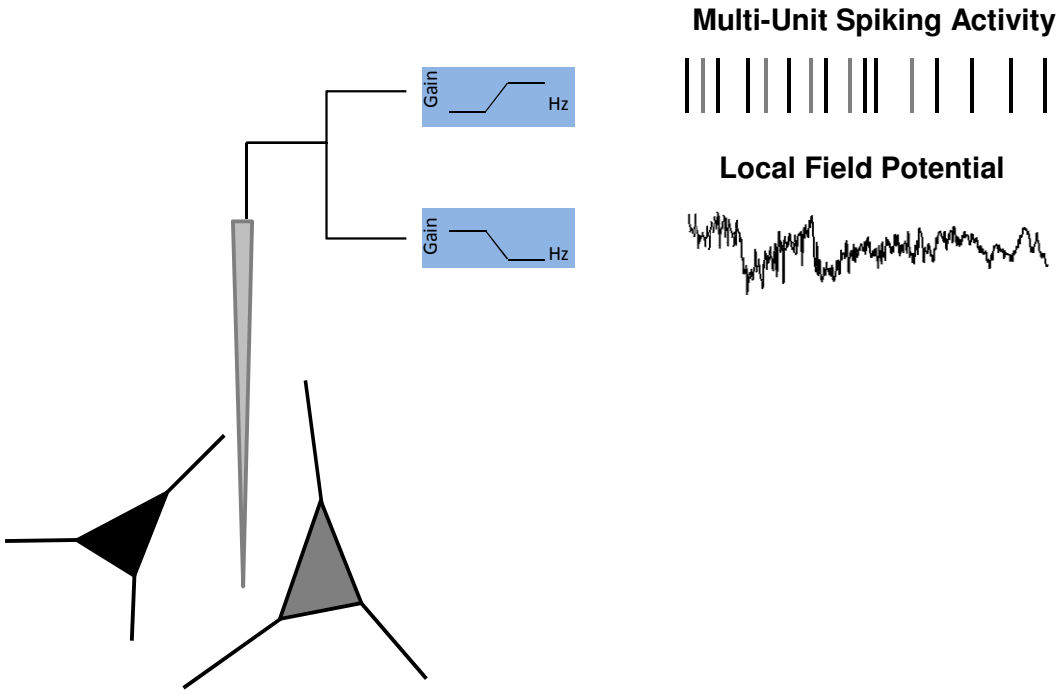

Figure 4.1. Neuronal signals and LFPs
An extracellular electrode placed in the brain measures the mean extracellular field potential, an aggregate signal originating from the population of neurons near the electrode tip. To obtain multi-unit spiking activity, the recorded voltage trace is high-pass filtered and individual action potentials are detected (top). The LFP is comprised of the low frequency components of the extracellular field potential up to 200 Hz (bottom). The frequency composition varies over time (adapted from Berens et al., 2008).

Even though LFPs are considered a measure of the average activity of numerous locally interconnected cells, they are surprisingly well modulated by contrast (Henrie and Shapley, 2005), orientation (Frien et al., 2000), and complex features such as objects (Kreiman et al., 2006) or semantic categories (Kraskov et al., 2007; in human subjects). Both perceptual and cognitive research has implemented aspects of LFP analysis, which is widely accepted, but the mechanism(s) underlying LFP modulation and precise spatial resolution are not fully understood.

According to Berens et al., (2008) one prevailing hypothesis is that the LFP is originated by a weighted average over potential changes in the nearby vicinity of the recording electrode, generated by current sinks and sources (Mitzdorf, 1985; Goense and Logothetis, 2008). That is, when synchronous excitatory synaptic activity occurs in the dendrites of a neuron, it creates a current sink at the dendrite and a resulting current source at the soma. When a sink and source are separated by a distance, this is commonly referred to as a dipole. A dipole in this context contributes to the LFP given the unique structure of the neuron with respect to the local population. An example of this is most clearly seen in pyramidal cells, which make up 80% of all cortical neurons and have large dendritic arbors facing in one direction away from the soma (Johnston and Wu, 1995). Researchers suggest that pyramidal cells strongly modulate LFP activity in the cortex. Recently, other sources such as inhibitory synaptic input (Hasenstaub et al., 2005), subthreshold membrane oscillations (Kamondi et al., 1998), and after potentials of somatodendritic action potentials (Buzsaki, 2002) have been found to contribute significantly to generation of the LFP signal.

Very little is known about the relationship between the mechanisms generating the LFP signal and the local cortical circuit. However, the spectral coherence between LFPs from neighboring recording sites falls off with increasing distance (Leopold and Logothetis, 2003). Indeed, the fall-off is steeper for frequencies greater than 30 Hz than for lower ones. Importantly, other researchers even those recording from neurons up to 1.5 mm apart, still report a gamma-band coherence of 0.7 (Juergens et al., 1999). Analysis of LFPs can help to identify synchronous activity between distant cortical populations, which may have functional implications concerning the efficient transfer of sensory information.

Fries et al., (2007) proposed that LFP responses could be used to measure the communication between neuronal ensembles. Indeed, accumulating evidence suggests that the synchronization between local populations, especially in the gamma-band (40-80 Hz), subserves information routing, grouping, attention, and behavioral reaction time (Gray et al., 1989; Engel et al., 1991a; Fries, 2005; Womelsdorf et al., 2007). For instance, gamma oscillations can be used to control efficient signal propagation by allowing groups of neurons in many brain regions to synchronize their responses. Fries and his colleagues have proposed that neuronal communication is performed by phase locking between the oscillations of interacting populations by alternately opening and closing their communication window (**Figure 4.2**). That is, coherent LFP oscillations regulate neuronal interactions and the flow of information (Fries, 2005; Schoffelen et al., 2005; Womelsdorf et al., 2007).

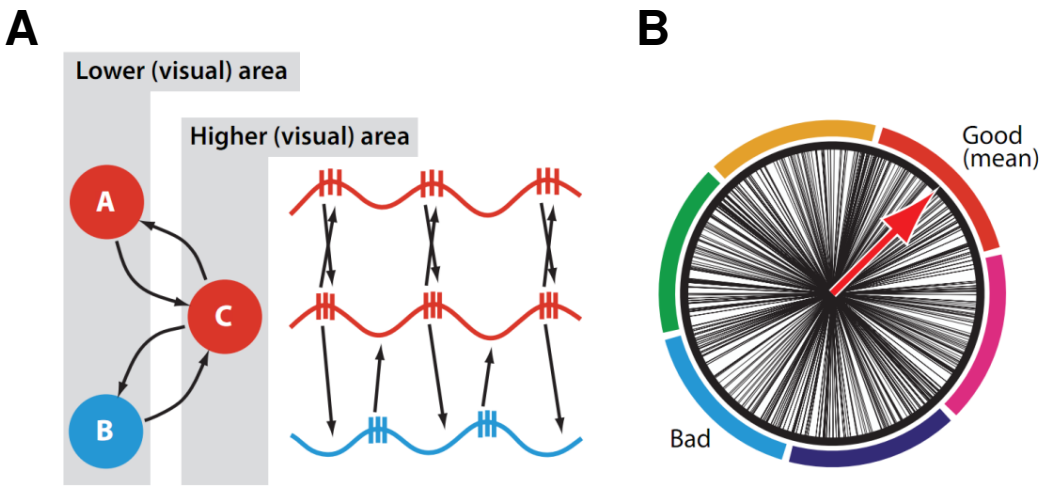

Figure 4.2. Communication is influenced by timing between neuronal activities
(**A**) Three neuronal groups (A, B, and C). The neurons inside group A are rhythmically synchronized as indicated by the undulating lines with spikes around the peaks. The same holds for the neurons inside groups B and C. However, C is in-phase synchronized exclusively to A and not to B. (**B**) Each vector corresponds to the relative gamma-band phase in a 250-ms-long epoch between gamma-band rhythms in two separate neuronal groups recorded in awake cat visual cortex. The thick red arrow indicates the mean relative phase across all epochs. The outer ring segments illustrate the sorting of epochs according to their relative phases (provided by Womelsdorf et al., 2007; reprinted with permission).

Communication between neuronal groups has also been shown to influence the grouping and selection of information (Engel et al., 2001) as well as cognitive function, such as expectancy or attention (Fries, 2005). An important measure of information transmission in neuronal circuits is the extent to which neuron spiking activity is synchronized with the underlying oscillatory population response (Jensen et al., 2007). In agreement with experimental and theoretical evidence network activity oscillating in the gamma-band, compared to lower frequency bands, has a more robust influence on post-synaptic targets due in part to the high temporal precision with the underlying neuronal network. For instance, attention increases gamma-band synchronization between spikes and LFPs (Fries et al., 2001). The effects of spike-LFP synchronization can also modulate visual behavior. For example, gamma-band synchronization in V4 has been correlated with decreased reaction times in a change detection task (Womelsdorf et al., 2006). These results support the hypothesis that efficient information transmission would occur whenever two networks are synchronous in their excitability peaks, which could constitute an energy-efficient mechanism for temporal coordination (Castro-Alamancos, 2004). In order to understand the basis of network synchronization, the next section will focus specifically on three key frequencies each involved in various aspects of cognitive and/or perpetual processing – alpha, beta, and gamma bands.

4.3 Frequency and laminar dependent synchronization

4.3.1 Alpha-band (8-14 Hz)

Alpha activity is characterized by a spectral maximum between 8-13 Hz and has been predominantly observed during the awake-state (Hughes and Crunelli, 2005). Recently, alpha activity has been shown to subserve an active, suppressive role for cortico-thalamic information processing during attentive processing and stimulus expectancies (Bollimunta et al., 2008; Jensen and Mazaheri, 2010; Bollimunta et al., 2011). Still, there is much debate about the true role of alpha-band synchronization in cognitive processing. Many of the theories concerning the function of alpha activity center on the observation that alpha activity is at its largest during periods of eye closure. Conversely, when eyes are open and the subject is engaged in a visual attention task, alpha synchronization is greatly reduced (Steriade et al., 1990) suggesting alpha rhythms may reflect an idling of the brain or an active input suppression (Worden et al., 2000). Others have argued this idea, citing work describing an increase in alpha during 'rejection tasks' or when attention is directed internally (Ray and Cole, 1985; Palva and Palva, 2007). Chapter 6 will investigate the role of network synchronization in the alpha frequency range during a rapid adaptation task. In addition, the role of alpha activity in laminar cortical processing will be addressed. Yet in order to understand the importance of alpha as a mechanism for neuronal communication, it is important to have an idea of the physiological mechanism(s) that generate alpha rhythms.

Even though the existence of alpha activity is widely observed across a variety of visual cortices, research identifying the mechanisms underlying alpha-band synchronization are still not fully understood. The general hypothesis was that alpha activity originated in the thalamus (Andersen and Andersson, 1968). However, further research (da Silva et al., 1973a, b; Lopes da Silva et al., 1980) identified that alpha rhythms were generated from layer 5 pyramidal neurons acting as pacemakers (Lopes da Silva, 1991). This work was later bolstered by studies using *in vitro* preparations that showed cortical neurons can oscillate intrinsically in the alpha range in response to repetitive stimulation at 10 Hz (Steriade et al., 1990; Connors and Amitai, 1997). They also observed, consistent with earlier work, the existence of such alpha pacemakers in layer 5. This experimental work led computational neuroscientists modeling laminar cortical processing to include alpha pacemakers in layer 5 (Jones et al., 2000; Karameh et al., 2006). Recent work from Bollimuta el at., (2011) measured alpha activity across cortical layers in V1 of awake-behaving monkeys during a selective attention task and analyzed the Granger causality between signals in different layers. This was the first study to measure alpha activity across cortical layers and to provide evidence for the existence of layer 5 alpha pacemakers (**Figure 4.3**). Briefly, Granger causality requires two simultaneously measured continuous signals or time series (e.g. LFPs or coherence values). Granger (1969) stated "if the variance of the prediction error for the second time series at the present time is reduced by including past measurements from the first time series in the linear regression model, then the first time series is said to have a directional or driving influence on the second time series". That is, Granger causality as a measure is based on time series predictions (Geweke, 1982; Ding et al., 2006). A causal relationship is said to occur between two time series when predicting the second series depends on the past information of the first series. The same interpretation is used to describe

measurements that occur in the opposite direction. This measure is useful because it allows one to identify to what extent laminar-specific frequency generators influence synchronization between layers.

Despite the fact that pyramidal neurons are acting as alpha pacemakers in layer 5, little is known to explain the observation that alpha activity patterns persist as you travel up the ventral pathway given the cortical cellular morphological heterogeneity between areas. Importantly, Bollimuta et al., (2008) observed that in layer 5 visual areas there is an increase in spontaneous activity, which they conclude is a signature of alpha pacemaker. This claim is further supported by the fact that greater spontaneous activity is thought to arise because deep layers contain a greater amount of long-range horizontal projections (Telfeian and Connors, 2003; consistent with our conceptual model of the spatial spread of intracortical connections discussed in chapter 5).

4.3.2 Beta-band (15-30 Hz)

Beta-band activity (15-30 Hz) was initially observed in the primary motor cortex by Hans Berger in 1931 (Wang, 2011). Pioneering work using intracranial electroencephalography (iEEG) recordings from patients with epilepsy, Jasper and Penfield (1949) noted that the beta rhythm occurred during movement "readiness" or preparation, but ceased at the initiation of a movement. Continuing this line of research, electrophysiological studies in humans and monkeys have confirmed the notion that beta band activity is associated with both the preparation and control of the motor system. Therefore, beta power is known to decrease at the

onset of movement execution and increase when a response is withheld (Bouyer et al., 1987; Sanes and Donoghue, 1993; Baker et al., 1997; Swann et al., 2009). The restriction of beta oscillations to the motor system has been argued with suggestions that beta activity might be more generally involved in sensorimotor integration and top-down signaling. Unfortunately, there is no unifying hypothesis describing the mechanisms by which beta rhythms emerge. The following section will argue that beta band activity is intimately involved in both motor control as well as cognitive processing.

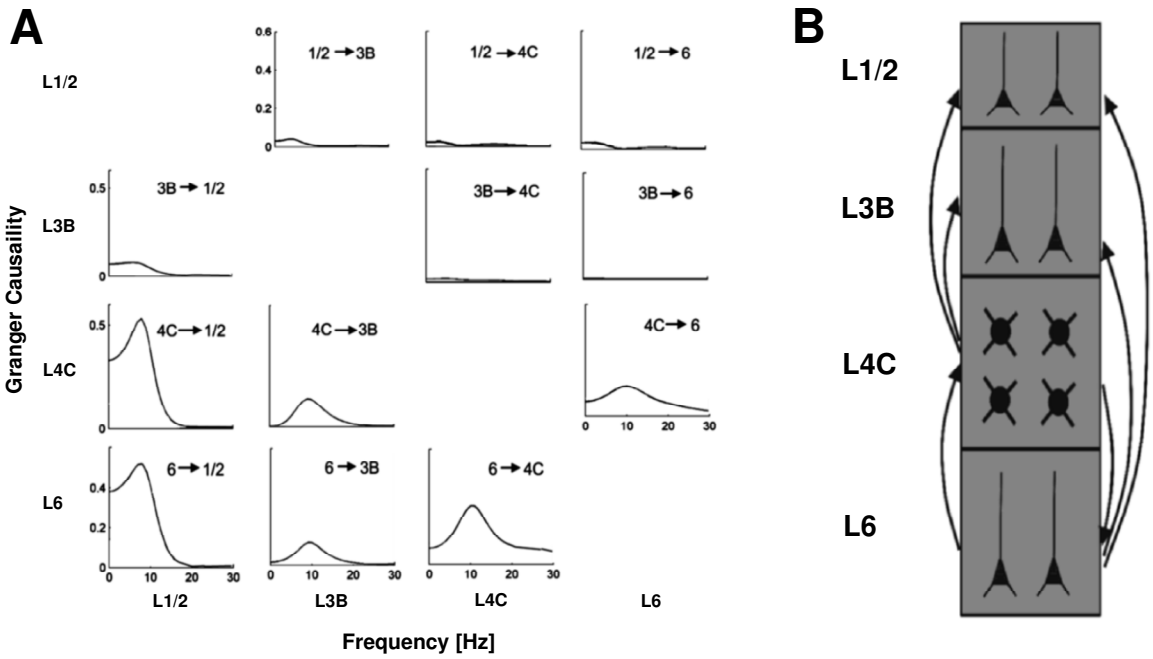

Figure 4.3. Laminar origin of alpha activity and Granger causality between layers
(**A**) Granger causality spectra for different alpha current generator pairs. The *y*-axis is the driver and *x*-axis is the target (i.e., panel *xy*, where *x* is the row index of the panel and *y* is the column index, shows the Granger causality spectrum for $y \rightarrow x$). (**B**) Schematic representation of interaction between different alpha current generators. An arrow is understood in the sense of significant Granger causality (n > 4) penetrations showed significant causality in response to the auditory condition (provided by Bollimunta et al., 2011; reprinted with permission).

Several lines of evidence have concluded that pronounced beta activity occurs in the motor system during steady contractions and holding periods following movements. Beta activity was observed to have been attenuated by voluntary movements (Sanes and Donoghue, 1993; Baker et al., 1997; Baker, 2007; Klostermann et al., 2007) and often inhibited by motor imagery (de Lange et al., 2008). During the preparation and execution of a movement plan, gamma-band activity replaces beta activity because of its faster rhythms and relationship with efficient communication of information (previously covered in Section 4.2). The role of beta activity in steady contractions is widely observed across numerous cortical and subcortical areas of the brain involved in movement planning: motor and premotor cortex, the basal ganglia, the cerebellum, and peripheral motor units (Baker, 2007; Brown, 2007). Taken together, these results led researchers to suggest that beta rhythms, given their increased activity during periods of inactivity, can be viewed as a sort of "idling rhythm" (Pfurtscheller et al., 1996). Recent research has challenged the role of beta activity as a rhythm reflecting a lack of movement. However, rather than signaling a lack of movement, beta activity may be a more active process that promotes an existing motor set while integrating neuronal processing of new movements (Gilbertson et al., 2005; Baker, 2007; Pogosyan et al., 2009; Swann et al., 2009). A review from Engel and Fries (2010) suggests that beta activity "may signal the tendency of the sensorimotor system to maintain the status quo." This theory is very controversial because it suggests that beta activity is an active signal as opposed to a passive rhythm and involved in feedback communication and recalibrating the motor system.

Based on findings from the motor system, many theories have proposed a possible role for beta activity modulation during various cognitive processes. It has been suggested that beta

activity can be modulated in three ways: (i) beta activity would remain unchanged if there is no change in the current cognitive processes or perceptual information, (ii) beta activity would increase with active maintenance of the current cognitive processes, and (iii) beta activity would decrease with a disruption in the current cognitive processes due to a novel or unexpected event (Engel and Fries, 2011). These predictions can be viewed in terms of either an endogenous event, involving top-down modulation and an increase in beta activity, or an exogenous event, in which the outcome of a given task is determined by bottom-up factors and a decrease in beta activity (Engel et al., 2001; Engel and Fries, 2011). There is increasing evidence that supports this idea of beta activity in cognitive processing (Engel and Fries, 2011), but understanding how various top-down and bottom-up processes influence beta activity is still an unanswered question in systems neuroscience.

Experimental evidence is consistent with the above predictions. Tasks that rely on stimulus-driven activity (i.e. tasks with a weak endogenous component) show a consistent decrease in beta during the presentation of new stimulus. Noteworthy, the observed decrease in beta activity corresponds with an increase in gamma-band oscillations (Engel et al., 2001; Fries, 2009). A number of recent studies suggest that beta activity is involved in top-down processes. One relevant study showed an enhanced association with beta-activity in response to an ambiguous stimulus generated purely from endogenous factors. Using magnetoencephalography (MEG) researchers measured beta activity of subjects during an auditory task. Subjects were instructed to manipulate an auditory tone by mentally placing downbeats and as a result, brain activity, during these trials, was said to arise from endogenous interpretation (Inversen et al., 2009). Even work using awake-behaving monkeys have observed that during

an endogenously directed search task, there is higher beta activity when compared to the same task when subjects are given explicit search instructions (Pesaran et al., 2008). Further research exploring beta oscillations and attentional processing has proposed that top-down attention is associated with large-scale network communication. Conversely, coupling at higher frequencies (i.e. gamma-band) occurs when bottom-up signals need to be conveyed to other cortical areas (Buschman and Miller, 2007, 2009).

One important and often neglected factor explaining some of the variability between attentional studies observing changes in beta activity seems to be the cortical layer in which recordings are performed. A recent study from Buffalo et al. (2011) found that stimulus-induced gamma-band activity was restricted to superficial layers. Indeed, they also observed in V1, V2, and V4 of awake-behaving monkeys that lower frequencies (i.e. alpha and beta) are more prominent in deep layers compared to superficial layers. Indeed, other groups have shown that there is a clear difference between synchronous activity in superficial layers compared to deep (Maier et al., 2010; Maier et al., 2011). We also observed a layer-specific relationship between cortical oscillations during a rapid adaptation task (chapter 6). To summarize this section, beta activity appears to playing similar roles during motor and cognitive processing. Particularly, in cognitive processing beta activity may serve to maintain a given set of perceptual information for future processing. This idea and the interplay between beta and gamma activity associated with the maintenance and changing of the status quo is summarized in **Figure 4.4**.

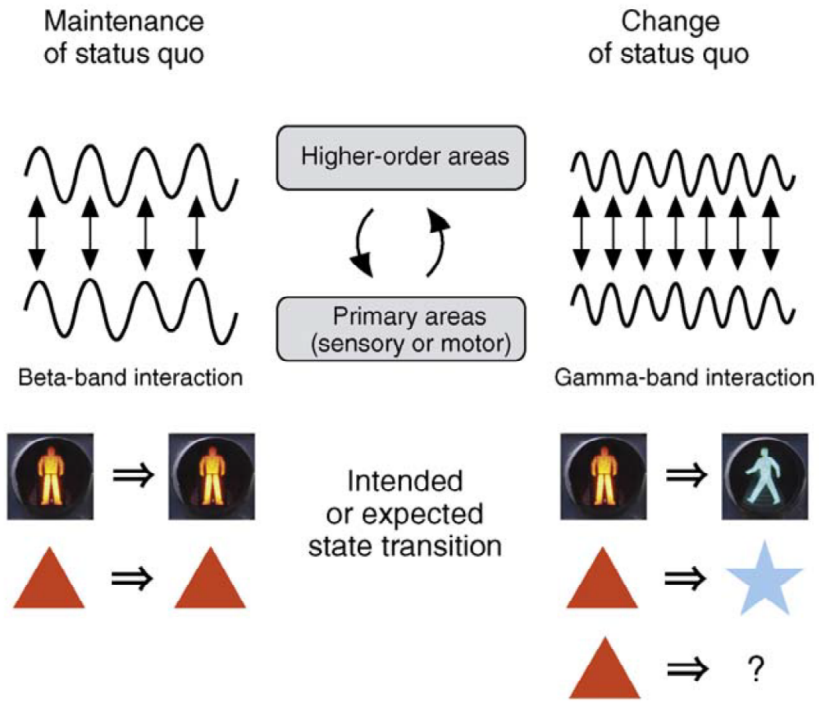

Figure 4.4. Beta band activity in sensory and motor circuits
According to the hypothesis, beta activity is important for the maintenance of a given sensorimotor state. For example, beta activity would be high when a 'no walk' sign continues to signal not to walk or when a stimulus such as a triangle does not change. On other hand, gamma activity increases when the system is ready to process novel sensorimotor information. For example, the 'ok to walk' sign or a new shape (provided by Engel and Fries, 2011; reprinted with permission).

4.3.3 Gamma-band (30-80 Hz)

Research in the neocortex led by Rougeul and colleagues identified a peculiar 40-50 Hz oscillation in the parietal and frontal areas when cats were engaged in watching prey enter the room (Bouyer et al., 1987). They referred to this oscillation as the "hyper vigilance rhythm", and while gamma activity (30-80 Hz) is never referred to by this name today, it accurately describes the behavioral context in which gamma is often modulated. In the late 1980s and 1990s, the next major advance in our understanding was that gamma-band synchronization in the visual cortex of anesthetized cats and monkeys was strongly enhanced when cortical

neurons were exposed to either moving bars or gratings (Gray et al., 1989; Gray and Singer, 1989; Engel et al., 1991a; Engel et al., 1991c; Engel et al., 1991b). More recently, other groups have induced such gamma synchronization with stationary squares (Rols et al., 2001) and smooth, deforming shapes (Taylor et al., 2005). There has also been a report that during free-viewing, gamma synchronization is modulated by exploration of a static visual scene (Bichot et al. 2005).

Given such a wide range of brain areas and tasks that claim to modulate gamma-band synchronization, there is also a high degree of specificity. For example, in the visual cortex, gamma-band synchronization has been shown to be selective for stimulus orientation (Gray and Singer, 1989). Moreover, in the lateral intraparietal area, reports claim directional selectively of gamma-band activity during a delayed saccade task (Pesaran et al., 2008). While much of the focus has been placed on measuring coherence within a particular area, more emphasis is being placed on coherence between areas (i.e. V4 and FEF) as was the subject of a recent study by Gregoriou et al. (2010). They observed that gamma-band activity was enhanced in neuronal populations when attention was directed to the stimulus in the overlapping receptive fields. Many theoretical approaches have begun to emerge about the role of gamma-frequency synchronization between neuronal assemblies. The suggestion that gamma activity is important in the integration of sensory information (Gray, 1994; Gray et al., 1995) is a hypothesis that has created new momentum in the systems neuroscience field, with the goal of understanding gamma rhythms and their functions.

Before understanding the role of gamma activity and its relevance in cognitive functions, a general hypothesis for the role of the gamma cycle must be defined. While much attention has focused on gamma-band activity (30-80 Hz), with such measures as power and coherence, analysis of the processes that occur during the gamma cycle is still largely unknown. During a gamma cycle (i.e. a sequence of neuronal processes that reoccur within each oscillation cycle), the excitatory input to a pyramidal cell is transformed into a time-based code which computes the amplitude of excitation as the time of occurrence of output spikes relative to the phase of the gamma rhythm (Fries et al., 2007). In other words, the stronger the input, the earlier the response is to the relative peak of the gamma cycle. This is seen when converting the amplitude into phase, which indicates how many spikes arrive prior to the peak of a gamma cycle.

While there is a great deal to learn about the role of gamma activity in various cognitive tasks, there is noteworthy research at the neuronal level as to how such rhythms are generated. The foundation of gamma synchronization begins at the level of the inhibitory interneuron network (Whittington et al., 1995; Jefferys et al., 1996; Singer, 1996; White et al., 1998; Hasenstaub et al., 2005; Vida et al., 2006; Bartos et al., 2007). Many studies have shown pharmacologically that an emergent property of these networks is their ability to generate synchronized gamma-band activity (Cunningham et al., 2004). Further studies using sophisticated computational models have confirmed such inhibitory networks require only synaptic inhibition and gap junction coupling in order to produce gamma-band oscillations (Whittington et al., 1995; Vida et al., 2006; Bartos et al., 2007). Importantly, it is also well established that these networks require activation, which is due to excitatory drive. During

physiological conditions, pyramidal cells have been suggested to provide such input. The activity between interneurons and pyramidal cells must be precisely modulated to produce gamma-band activity. What has been observed in hippocampal recordings from awake-behaving rats (Csicsvari et al., 2003) and more recently in ferret prefrontal cortex (Hasenstaub et al., 2005) is a precise phase relationship with the interneurons leading the pyramidal cells by a few milliseconds. The majority of this work has also been verified in simulations of networks with coupled pyramidal cells and interneurons in which synchronization with similar properties was observed (Borgers and Kopell, 2005).

Briefly, consider an idealized network (**Figure 4.5**) composed of three neurons (red traces) whose firing patterns are synchronized with the local gamma activity (green trace). Now, imagine to what extent this network will succeed in influencing a downstream neuron. When the firing patterns of the neurons in the network is synchronized in the gamma band, their effect on the receiving neuron increases. This is due to the high temporal precision associated with gamma activity. Thus, when a network of neurons is synchronized to their local gamma rhythm, the information arriving onto the postsynaptic potential is integrated over a given period. If the presynaptic potentials arrive at the same time (i.e. high temporal precision) from the network it will have a greater influence on how well that postsynaptic cell responds. When compared to the same network oscillating in the alpha band (8-14 Hz) there is a greater amount of temporal smearing. This lack of precision is caused by the presynaptic potentials arriving at random times, reducing the influence on the postsynaptic cell (c.f. size of the arrows to right between gamma and alpha). Presumably, phase-specific synaptic input, in relation to the gamma rhythm, can improve synaptic plasticity and as a result may have larger implications

for processing long-term memory. The cartoon suggests that when spiking occurs in phase with gamma activity there will be stronger synaptic strengthening even at the level of sub threshold activity.

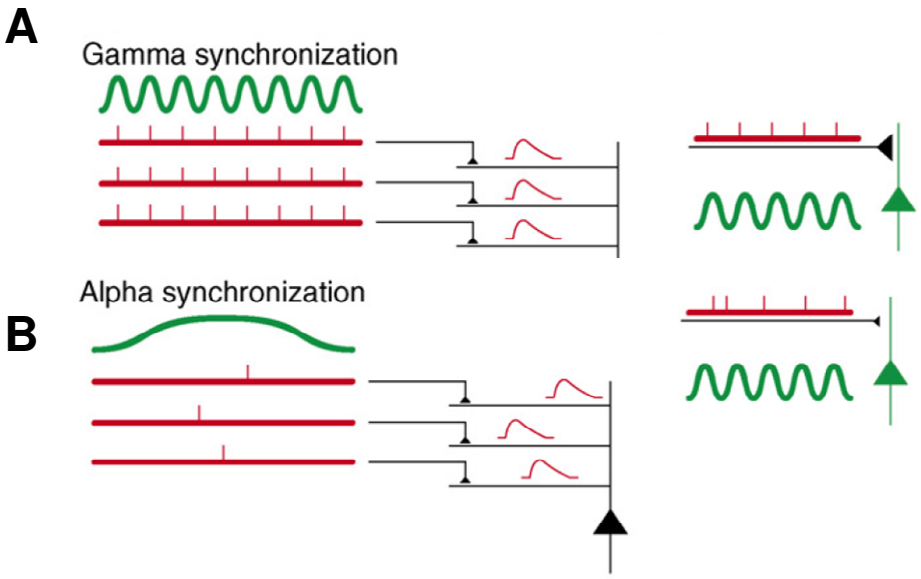

Figure 4.5. Functional role of gamma-band and alpha-band synchronization
(**A**) An idealized network composed of three neurons (red traces) whose firing patterns are synchronized with the local gamma activity (green trace). When the firing patterns of the neurons in the network are synchronized, their responses occur at the same time as a result the activity on the receiving neuron increases. This is due to the high temporal precision associated with gamma activity. (**B**) The same network under alpha synchronization lacks the temporal precision needed to influence the postsynaptic cell (provided by Jensen et al., 2007; reprinted with permission).

While numerous aspects of network synchronization based on the importance of alpha, beta and gamma band frequencies has been described, their functional significance is not yet clear. Possibly these rhythms, known to be important in cognitive function, are an irrelevant epiphenomenon given that the time differences and overlap between oscillatory activities across various frequency bands is only a few milliseconds. Two of the goals of this thesis are to: (i) provide some insight from our own work that characterizes the laminar network in V1 according the principles of network synchronization and (ii) extend the concepts of laminar

circuitry and network synchronization by exploring these effects during a behavioral discrimination task. To complete the first goal, we report that during a rapid adaptation task, we find very consist laminar changes in gamma activity, which is related to the discrimination performance of neurons within the same layer (chapter 6). For the second goal, we report that there is an important difference between beta and gamma activity that emerges during correct and incorrect decisions (chapter 7). Taken together, network synchronization is a powerful framework by which to analyze how the brain efficiently processes visual information across laminar circuits.

“The important thing in science is not so much to obtain new facts as to discover new ways of thinking about them.”

— William Bragg, Sr.

5. CORRELATED VARIABILITY IN LAMINAR CORTICAL CIRCUITS

5.1 Introduction

The strength of correlated neuronal activity reported in previous work has recently been challenged by evidence describing spike count correlations in sensory cortex on the order of 10^{-2} (Ecker et al., 2010; Renart et al., 2010). This poses a problem because clarifying whether cortical networks operate in a correlated or decorrelated state is fundamental for understanding how neuronal populations encode information. A decorrelated state of the cortex is arguably more advantageous for information processing by reducing the number of neurons necessary to achieve highly accurate network performance (Abbott and Dayan, 1999; Averbeck and Lee, 2004; Ecker et al., 2010; Shadlen and Newsome, 1998). Clarifying whether cortical networks operate in a correlated or decorrelated state is fundamental for understanding how neuronal populations encode information.

We reasoned that since responses of cortical neurons are significantly influenced by the inputs from other neurons in their local network, measurements of correlations may depend on the network environment (i.e. cortical layers) in which recorded neurons are embedded. Indeed, cortical layers are ubiquitous structures throughout neocortex (Nassi and Callaway, 2009) consisting of highly recurrent networks (Gilbert and Wiesel, 1983) and characterized by distinct connection patterns. Correlation analysis has provided significant information about the connectivity in neuronal networks (Alonso and Martinez, 1998; Greschner et al., 2011; Reid and Alonso, 1995). Not only does the distribution of cortical connectivity influence the correlation structure, the distribution of synaptic conductances is instrumental in modulating

correlation. For example, in a network modeling heterogeneity in the orientation tuning curves in V1 (Ringach et al., 2002), the noise correlation is significantly lower , ensuring better discrimination orientation performance, than in a network with non–heterogenous tuning curves (Chelaru and Dragoi, 2008).

Our central hypothesis is that the strength of noise correlations depends on the cortical layer from which they are measured. Since the main source of correlations is common input, one would expect that differences in the source and strength of inputs to neurons in different cortical layers would cause changes in correlations. For instance, one important distinction between cortical networks in the middle and superficial/deep layers is the spatial spread of intracortical connections. In the granular layers, where neurons receive geniculate input, the spatial spread of connections is small (Adesnik and Scanziani, 2010; Briggs and Callaway, 2005; Feldmeyer et al., 2002; Gilbert and Wiesel, 1983), whereas in supragranular and infragranular layers neurons receive recurrent input from larger distances (up to several millimeters) via long–range horizontal circuitry (Angelucci et al., 2002; Bosking et al., 1997; Gilbert and Wiesel, 1983; Malach et al., 1993; Shmuel et al., 2005; Ts'o et al., 1986). The heterogeneity of intracortical inputs to neurons in different cortical layers raises the possibility that pairs of cells may exhibit correlations whose strength varies in a laminar–dependent manner. Clearly, elucidating whether cortical networks operate in a correlated or decorrelated state is fundamental for understanding how neuronal populations encode information. Understanding the computational and functional connectivity across neuronal circuits requires delicate surgical and recording techniques capable of examining the collective neuronal activity of a population of neurons during a particular task.

5.2 Methods

All experimental procedures were performed in accordance with protocols approved by the US National Institutes of Health Guidelines for the Care and Use of Animals for Experimental Procedures.

5.2.1 Surgical procedure

Two rhesus monkeys, *Macaca mulatta,* were used for the following experiments that included behavioral training (fixation task) and awake-behaving electrophysiology. Monkeys used were five and seven years old and weighed 10 and 17 kg. The second monkey was utilized to confirm changes in visual behavior observed in the first monkey (individual behavior is often variable on a day-by-day basis). Each monkey underwent two surgical procedures. The first surgery was to implant a head-post to eliminate head movement during visual behavior. The second surgery was to implant a recording chamber implant and perform a craniotomy exposing area V1 of the visual cortex. Prior to surgery, monkeys were sedated with an IM dosage of ketamine (10 mg/kg). During the course of the surgical procedure, the monkeys were maintained on a 1-2% isoflurane inhalation. The appropriate level of anesthesia was determined by careful observation of EKG, CO_2, and pO_2 levels.

Once properly sedated, a midline incision was made to expose the skull and overlying tissues. The temporalis muscle was retracted to allow access to the top of the skull and the visual cortex (using stereotaxic coordinates) of one hemisphere. Small holes were drilled in the

skull to implant small titanium screws that will anchor the implant. The titanium head-post has 6 legs extending from the center post, which were mechanically adjusted to trace the shape of the skull. The head-post was surgically implanted to the skull using self-tapping bone screws of 4-6 mm. When the stainless steel recording chamber (approx. 19 mm outer diameter and a 16 mm inner diameter) was implanted, the chamber was firmly cemented to the skull within a ring of screws. The dura was exposed inside the recording chamber using a handed trephine whose outer diameter equals the chamber's inner diameter (i.e. 16 mm). The bone was carefully removed in order to keep dura intact (this reduces the risk of infection as all recordings were performed by using sharp single electrodes or laminar probes that perforate the dura).The chamber was subsequently sealed with antibiotic ointment and closed with a chamber cap. The remaining temporalis muscles were repositioned and sutured against each other. The scalp was closed using a buried suture technique combined with sterile staples and suture glue. Sterile Tobramycin was also added to the cement to produce an acrylic matrix that slowly releases the antibiotic over the life of the implant. The addition of Tobramycin into the cement was used to reduce the incidence of infection. Recovery from anesthesia was assessed by CO_2 and pO_2 values, which are used to determine that adequate respiration has been achieved. The monkey is then removed from the ventilator. The monkey returns to their home cage where they are given water; food is provided the next morning. All surgeries were done in an experimental surgical suite and under the supervision of a veterinarian and surgical assistants.

5.2.2 Electrophysiological recordings

We conducted 34 recording sessions in two monkeys using laminar electrodes. On average, we were able to identify LFPs across all 16 contacts and 6-10 single-units per recording session for each electrode. Each laminar electrode consisted of a linear array of 16 equally spaced contacts positioned to sample from all cortical layers simultaneously (Plextrode® U-Probe, Plexon Inc.; **Figure 5.1**). Analysis of real-time neuronal signals from multiple contacts along the electrode shaft (simultaneous 40 kHz A/D conversion on each channel) were recorded and amplified using a Multichannel Acquisition Processor system (MAP, Plexon Inc.) capable of recording up to 64 channels of spiking and continuous data. Single-unit recordings were amplified, filtered, and verified visually using an oscilloscope and audibly by listening to them through a speaker. The spike waveforms were sorted using Plexon's offline sorter program that implemented waveform clustering based on parameters such as principle components (**Figure 5.2**), action potential width, valley, and peak. When a single-unit was isolated, its receptive field was mapped using a reverse correlation stimulus, while the animal maintained fixation. Recording sites were selected based on the quality of the signal (signal-to-noise ratio, SNR) and their receptive field position. Using custom software scripts in MATLAB and Plexon's Offline Sorter, we analyzed the unit's waveform characteristic (i.e. width and peak), firing rate, and orientation selectivity. Single-units measured during spontaneous activity which abruptly changed their responses across trials (i.e. increases or decreases in firing rate and/or changes in orientation selectivity) were removed and only those units with stable firing rate and orientation selectivity were kept for further analysis.

5.2.3 Electrode drive construction

We utilized the U-Probe in combination with the computer-controlled NAN electrode drive system. We begin by assembling the NAN tower, which includes a 4-tower base (**Figure 5.3** A), the NAN chamber (**Figure 5.3** B), the grid with 1 mm spacing (**Figure 5.3** C), 1-4 screw microdrives (**Figure 5.3** D), 1-4 guide tubes (**Figure 5.3** E, 500 µm diameter and cut to about 5-7 cm), and 1-4 microdrive towers (**Figure 5.3** F). For simplicity, we will describe the procedure for building the NAN system with one electrode drive tower and one U-Probe. To construct the NAN electrode drive assembly, first assembly all the tools and pieces you will need (e.g. guide tubes, guide wire, a complete dremil set, NAN tools, and the U-Probe). Measure the depth of the recording chamber and the guide tubes so when attached to the recording device they are long enough to rest on top of the dura without damaging it. While cutting the guide tubes, ensure that no metal fragments enter inside the tube. Use a stiff wire smaller than the inner diameter of the guide tube to remove any metal fragments. Next, place the NAN grid into the NAN base. Tighten the clamp screw and grid screw. Once the base and grid are secured, identify the recording region of interest and advance the guide tube through the bottom of the NAN grid. Pass the guide tube through the grid until it is about 1-2 mm outside the NAN chamber. Once the guide tube is at the desired position, begin assembling the NAN microdrive tower. On each NAN microdrive tower, there are two clamps: a motor drives the top clamp, while the bottom clamp is fixed in place. Attach the top clamp to the reinforcement tube of the U-Probe. Attach the bottom clamp to the guide tube and apply a small amount of superglue to secure the guide tube in place. This system is both more stable and more precise due to the two clamps that are attached to the reinforcement tube of the U-

Probe. Carefully, align the tip of the U-Probe with the top of the guide tube and pass the U-Probe through the guide tube until you can secure the tower to the NAN base. Adjust the tower position with the thumbscrew so that there is no added tension on the U-Probe or guide tube. Once construction is completed, (**Figure 5.3** G), the U-Probe is connected to Plexon's pre-amplifier via dual headstage Omnetics connectors.

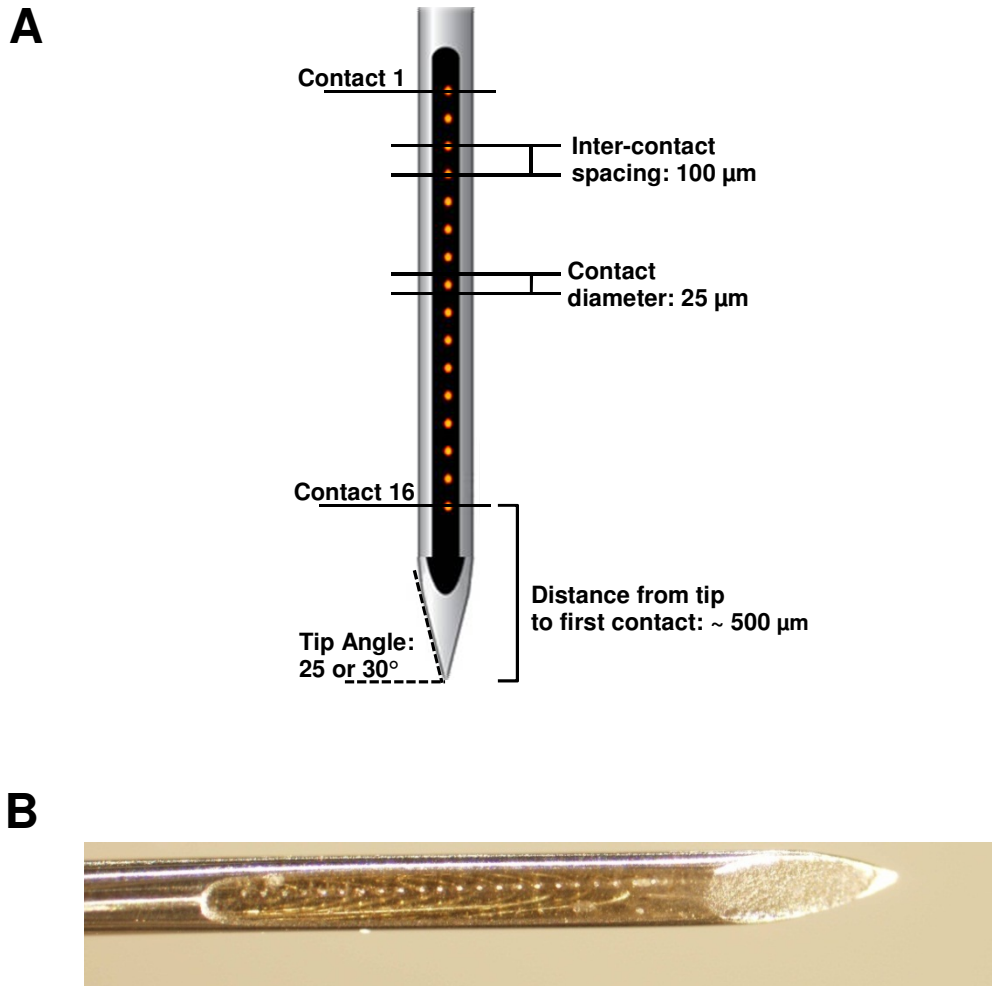

Figure 5.1. Multi-contact laminar electrode
(**A**) Using multi-contact laminar electrodes, we recorded simultaneously spiking activity from isolated individual neurons and LFP signals across cortical layers of V1. Each probe consists of 16 equally spaced (100 µm) electrode contacts spanning a total length of 1.6 mm. Each electrode contact is 25 µm in diameter and is composed of platinum iridium (**B**) Actual U-Probe under high magnification. Notice the contacts in white and the wires running up the shaft (image provided by Plexon, Inc.).

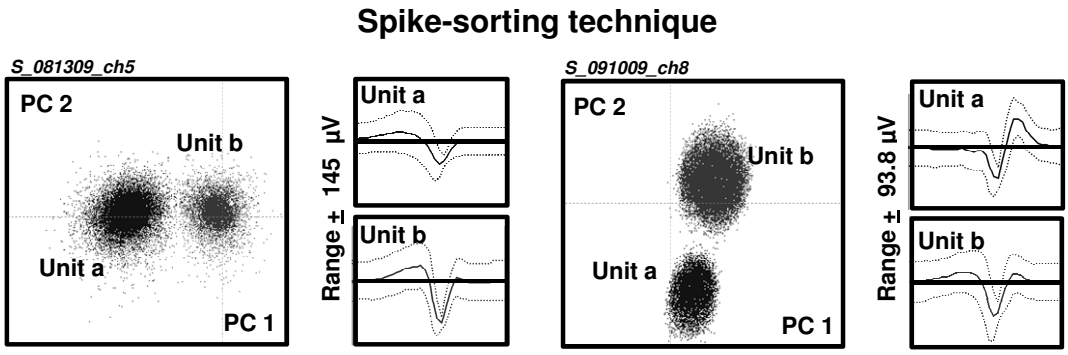

Figure 5.2. Single-unit isolation
Two representative examples of spike waveforms isolated on the same contact. Cluster analysis was performed by using Principal Component Analysis (left panel) and spike waveform characteristics. The average spike waveforms are shown in solid line; standard deviations are shown in dashed line (right panel).

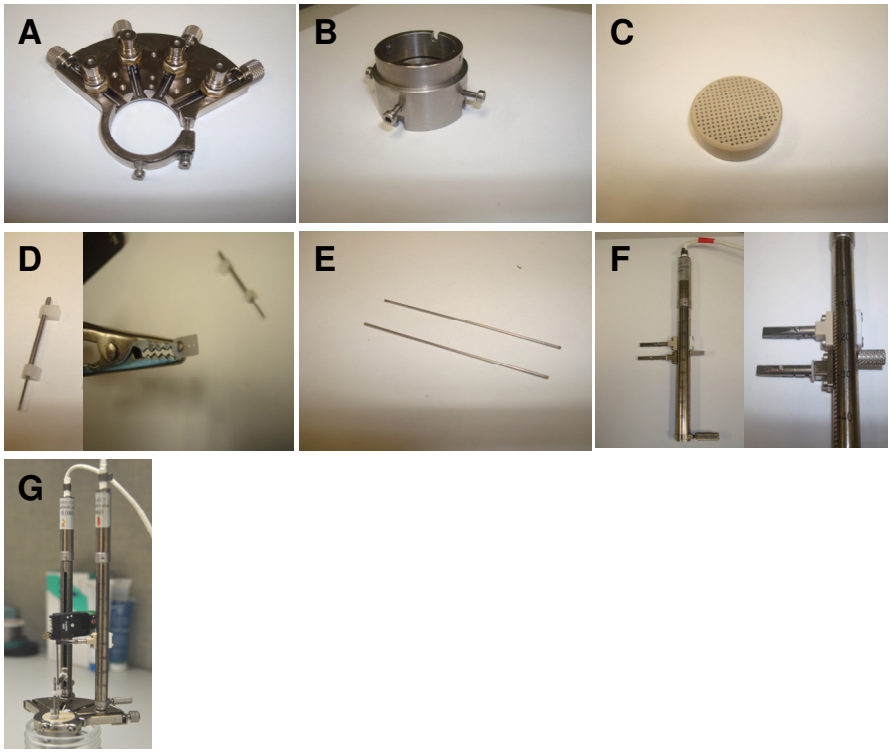

Figure 5.3. NAN grid construction
Each group of electrodes is independently manipulated in the Z direction within a user defined working depth (up to 100 mm) and variable speed range from 0.001 mm /sec to 0.5 mm/sec and a high resolution of 1 micrometer. (**A**) 4-channel base, (**B**) the NAN chamber, (**C**) the grid with 1 mm spacing, (**D**) 1-4 screw microdrives, (**E**) 1-4 guide tubes (500 µm diameter and cut to about 5-7 cm), (**F**) 1-4 microdrive towers and (**G**) the completed NAN system (Hansen et al., 2011).

5.2.4 Local field potential analysis

LFPs were filtered using high-pass and low-pass equirriple finite impulse response (FIR) filters with cutoff frequencies of 0.5 Hz and 100 Hz respectively with 60 dB stopband attenuations. In order to remove line artifacts, we applied a digital notch at 60 Hz (4th order elliptic filter, 0.1 db peak-to-peak ripples, 40 db stopband attenuation; the cross-correlation between the monitor 60 Hz refresh pulses and spikes and LFPs for our entire population failed to find a signature of locking). All filtering was applied by using forward-backward filtering to obtain zero phase shifts. To correct for the time delays induced in the LFP signals by the filters in headstages and pre-amplification boards, we used the software correction FPAlign provided by Plexon (http://www.plexon.com/downloads.html). We discarded all LFPs that had more than 3 points outside the mean ± 4 standard deviations to avoid influence of irregular artifact noise associated with experimental noise or movement artifact. In these experiments, the primary use of the LFPs was for computing the current-source density to identify cortical layers.

5.2.5 Cortical layer identification

For each recording session, we verified the laminar position of the electrode contacts by computing the ERP profile for brief visual stimulation during a passive fixation task. Briefly, monkeys were exposed to a full-field black screen that flashed white for 100 ms, and then returned to black (**Figure 5.4** A). The LFP responses recorded with the laminar probe were processed to obtain ERP traces for each contact (ERPs were recorded for 100 trials; **Figure 5.4** B). Schroeder and colleagues have previously combined laminar recording, microlesion, and

histological reconstruction to validate the effectiveness of the ERP method in the functional identification of cortical layers in V1 (Mitzdorf and Singer, 1979; Schroeder et al., 1991; Schroeder et al., 1998). We computed the current source density (CSD) according to the second spatial derivative of the LFP time-series across equally-spaced laminar contacts and utilizing the iCSD toolbox for MATLAB (http://software.incf.org/software/csdplotter/home; Mitzdorf, 1985; Pettersen et al., 2006) allowed us to accurately identify the polarity inversion accompanied by the sink-source configuration at the base of layer 4 (the sink is inside layer 4; **Figure 5.5**). Using homemade MATLAB programs, we analyzed the laminar CSD profile to verify the presence of a primary sink in the granular layer in each of the 34 recording sessions. This was accomplished by locating the sink driven negative polarity in the CSD plot, and then computing the center-of-mass of the granular sink. We obtained a single coordinate from this analysis consisting of the contact number and the time (in ms) when the sink was largest (centroid). The contact with the sink centroid served as the granular layer reference at 0 μm. We then analyzed all the contacts above and below the reference and grouped them (based on their sink/source waveform characteristics) into one of three possible layers: supragranular, granular, and infragranular.

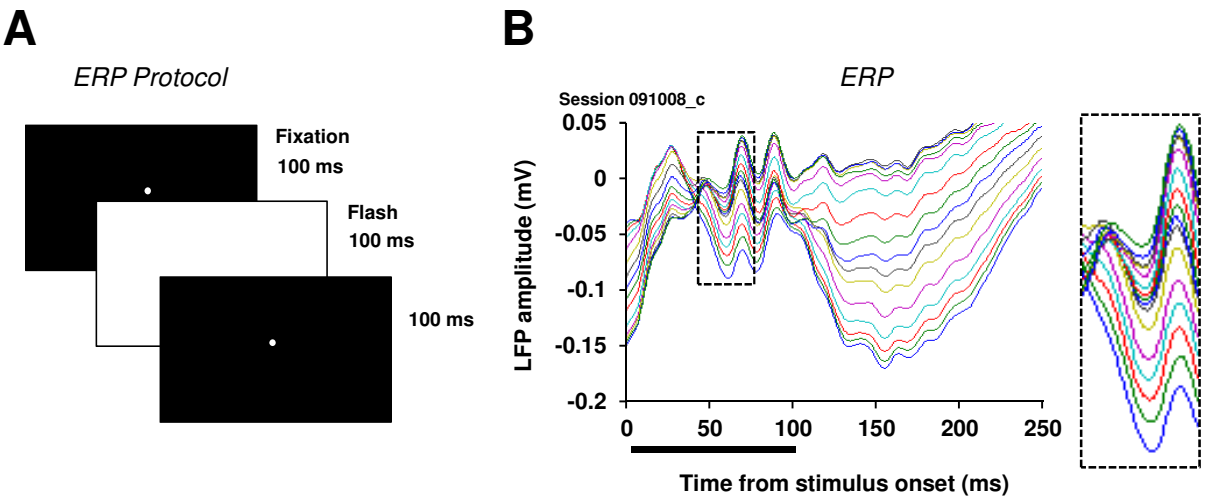

Figure 5.4. Evoked-response potentials
(**A**) To identify cortical layers, we measured the evoked response potential (ERP) during a passive fixation task while monkeys were exposed to a full-field black screen that flashed white (~1 Hz) for 100 ms, and then returned to black. (**B**) The LFP responses recorded with the laminar probe were processed to obtain ERP traces for each contact. This allowed us to detect an initial negativity in the LFP amplitude at ~ 50 ms followed by an inversion to positive complex stretching ~ 90-100 ms from stimulus onset.

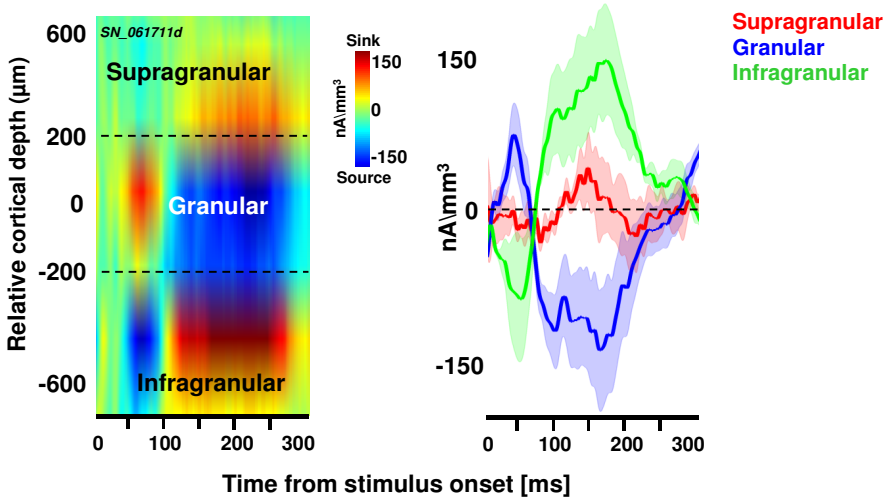

Figure 5.5. Layer-identification
Current-source density (CSD) analysis is used to identify the polarity inversion accompanied by the sink-source configuration at the base of the granular layer. The current sink (red region) represents the granular layer and spans ~ 400 µm. The CSD traces (right) represent the average of those contacts assigned to a given layer. This allowed us to determine the precise timing of the initial sink (in this example ~ 50 ms). CSD trace envelopes represent standard deviation (Mitzdorf, 1985; Pettersen et al., 2006).

5.2.6 Experimental paradigm

Two rhesus monkeys were trained to fixate a small spot (0.1°) presented on a video monitor placed at a distance of 57 cm from each monkey's eye. Stimuli were generated with Psychophysics Toolbox using MATLAB and presented on a 19'' CRT color video monitor (Dell, 60 Hz refresh rate). Monkeys performed a passive fixation task in which static, 5° circular sine-wave gratings with a spatial frequency of 1.4 cycles per deg and a 50% contrast level were presented binocularly (**Figure 5.6**). Monkeys triggered the beginning of each trial by holding a bar, and after 300 ms of fixation, a stimulus of random orientation (8 equally spaced orientations spanning 0-180°; random spatial phase for each orientation) was flashed in the center of the neurons' receptive fields. Each orientation was randomly presented 50 times. Stimulus presentation and eye tracking were recorded and synchronized with neuronal data using the ECM (Experiment Control Module) programmable device (FHC Inc.). If monkeys maintained fixation throughout the entire trial they were rewarded with a 3 drops of juice.

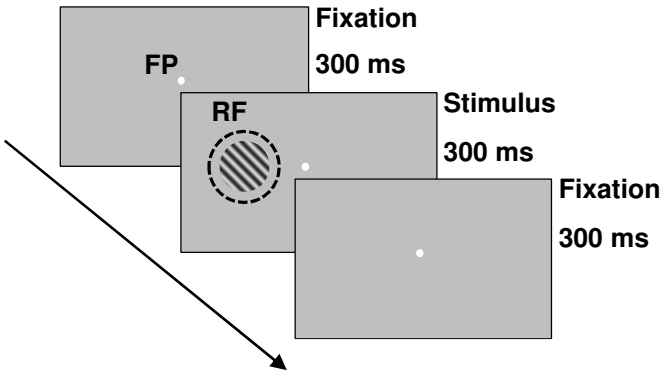

Figure 5.6. Schematic representation of the stimulus sequence
While monkeys fixated a white dot at the center of a computer screen, oriented grating stimuli were flashed for 300 ms in the center of the neurons' receptive field. Stimulus orientation ranged from 0-180° in 22.5° steps and was randomly varied across trials (n = 400). After the second fixation, monkeys were rewarded if they maintained fixation throughout the whole trial.

5.2.7 Noise correlations

We measured the layer-specific noise correlations between pairs of neurons for each of the 8 orientations (spanning 0-180°; random spatial phase for each orientation). The Pearson spike count correlation coefficient between two cells r_{sc} is defined as:

$$r_{sc} = \frac{\sum_{i=1}^{N} (r_1^i - \overline{r_1}) \cdot (r_2^i - \overline{r_2})}{\sigma_1 \cdot \sigma_2} \tag{5.1}$$

where N is the number of trials, r_j^i is the firing rate of cell j in trial i averaged over the entire range of oriented stimuli, $\overline{r_j}$ represents the mean response of neuron j, and σ is standard deviation of the responses (Kohn and Smith, 2005). For each cell pair, we computed mean firing rate as well as the geometric mean of the cells' firing rates defined as:

$$\sqrt{(\overline{FR}_1 \cdot \overline{FR}_2)} \tag{5.2}$$

Importantly, we found no laminar dependence on the mean firing rate of the cell pairs (population result: one-way ANOVA, F (2, 324) = 0.36, $P > 0.69$). We also calculated the correlation between r_{sc} and geometric mean and found no significant relationship (SG: r = -0.07; G: r = -0.01; IG: r = -0.03, Pearson correlation). In order to remove slow-wave fluctuations in responses across trials, all the neurons used in the correlation analysis underwent a detrending procedure (Kohn and Smith, 2005) in which the spike counts for each trial were high-pass filtered using a linear-phase Finite Impulse Response (FIR) filter having a 0.1 normalized cut-off frequency.

5.2.8 Eye movement analysis

Eye position was continuously monitored using an eye tracker system (EyeLink II, SR Research Ltd., Osgoode, ON, Canada) with a binocular 1 kHz sampling rate. Eye position was calibrated before each experiment using a 5-point calibration procedure in which the animal was required to fixate on each one of 5 points (1 in the center, 2 in the vertical, and 2 in the horizontal axes) in steps of 4°, 8°, and 12° from the central fixation spot. The eye-tracker gains were adjusted such as to be linear for the horizontal and vertical eye deflections. The fixation pattern was analyzed to rule out any systematic bias and inconsistency during fixation. Microsaccades were analyzed every 10 ms by using a vector velocity threshold of 10°/s (this corresponds to a 0.1° eye movement between consecutive 10 ms intervals). It is possible that due to common input microsaccades could partially contaminate our laminar correlation results. To control for eye movements we first explored trial-by-trial changes in amplitude according the formula:

$$\sqrt{(x_1 - x_2)^2 + (y_1 - y_2)^2} \tag{5.3}$$

where x and y represent two locations of the eye on the computer screen. After obtaining the microsaccade amplitude and velocity for each trial, we removed those trials in the 1st and 2nd quartile.

5.3 Results

5.3.1 Identification of cortical layers

We examined the laminar dependence of trial-to-trial fluctuations in responses, or correlated variability, and measured spike count (noise) correlations using multi-contact laminar electrodes (**Figure 5.1**). This technique allowed us to record the responses of individual cells and local field potentials (LFPs) simultaneously across all layers of V1 from two macaques. To identify cortical layers, we measured the evoked response potentials (ERPs) of LFPs across equally spaced contacts (inter-contact distance = 100 um) in response to a full-field flashed stimulus. We then performed current-source density (CSD) analysis (**Figure 5.5**) of the LFP time-series to identify the polarity inversion accompanied by the sink-source configuration at the base of layer 4; the sink is inside layer 4, subsequently referred to as the granular layer (Mitzdorf and Singer, 1979; Schroeder et al., 1991; Schroeder et al., 1998). Current-source density analysis is useful because it provides an index of the location, direction, and density of transmembrane current flow, allowing us to accurately position electrodes to record from all layers in a single penetration. The CSD traces shown to the right of **Figure 5.5** represent the average of those contacts assigned to a given layer. In this example, the granular layer undergoes a clear increase in CSD amplitude at ~ 50 ms. We defined the granular sink, as a reference to assign electrode contacts above and below the granular layer to supragranular and infragranular layers, respectively (the contact with the largest sink center-of-mass served as the granular layer reference at 0 μm). Several controls were performed to test the reliability of our measure in identifying cortical layers: (i) we observed that micron advancement of the laminar

electrode was highly correlated with a corresponding shift in the center-of-mass of the granular sink (r = 0.89, $P < 0.001$, Pearson correlation), (ii) shuffling electrode contacts as a function of cortical depth destroyed the laminar CSD profile, and (iii) vertical penetrations across all layers revealed a columnar organization based on the orientation preference of spike responses (**Figure 5.7**).

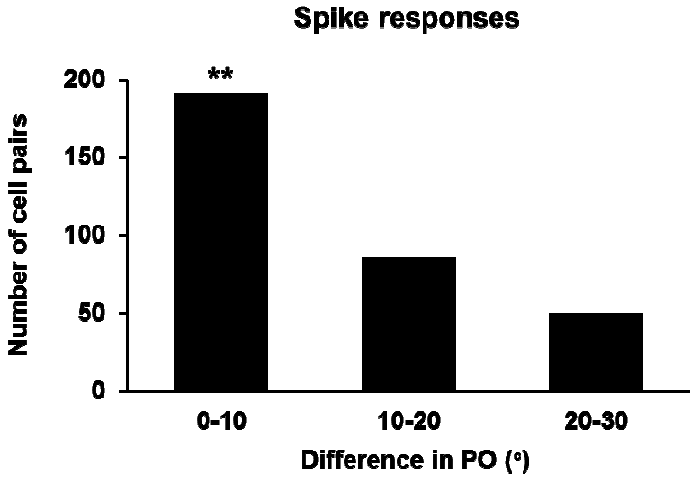

Figure 5.7. Difference in preferred orientation (*PO*) across cortical layers
For each single-unit pair we computed the difference in preferred orientation (determined using the vector averaging method between the cells in a pair. For the majority of pairs, the orientation preference difference was within 10°. This indicates that the advancement of the laminar electrode remained isolated to a single cortical column in V1 (** $P < 0.01$, Wilcoxon signed-rank test).

5.3.2 Layer-dependent changes in correlated variability

Cells recorded on laminar probes had highly overlapping receptive fields and similar preferred orientations (**Figure 5.7**; the difference in preferred orientation for over 58% of the pairs of neurons was within 10°, $P < 0.01$, Wilcoxon signed-rank test). Single-unit isolation on the laminar electrode was performed manually, and distinct clusters were identified based on spike waveform properties such as the weight of the first and second principle components (**Figure**

5.2), action potential width, valley, and peak. Two examples of average waveforms and their standard deviation for two units that were isolated on one contact are shown in **Figure 5.2**. We collected data from 34 sessions in two monkeys (W – 27; P – 7) and were able to isolate 199 single-units (W – SG: 54, G: 57, IG: 47; P – SG: 12, G: 11, IG: 18) that exhibited significant response modulation by stimulus orientation (responses were measured throughout stimulus presentation). We measured noise correlations for our population of 327 pairs of recording sites assigned to different cortical layers (W – SG: 91, G: 98, IG: 74; P – SG: 22, G: 16, IG: 26). Since our laminar probes were able to record single-units that belonged to the same cortical column within a vertical penetration, we initially expected strong spike count correlations between nearby cells in each cortical layer.

Figure 5.8 shows six examples of spike count correlations for a pair of cells recorded simultaneously in a given layer. Surprisingly, whereas the supragranular (**Figure 5.8** A, red) and infragranular (**Figure 5.8** B, blue) layer pairs showed high noise correlations, the pairs in the granular layer (**Figure 5.8** C, green) showed almost no correlated variability. These results were confirmed across our population of 327 pairs (**Figure 5.9**). We found that correlated variability in the supragranular layers was 0.29 ± 0.03 (mean ± SEM) with ~ 84.0% of all pairs significantly different from zero ($\alpha = 0.05$, two-sample t test; positive 78.8%, negative 5.3%), similar to the values previously reported in V1 (Bair et al., 2001; Kohn and Smith, 2005; de la Rocha et al., 2007; Gutnisky and Dragoi, 2008; Smith and Kohn, 2008; Nauhaus et al., 2009).

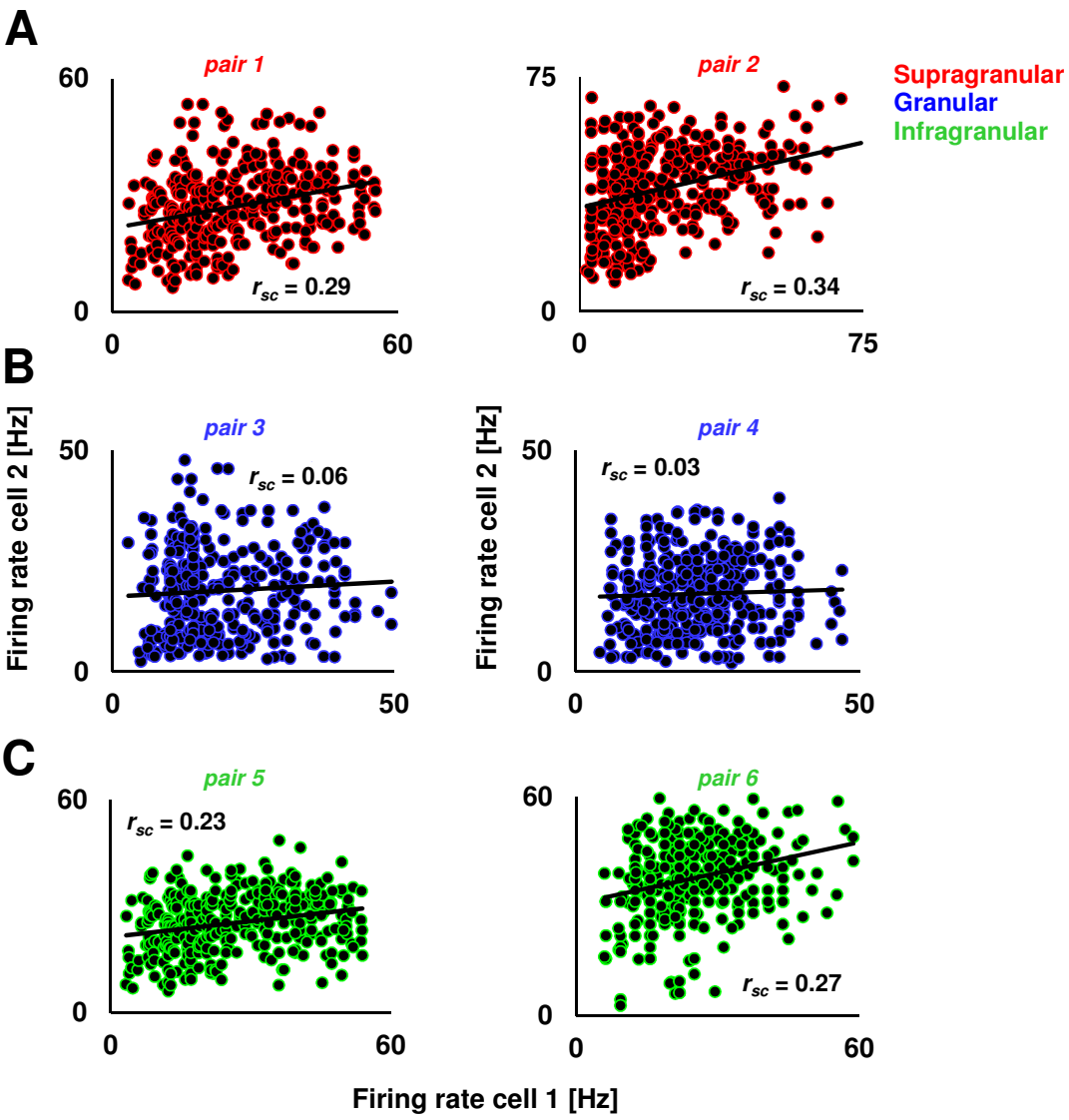

Figure 5.8. Layer dependent changes in spike count correlations
Each scatter plot represents the trial-by-trial responses of a pair of cells recorded simultaneously either in the supragranular (**A**), granular (**B**), or infragranular (**C**) layer. Each dot represents the firing rates of both cells in a given trial. The trend line represents the linear regression fit for each pair of cells; r_{sc} represents the Pearson correlation coefficient.

However, in the granular layer, correlation values were exceedingly low (0.03 ± 0.01) with only ~ 16.7% significant pairs (positive 7.02%, negative, 9.65%) consistent with recent reports in V1 and primary somatosensory cortex (Ecker et al., 2010; Renart et al., 2010). In the infragranular layers, the value of correlated variability was high again and comparable to that

found in supragranular layers (0.24 ± 0.03) with ~ 81% of significant pairs (positive 76%, negative 5%). **Figure 5.9** summarizes the results obtained in each monkey – not surprisingly, the laminar dependence of noise correlations was consistent across animals (W: SG: 0.31 ± 0.03, G: 0.03 ± 0.01, IG: 0.26 ± 0.04; P: SG: 0.22 ± 0.04, G: 0.04 ± 0.02, IG: 0.19 ± 0.02). We also observed a significant difference in mean correlations across layers (W: one-way ANOVA, $F(2, 260) = 27.7$, $P < 10^{-11}$; P: one-way ANOVA, $F(2, 61) = 8.66$, $P < 0.0005$).

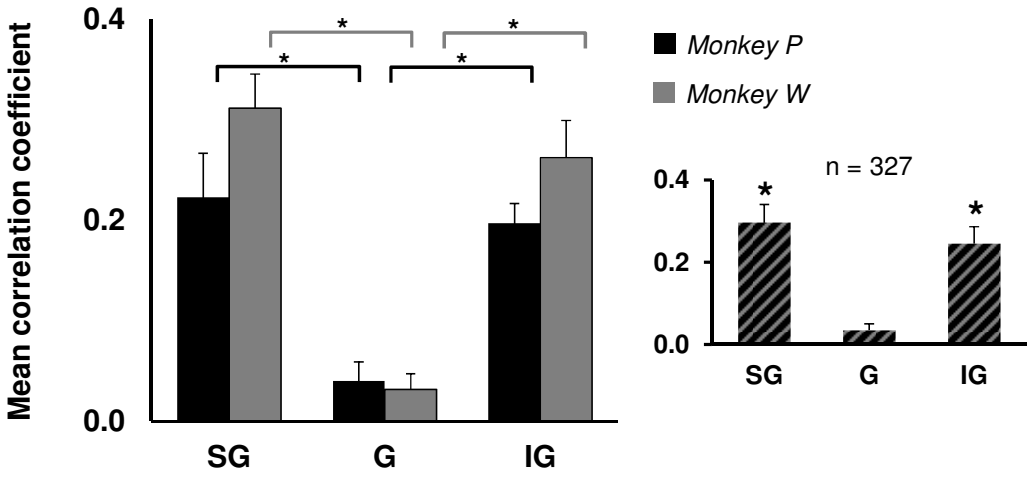

Figure 5.9. Spike count correlation analysis for the population of cell pairs
Laminar-dependent noise correlations for each of the monkeys used in the experiments (monkey W: SG – 0.31 ± 0.03, G – 0.03 ± 0.01, IG – 0.26 ± 0.04 (black bars); monkey P: SG – 0.22 ± 0.04, G – 0.04 ± 0.02, IG – 0.19 ± 0.02 (grey bars)). Inset striped bars: Population noise correlations for our 327 cell pairs located across cortical layers – SG layers: 0.29 ± 0.03; G layers: 0.03 ± 0.01; IG layers: 0.24 ± 0.04.

In principle, it is possible that the laminar differences in noise correlations will have been due to differences in firing rates of the pairs identified across cortical layers. Indeed, some studies (de la Rocha et al., 2007) have suggested that spike count correlations are positively correlated with the mean responses of the cells in a pair (but see Bair et al., 2001; Kohn and Smith, 2005; Gutnisky and Dragoi, 2008; Smith and Kohn, 2008; Nauhaus et al., 2009).

However, we found that the mean firing rates of the cells in our population did not differ across cortical layers for either animal (**Figure 5.10**; one-way ANOVA, F (2, 324) = 0.36, $P > 0.69$) and that, within each layer, noise correlations did not depend on the geometric mean firing rates of the cells in a pair (SG: r = -0.07; G: r = -0.01; IG: r = -0.03, Pearson correlation, $P > 0.1$).

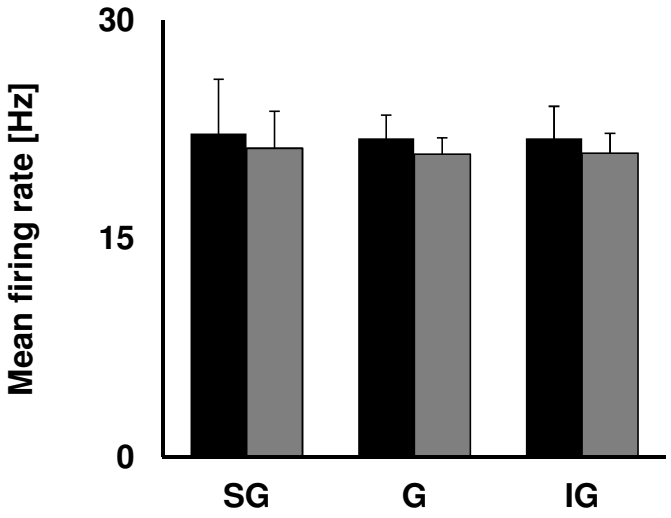

Figure 5.10. Firing rate analysis
Mean firing rates during the stimulus period (300 ms spike-count window) do not vary by cortical layer. Each bar represents the average firing rate of the cells recorded in the corresponding cortical layer for the two different monkeys (monkey W: black bars; monkey P: grey bars).

Previous studies have shown that noise correlations depend on the precise time scale at which spike rates are counted (Kohn and Smith, 2005; Yu and Ferster, 2010). We addressed this issue by recalculating spike count correlations for varying spike-count windows during stimulus presentation. **Figure 5.11** summarizes our results: although the mean correlation coefficient increased in all layers as the time window approached the stimulus duration, correlations values in the granular layer continued to remain significantly lower than correlations in the supragranular and infragranular layers (one-way ANOVA, $P < 10^{-11}$). This

result indicates that the laminar differences in noise correlations are pronounced even when short spike count windows are used to measure correlations.

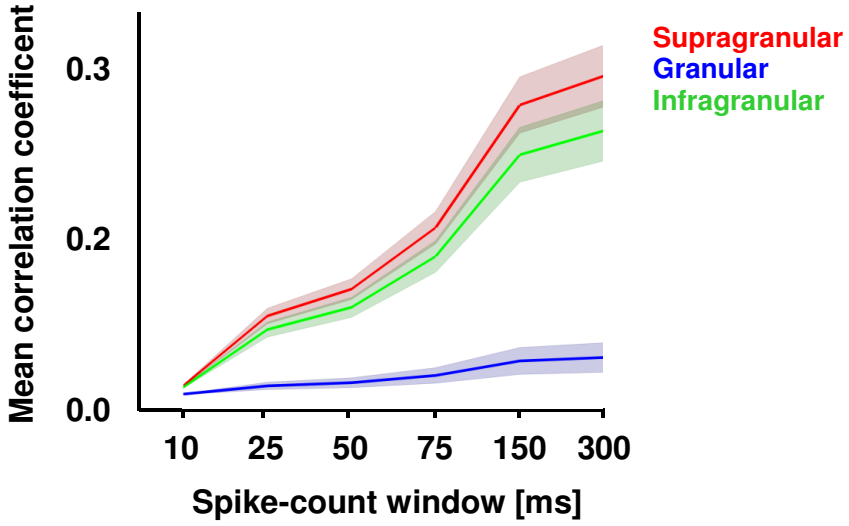

Figure 5.11. Timescale of laminar noise correlations
Using a range of spike-count windows, we observed a steady increase in the mean correlation coefficient in all layers. Shaded envelopes represent the SEM.

Figure 5.12 shows the laminar distribution of correlations – while correlation coefficients in supragranular and infragranular layers are skewed toward high values, those in the granular layer have much lower values. The average correlation coefficient for all the pairs in our population (irrespective of cortical layer) is r_{sc} = 0.18. In **Figure 5.13**, we calculated noise correlations for neuron pairs originating from different layers and found that correlations between neurons in the granular layer and those in other cortical layers (SG-G: 0.10 ± 0.01 and IG-G: 0.09 ± 0.02) were significantly weaker than correlations between neurons in supragranular and infragranular layers (SG-IG: 0.19 ± 0.02; one-way ANOVA, F (2, 155) = 14.73, P = 1.38 10^{-6}; post-hoc multi-comparison, Tukey's Least Significant Difference). Consistent with our hypothesis, the reason for this result is the source of common input to

cortical neurons in different cortical layers. Thus, whereas SG and IG neurons receive common inputs through long-range horizontal axons, the fact that the spatial scale of intracortical connections differs between supragranular/infragranular and granular layers ensures that noise correlations between SG-G and IG-G neurons are lower than those between SG-IG neurons.

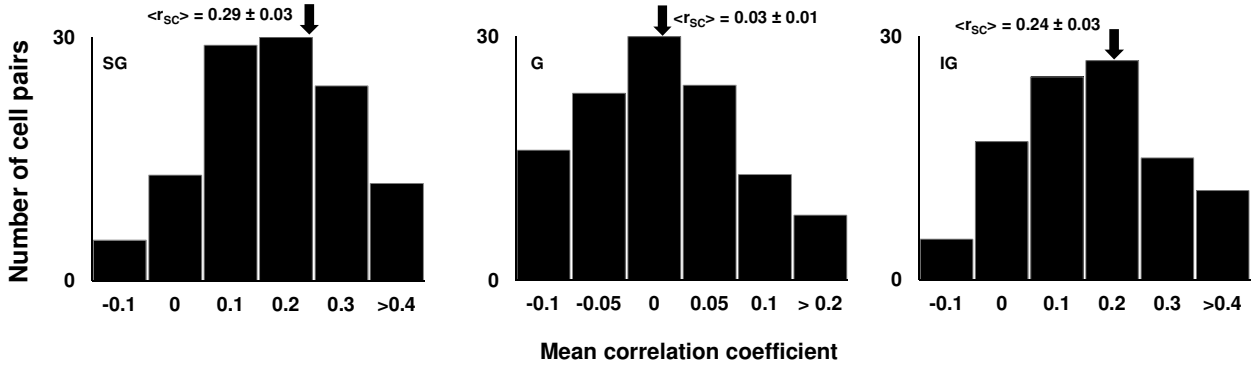

Figure 5.12. Distribution of r_{sc} values for each cortical layer
Distribution of r_{sc} values for each cortical layer. While correlation coefficients in infragranular and supragranular layers are skewed toward high values, those in the granular layer have much lower values. Left to right: SG, G, and IG number of cell pairs as a function of the mean correlation coefficient.

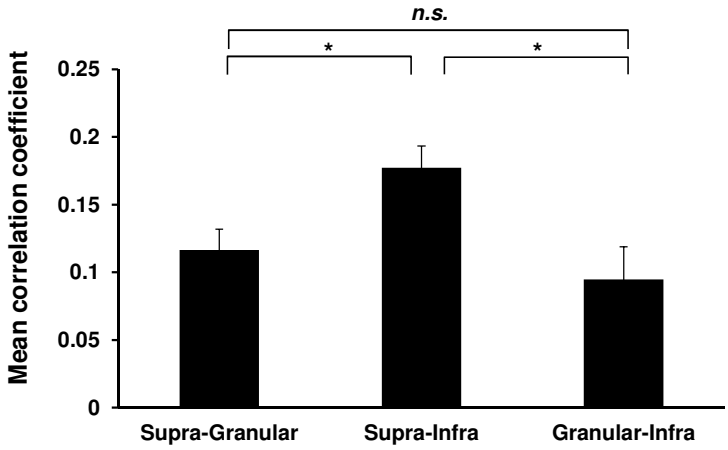

Figure 5.13. Correlations between cells in different layers
Correlations between neurons in the granular layer and those in other cortical layers (SG-G: 0.10 ± 0.01 and IG-G: 0.09 ± 0.02) were significantly weaker than correlations between neurons in supragranular and infragranular layers (SG-IG: 0.19 ± 0.02; one-way ANOVA, F (2, 155) = 14.73, P = 1.38 10^{-6}; post-hoc multi-comparison, Tukey's Least Significant Difference).

Next, we investigated the effect of distance between laminar contacts on correlated variability (we were able to record from pairs of cells up to 400 µm away). Therefore, we computed the number of cell pairs as a function of electrode contact distance across layers and found that ~77% of cell pairs were within 200 µm (**Figure 5.14** A). In addition, the correlation coefficient did not depend on contact distance irrespective of cortical layer (**Figure 5.14** B; $P >$ 0.35; Wilcoxon rank sum test).

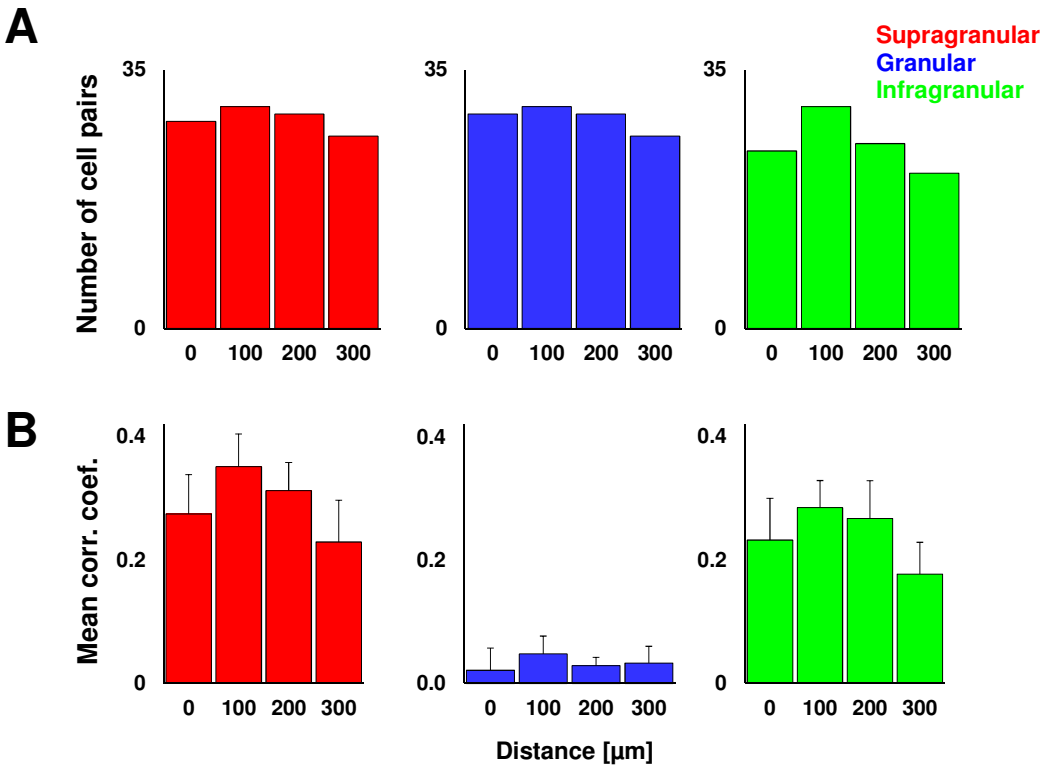

Figure 5.14. Laminar distribution and the effect of contact distance
(**A**) We computed the percentage of pairs corresponding to each pair distance across layers and observed that ~77% of all the cell pairs were within 200 µm. (**B**) Computing the distance between cell pairs we observed that r_{sc} does not depend on contact distance irrespective of cortical layer.

5.3.3 The effects of eye movements on noise correlations

One possible confound in our measurement of noise correlations is eye movements during fixation (microsaccades). Indeed, minute eye movements could modulate the firing rates of all the neurons recorded simultaneously to possibly increase correlated variability. Although the eye movement modulation of firing rates has not been demonstrated to depend on cortical layer, one cannot totally exclude the possibility that this modulation could be larger in supra and infragranular layers of V1 to contribute to an increase in noise correlations. To control for this possibility, we removed from the analysis those trials with large amplitude and velocity eye movements (the 1^{st} and 2^{nd} quartiles), and recalculated spike count correlations for the remaining trials. We found a significant overlap, ~87.4% of trials, between the largest eye movement amplitude and velocity trials when the 1^{st} and the 2^{nd} quartile eye movements were compared. However, while this analysis significantly reduced the number of trials used in our calculation of noise correlations, our main result remained unchanged – removing trials with high amplitude and velocity eye movements reduces noise correlations but preserves their laminar dependence (**Figure 5.15**; average of all 327 pairs; 1^{st} quartile: one-way ANOVA, $F(2, 324) = 30.75$, $P = 5.93\ 10\text{-}13$; 1^{st} & 2^{nd} quartile: one-way ANOVA, $F(2, 324) = 17.27$, $P = 7.44\ 10\text{-}8$; post-hoc multi-comparison, Tukey's Least Significant Difference).

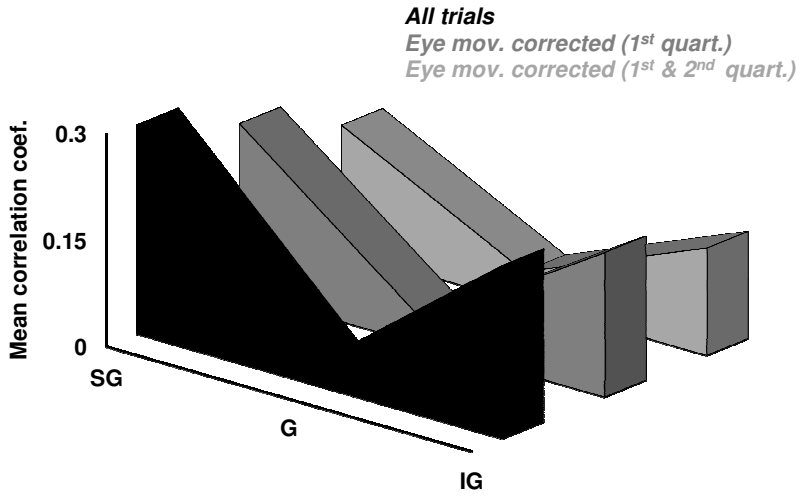

Figure 5.15. The effects of eye movements on laminar-specific correlations
We identified the trial–by–trial changes in microsaccade amplitude and velocity and removed from the calculation of noise correlations the 1st and 1st and 2nd quartile trials. The 'all trials' (black) region represents the layer-specific mean noise correlation from our main experiment (cf. **Figure 3** A). The gray areas represents the layer–specific mean noise correlation coefficient after removing the 1st quartile microsaccade amplitude and velocity trials (gray; one–way ANOVA, F (2, 324) = 30.75, $P = 5.93\ 10^{-13}$), and the layer–specific mean noise correlation coefficient after removing the 1st and 2nd quartiles for microsaccade amplitude and velocity trials (light gray; one–way ANOVA, F (2, 324) = 17.27, $P = 7.44\ 10^{-8}$; post–hoc multi–comparison, Tukey's Least Significant Difference).

5.3.4 Possible network mechanisms

The network mechanism behind our noise correlation results described in chapter 1 (**Figure 4.3**) predict that a broad tuning of intracortical inputs, as in the granular layer, would decorrelate responses of nearby neurons, whereas a sharper tuning of intracortical inputs due to long-range horizontal connections, as in the supragranular and infragranular layers, would cause strong response correlations (**Figure 5.16**). This idea critically rests on experimental evidence that the spatial spread of connections in the granular layers is small, whereas in supragranular and infragranular layers neurons receive recurrent input over larger distances (up

to several mm) via horizontal and feedback circuitry (Gilbert and Wiesel, 1983; Ts'o et al., 1986; Malach et al., 1993; Bosking et al., 1997; Angelucci et al., 2002; Shmuel et al., 2005).

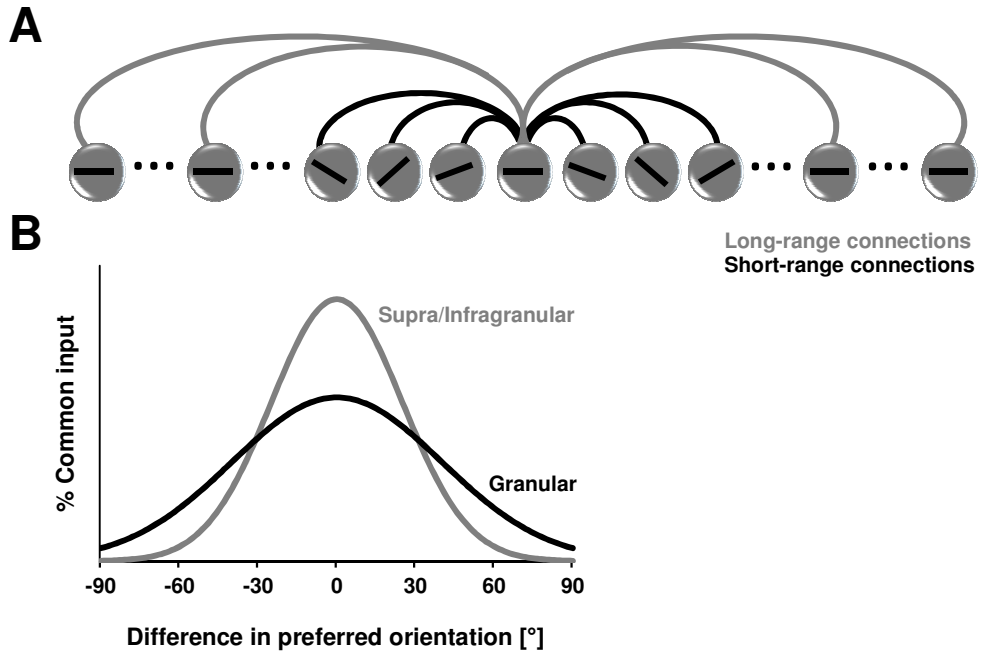

Figure 5.16. Cartoon illustration of short and long-range intracortical connections
(**A**) The granular layer is mainly characterized by short-range connections (black lines), and the orientation distribution of intracortical inputs is relatively broad. In contrast, the supragranular and infragranular layers are characterized by both short-range and long-range horizontal connections (gray lines). Because long-range horizontal inputs are predominantly iso-oriented, the orientation distribution of intracortical inputs is narrow. (**B**) The percentage of common input as a function of the difference in preferred orientation for a pair of neurons is represented according to the specific layer properties. Since long-range horizontal connections preferentially target iso-oriented cells, supragranular and infragranular layer cells (gray line) would receive a larger fraction of iso-oriented common inputs than neurons in the granular layer (black line).

We sought to determine if similar patterns of connectivity exist outside V1. We addressed this issue by exploring previous studies that examined the specificity of local intracortical connections in extrastriate cortex as well as other early sensory cortical areas (i.e. primary auditory cortex (A1) and primary somatosensory cortex (S1)). In area V2 of macaque

visual cortex, biocytin-labeled pyramidal neurons of layers 2/3 and layer 5 have been shown to provide laterally spreading axon projections that terminated in discrete patches (250-300 microns diameter), primarily in layers 2/3, and distributed in an elongated field orthogonal to the stripe compartments (Levitt et al., 1994). There were prominent patchy connections within, as well as between, individual compartments, perhaps reflecting functional substructures within stripes. In area V4 of macaque visual cortex, pyramidal neurons of layers 2/3 make extensive lateral projections with oval or circular patches of terminals in layers 1-3 (Yoshioka et al., 1992). Additionally, any small patch of tissue (approximately 250 microns wide) injected in the superficial layers connects reciprocally to patches scattered up to 3 mm around the injection. In contrast, small injections in layer 4 did not produce similar patch-like lattice connections, while injections in layer 5 gave relatively weak rising contributions compared to the superficial layer patch system. These findings indicate a functional repeat distance of 450-600 μm in area V4 with a patchy, discontinuous layout.

In addition to visual cortex, other sensory cortical areas are characterized by similar intracortical connectivity patterns. For instance, in cat primary auditory cortex (A1), it has been reported using retrograde anatomic tracing and topographic physiologic mapping of acoustic responses that layers 2/3 are characterized by long-range (> 1.5 mm) connections between patches with similar acoustic properties, whereas connections in layer 4 are mostly local (Read et al., 2001). Similarly, layer 3 of cat primary somatosensory cortex (S1) is characterized by long-range horizontal axons that can travel for up to 2.5 mm (Schwark and Jones, 1989), whereas layer 4 connections are mostly local. Importantly, long-range horizontal connections in cat S1 are patchy and connect neurons tuned to the same whisker.

5.3.5 The effects of stimulus size on noise correlations

To test this mechanism relying on the layer-specific spread of horizontal connections, we performed additional experiments in which we measured the laminar-dependent distribution of noise correlations as a function of stimulus size (large gratings, 5 deg, and small gratings, 1.5 deg). Our hypothesis is that a large stimulus will strongly activate the iso-orientation columns outside the receptive fields of nearby neurons targeted by our laminar probe, whereas a small stimulus will only weakly activate the iso-orientation columns outside the receptive fields of nearby cells. That is, a small stimulus will make supragranular and infragranular layers 'behave' as the granular layer, and thus noise correlations will be relatively small and not exhibit layer dependency. In contrast, but in agreement with our hypothesized mechanism, a large stimulus (identical to the stimulus used in the experiments in **Figure 5.6**) will produce large noise correlations in the supragranular and infragranular layers, and much smaller correlations in the granular layer.

We performed 5 additional recording sessions and isolated 41 single-units (SG – 13, G – 13, IG – 15) that exhibited significant response modulation by stimulus orientation. We measured noise correlations for our population of 72 pairs of recording sites assigned to different cortical layers as follows: SG – 24, G – 24, IG – 24. In each session, we randomly varied the orientation and size of the gratings (small and large). For each session we presented 400 trial, (200 small and 200 large) with each orientation (0-180° in steps of 22.5°) presented 50 times. For our large grating stimulus (**Figure 5.17**), we found that correlated variability in the supragranular layer was 0.20 ± 0.02 (mean ± SEM). However, in the granular layer, correlation values were much lower 0.07 ± 0.04, whereas in infragranular layers, the value of

correlated variability was high again and comparable to that found in supragranular layers (0.19 ± 0.04). There was a significant difference in layer mean correlations (one-way ANOVA, F (2, 69) = 6.77, P = 0.0021) between SG-G and IG-G, but not between SG-IG layers (post-hoc multi-comparison, Tukey's Least Significant Difference). Interestingly, for small gratings we observed no layer specific change in correlations (SG: 0.07 ± 0.04; G: 0.07 ± 0.04; IG: 0.07 ± 0.03). Not surprisingly, there was no significant correlation difference across layers (one-way ANOVA, F (2, 69) = 0.01, P = 0.9945). Importantly, we did observe significant differences between conditions (large vs. small gratings) within supragranular (P = 0.006, Wilcoxon signed-rank test) and infragranular layers (P = 0.0223), but not the granular layer (P = 0.9030). The data supports our hypothesis that during the presentation of the small stimulus excites only short range connections and as a result difference in correlation values across cortical layer were not observed. Conversely, we report that in the same pairs of responsive neurons we are able to recover our laminar dependent result by presenting a large stimulus capable of invoking long-range connections. These results provide experimental support for our proposed mechanism of laminar dependency of noise correlations relying on the layer-dependent spatial spread of intracortical connections.

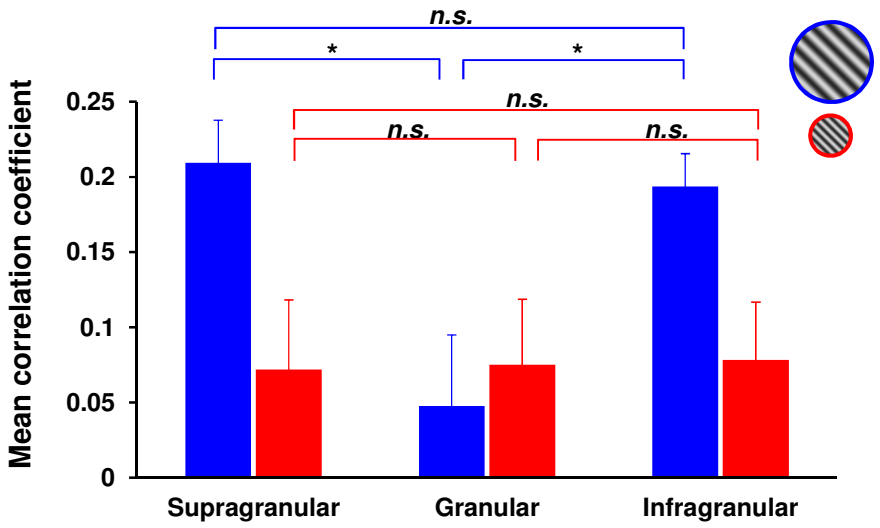

Figure 5.17. Layer-dependent correlations vary with stimulus size
Layer-dependent correlations vary with stimulus size. Within each session we randomly varied the size of the grating, i.e., large grating – 5 deg (blue), or small grating – 1.5 deg (red). We observed a significant difference in layer mean correlations (one-way ANOVA, F (2, 69) = 6.77, P = 0.0021) between SG-G and IG-G, but not between SG-IG layers (post-hoc multi-comparison, Tukey's Least Significant Difference). In the small grating condition, we observed no layer specific change in noise correlations.

Nonetheless, while a functional link between noise correlations and the laminar-dependent spread of recurrent connections could be established, it may be possible that other mechanisms could also be invoked to explain our results. For instance, cortico-cortical feedback projections from higher cortical areas (Felleman and Van Essen, 1991; Salin and Bullier, 1995) could, at least in principle, explain the effects described here. However, since top-down feedback, projections exclusively target superficial layers and avoid granular and infragranular layers (Dong et al., 2004; Angelucci and Bressloff, 2006), they might explain only the difference in correlations between the supragranular and granular layers, not the emergence of strong correlations in the deep layers of V1. Another possible explanation for the low correlated variability in the granular layers is the fact that the LGN inputs targeting

granular layer cells may be only weakly correlated. In principle, this mechanism may appear unlikely to explain fully our data as it ignores the fact that neurons in the granular layer receive most of their inputs from intracortical sources, including correlated inputs from infragranular and supragranular layer neurons. However, this argument is weakened somewhat by the fact that thalamocortical inputs are stronger than intracortical inputs. In sum, while the laminar dependence of the spatial spread of intracortical inputs appears to be consistent with layer-dependent noise correlations, future experimental and theoretical work is required to precisely determine the mechanism underlying changes in neuronal correlations and their relationship with network performance.

5.3.6 Noise correlations influence network accuracy

In collaboration with Mircea Chelaru, we further tested our hypothesis that noise correlations vary across cortical layers due to the laminar spread of intracortical connections. Specifically, he examined whether noise correlations in different cortical layers influence the information encoded in population activity. To this end, he tuned the parameters of a model previously used (Chelaru and Dragoi, 2008; the model was used to examine the accuracy of population coding in V1 networks) such as to reproduce the mean experimental correlation values observed in the supragranular, granular, and infragranular layers (cf. **Figure 5.9**). Subsequently, he examined the contribution of response correlations to network coding accuracy in each layer. A measure of the accuracy of population coding is the network discrimination threshold (the inverse of this threshold is proportional to the square root of Fisher information, which represents the upper limit of the accuracy with which any decoding mechanism can extract information about a

stimulus parameter), which he computed by using a linear decoder of stimulus orientation. The decoder was trained to maximize the Fisher information of population responses (Abbott and Dayan, 1999; Series et al., 2004) and, as a result, minimize the discrimination threshold between two nearby stimulus orientations. As expected, he found that the orientation discrimination threshold is lowest when the population of cells is virtually uncorrelated (granular layer), and is elevated when correlations are increased (consistent with **Figure 5.9** and **Figure 5.18**). The discrimination threshold is significantly smaller for the granular layer ($P < 0.05$, bootstrap method) than for the supragranular and infragranular layers, but is not significantly different between the supragranular and infragranular layers ($P > 0.05$). These results indicate that network discrimination in the granular layer is significantly greater than that in the superficial and deep layers of V1.

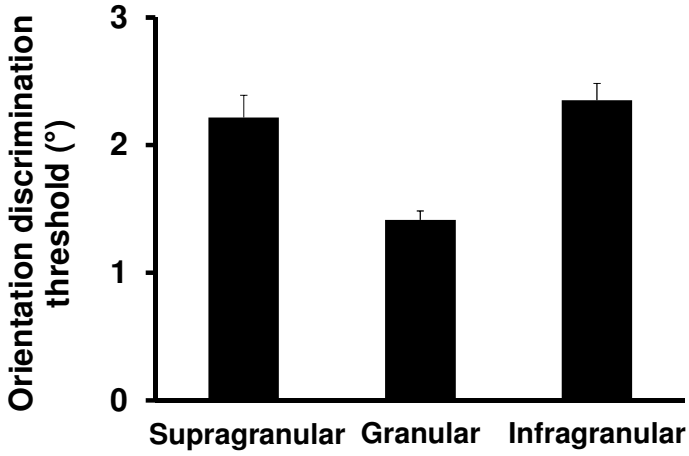

Figure 5.18. Functional connectivity and layer-dependent network information
The orientation discrimination threshold, computed using Fisher Information, is significantly smaller for the granular layer than for the supragranular and infragranular layers, but is not significantly different between the supragranular and infragranular layers. Stimulus orientation was decoded from the population response using a locally optimal linear estimator trained to minimize the discrimination threshold between the two adjacent stimulus orientations.

5.4 Conclusions

A fundamental issue in our understanding of brain circuits is how sensory information is encoded by networks in different layers of the cerebral cortex. For example, in primary visual cortex (V1), the granular layer (layer 4) receives feedforward thalamic inputs. Subsequently, neuronal impulses from the granular layer are transmitted first to neurons in supragranular layers (layers 2-3), and then infragranular layers (layers 5-6); both layers constitute outputs of V1. In recent years, significant progress has been made in our understanding of differences in response properties of neurons across cortical layers (Buffalo et al., 2011; Hansen and Dragoi, 2011; Lakatos et al., 2009; Maier et al., 2010; Maier et al., 2011), yet whether and how neuronal populations encode information in a laminar–dependent manner has remained unclear. Using laminar recording techniques in combination with evoked-response potentials and current-source density, we revisited the issue of correlated variability in V1 circuits. We found that correlations between neurons depend strongly on the local network context – whereas neurons in the granular layer showed virtually no correlated variability, neurons in supragranular and infragranular layers exhibited strong response correlations. Consistent with our results, Smith and Kohn (personal communication) measured spike count correlation between pairs of neurons at various depths in primary visual cortex, and found a striking dependence on cortical layer. Correlations between neurons in the superficial or deep layers could be as high as in the previous studies (in excess of 10%), but correlation between neurons in the intermediate layers was extremely low (as low as 2%). Thus, we conclude that the knowledge of cortical layers may help explain the discrepancy between measures of correlation.

Our study could potentially shed light on recent controversy in the field regarding the issue of correlated variability (Cohen and Kohn, 2011). Thus, despite the fact that strong trial-by-trial correlated variability has long been reported in primary visual cortex (Bair et al., 2001; Kohn and Smith, 2005; de la Rocha et al., 2007; Gutnisky and Dragoi, 2008; Smith and Kohn, 2008; Nauhaus et al., 2009), recent evidence from Ecker et al. (2010) has suggested that neuronal correlations are much lower than previously thought. Our study offers experimental evidence in support of the idea that correlations in the granular layer of V1 are an order of magnitude weaker than correlations in the output layers. While it is unlikely that Ecker et al. (2010) have recorded solely from the granular layers (they report a broad range of correlation coefficients), it is entirely possible that a significant number of pairs could have originated from the granular layers. Indeed, electrode arrays used in chronic recordings are often advanced up to 1 mm (within the range of the granular layers) in order to ensure recording stability (Gray et al., 1995; Nicolelis, 1999). In addition to cortical layers, other factors could have influenced the low correlation values reported by Ecker et al. (2010), such as the low mean firing rates. Indeed, as shown in **Figure 5.11**, low firing counts (due to small temporal windows) could lead to low correlation coefficients, particularly in the granular layers.

Other experimental variables might have affected the level of correlated variability reported here. As discussed by Ecker et al. (2010) improper spike sorting could inflate correlation coefficients at least by a factor of two by incorrectly measuring correlations between multi-unit, not single-unit, spike counts. However, besides the fact that the spike sorting methods used in our study are similar to those used by Ecker et al. (2010) incorrect spike sorting would have also affected single-unit isolation in the middle V1 layers, not only in

superficial and deep layers. Therefore, if spike sorting had been an issue in our study, one would have expected much higher noise correlations in the granular layer than those reported in **Figure 5.9**. Another variable affecting noise correlations is eye movements. Microsaccades would be expected to jointly increase or decrease neuronal responses such as to increase correlated variability. However, we found that although noise correlations were decreased somewhat by eliminating the large fixational eye movements, the layer dependency of correlations remained highly significant.

Surprisingly, we found that populations of neurons in different cortical layers may employ different coding strategies. While the resolution of our laminar recording technique is unable to identify unique sub layer contributions (such as 3B or 4A), our results should be viewed in terms of the major laminar circuits in V1 of macaque monkeys (See chapter 2). We propose that by operating in a virtually uncorrelated state, cells in the input (granular) layer, which receive afferents from networks in subcortical areas and have only local projections to other layers within V1, may encode incoming stimuli more accurately than cells in the supragranular and infragranular layers (based on the results of a model and using linear decoders). In contrast, the output layers (supragranular and infragranular), which send projections to other cortical and subcortical areas possibly encode information less accurately by exhibiting large correlated variability. While there are other thalamorecpient layers outside of 4C (e.g. K input to 3B and 4A) these connections are relatively sparse. Yet in theory, neurons that receive input from these projections should express lower noise correlations as we observed in our granular recordings (presumed layer 4C). However, current laminar techniques

likely miss their contribution given the larger percentage of neuron pairs exhibiting increased noise correlations present in supragranular cortex.

The fact that our results suggest that response decorrelation in the granular layer may be beneficial for sensory discriminations (**Figure 5.18**) raises the issue of whether the higher correlations in supragranular and infragranular layers are detrimental for the information that V1 transmits to other cortical areas. However, this is unlikely to be the case. Indeed, whereas neuronal responses in the granular layer may be optimized for sensory discrimination, the processing of information is mostly local. In contrast, neurons in the supragranular and infragranular layers use long-range cortical projections to process afferent inputs in a context-dependent manner (Gilbert and Wiesel, 1989; Feldmeyer et al., 2002; Briggs and Callaway, 2005). Importantly, long-range horizontal connections are essential for performing complex computations, such as contour grouping (Roelfsema et al., 2004) or figure-ground segregation (Salinas and Sejnowski, 2000), which may rely on strong correlations between neurons. In addition, theoretical studies have suggested that correlated inputs are transmitted more efficiently than decorrelated inputs (van der Togt et al., 2006), thus supporting the idea that the increase in correlations in the output layers of V1 may be functionally beneficial.

"The most exciting phrase to hear in science, the one that heralds new discoveries, is not 'Eureka! [I've found it!]*', but 'That's funny* [odd]*'"*

– Isaac Asimov

6. ADAPTATION-INDUCED SYNCHRONIZATION IN LAMINAR CIRCUITS

6.1 Introduction

A fundamental property of cortical neurons is the capacity to exhibit adaptive changes or plasticity. Little is known about whether adaptive changes in cortical responses are accompanied by changes in synchrony between individual neurons and local population activity. Importantly how adaptive changes emerge across cortical layers has never been studied experimentally. This issue is important as synchronized neural activity is hypothesized to play a vital role in propagating information in neuronal circuits within and between neuronal populations. We investigated this issue in the context of rapid, adaptation-induced plasticity in monkey primary visual cortex (area V1) where neurons have been shown to exhibit plasticity of feature coding even after brief exposure (on the time scale of a visual fixation) to a stimulus of fixed structure (Muller et al., 1999; Yao and Dan, 2001; Dragoi et al., 2002; Felsen et al., 2002; Gutnisky and Dragoi, 2008). We focused on rapid adaptation because this phenomenon has been previously demonstrated to depend on the local network context in which neurons are embedded (Dragoi et al., 2000; Dragoi et al., 2001), thus raising the possibility that the adaptive capacity of individual neurons may exhibit layer dependency.

Surprisingly, adaptation has never been directly investigated in relation to neuronal oscillatory activity, particularly in the gamma frequency range. Indeed, while gamma synchronization has been found to be involved in a variety of conditions (Gray et al., 1989; Engel et al., 1991a; Fries et al., 2001; Taylor et al., 2005; Womelsdorf et al., 2006; Cardin et

al., 2009; Gregoriou et al., 2009; Chalk et al., 2010), whether a fundamental feature of individual neurons, such as the capacity to exhibit adaptive changes, is influenced by synchrony in the gamma frequency band remains unclear. EEG studies in humans have shown that certain forms of associative learning may be accompanied by gamma synchronization (Miltner et al., 1999); yet, whether and how synchrony between individual neurons and local population activity is altered when neurons undergo adaptation remains unclear. Recently, several studies have addressed the relationship between neuronal synchronization and adaptive cortical changes during learning and memory (van Wingerden et al.; Masquelier et al., 2009; Rutishauser et al., 2010). However, these studies have focused on longer forms of plasticity while ignoring plastic changes occurring at more rapid time scales.

Another aspect yet to be studied experimentally is whether and how orientation adaptation induces effects on neuronal responses across cortical layers. Apart from a study in anesthetized cat V1 (Dragoi et al., 2000) reporting that adaptation changes the response properties of neurons irrespective of cortical depth, it is unknown whether networks of cells across cortical layers in V1 change their coding properties after rapid adaptation. However, in principle, the network structure could change after adaptation in a manner that depends on cortical layers. For instance, the facts that neurons in layer 4 of V1 receive direct input from the lateral geniculate nucleus (LGN) of the thalamus and that LGN responses tend to be highly correlated (Reid and Alonso, 1995), suggest there are possible differences in correlations between neurons in the granular layer. This could influence the communication between neuronal groups in a layer dependent manner.

We focused our analysis on two important effects of rapid adaptation: (1) the improvement in the ability of neurons to discriminate small changes in stimulus orientation (Muller et al., 1999; Yao and Dan, 2001; Dragoi et al., 2002; Felsen et al., 2002; Gutnisky and Dragoi, 2008), and (2) the improvement in neuronal precision (Muller et al., 1999) measured by a decrease in the variation of the interspike-interval (ISI). We tested the hypothesis that the adaptive capacity of neurons to improve their discrimination performance and reduce their ISI variation in different cortical layers is related to the local degree of synchronization between individual cells and field potential activity. We demonstrate that before adaptation (i.e. during control) the presentation of the test stimulus is accompanied by significant spike-field synchronization in the gamma band and is localized to those populations within the input (granular) layers of V1. However, after adaptation there is an increase in gamma band synchronization that is isolated to the superficial (supragranular) layers, known to provide the major cortical output of V1. Isolating individual neuron responses, we also computed two measures of feature coding and observed that neurons in the supragranular layers show the largest improvement in neuronal orientation discrimination performance and have the most precise neuronal firing. Based on these results we propose that the increase in gamma-band neuronal synchronization in the supragranular may enhance the adaptive capacity of individual neurons to optimize network processing across laminar circuits.

6.2 Methods

All experimental procedures were performed in accordance with protocols approved by the US National Institutes of Health Guidelines for the Care and Use of Animals for Experimental Procedures.

6.2.1 Surgical procedure

Overall, the methods are similar to those described in chapter five. Of noteworthy differences, in the following experiments the two male monkeys used were ages five and six years and weighted 10 and 12 kg.

6.2.2 Electrophysiological recordings

Unique to these experiments, we conducted 20 recording sessions using laminar electrodes. On average, we were able to identify 14 LFPs and 5 single-units per recording session for each electrode. Each laminar electrode consisted of a linear array of 16 equally spaced contacts (100 µm inter-contact spacing) positioned to sample from cortical layers simultaneously (Plextrode® U-Probe, Plexon Inc.; **Figure 5.1**). In half of the recording sessions, the electrodes were treated with carbon nanotube coating that gave impedance between 0.3–0.5 MΩ at each contact. The coating reduced the impedance by 25% without altering the area, resulting in an improvement in the signal-to-noise for both spikes (high-frequency bands) and local field potentials (lower-frequency bands). Combining the recordings from the uncoated sessions, we

did not observe any differences in the ability to isolate single-units or the overall signal-to-noise ratio (SNR). For all sessions, real-time neuronal signals recorded from multiple contacts along the electrode shaft (simultaneous 40 kHz A/D conversion on each channel) were analyzed using a Multichannel Acquisition Processor system (MAP, Plexon Inc.). Single-unit recordings were amplified, filtered, and viewed on an oscilloscope and heard through a speaker. The spike waveforms were sorted using Plexon's Offline Sorter program that implemented waveform clustering based on parameters such as principle components, spike width, valley, and peak. When a unit was isolated, its receptive field was mapped using a reverse correlation stimulus (**Figure 6.1**). As expected, given that our recordings spanned across cortical depth we observed highly overlapping receptive fields. Recording sites were selected based on the quality of the SNR and their receptive field position. Using homemade scripts in MATLAB and Plexon's Offline Sorter, we analyzed the unit's waveform characteristic (e.g. width and peak), firing rate, and orientation selectivity. Single-units that abruptly changed their responses (e.g. increased or decreased their firing rate and/or changed their orientation selectivity) were removed and only those units with stable firing rates and orientation selectivity were kept for further analysis.

6.2.3 Experimental paradigm

Two rhesus monkeys performed an orientation adaptation task (**Figure 6.2**). Monkeys were trained to fixate a small spot (0.1 deg) presented on a video monitor placed at a distance of 57 cm from each monkey's eye. If monkeys maintained fixation throughout the entire trial they were rewarded with a 3 drops of juice. Stimuli were generated with Psychophysics Toolbox

from MATLAB and presented on a CRT 19" color video monitor (Dell, 60 Hz refresh rate). All stimuli were static and consisted of a 5° circular sine wave grating of 1.4 cycles/deg spatial frequency and 50% contrast level presented binocularly. Monkeys triggered the trial by holding a bar. After 300 ms of fixation, an adapting stimulus was flashed for 300 ms in the center of the neurons' receptive fields.

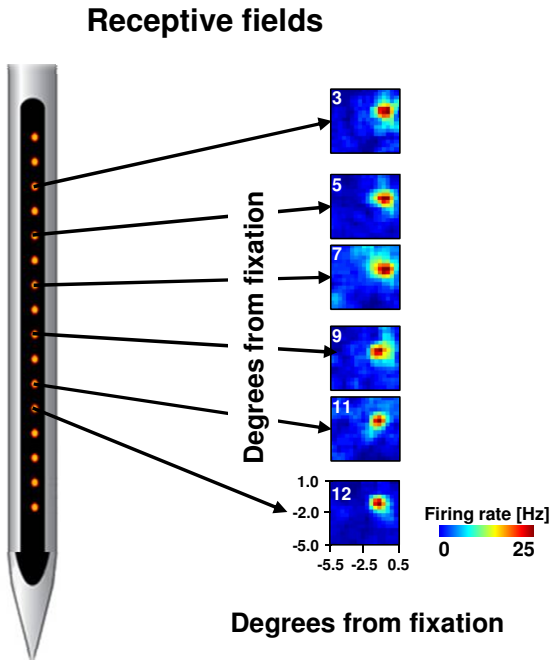

Figure 6.1. Identification of receptive field across laminar contacts
First, half a visual degree is calculated and doubled. Then, reverse correlation stimuli are presented in patches on a CRT monitor consisting of oriented gratings at 0, 45, 90 and 135 degrees. Firing rates for each neuron are calculated independently at 5 ms intervals between 40 to 120 ms after stimuli are presented for each spatial location. Second, the maximum firing rates are calculated and then the centroid for each time delay. Finally, at each delay the distance between the centroid and adjacent firing rate locations is calculated. The time delay with the minimum distance is chosen as the receptive field.

After a 100 ms blank, a 300 ms test stimulus of random orientation (eight equally spaced orientations spanning 0-180°; random spatial phase for each test orientation) was flashed at the same visual location. The adapting stimulus was either a five degree random dot patch (control condition) or a sine-wave grating of identical characteristics as the test stimulus (5 deg circular

sine-wave grating of 1.4 cycles/deg spatial frequency and 50% contrast level), but with a fixed orientation (0° , 45° , 90° or 135°; adaptation condition). The orientation range of the adapting stimulus was chosen based on our previous orientation adaptation experiments (Dragoi et al., 2002; Gutnisky and Dragoi, 2008) reporting strong effects when the adaptor is relatively close to the cell's preferred orientation. Both the adaptor and test stimuli had the same mean luminance. Each test orientation was randomly presented 50 times in each of the control and adaptation conditions (trials were randomly interleaved).

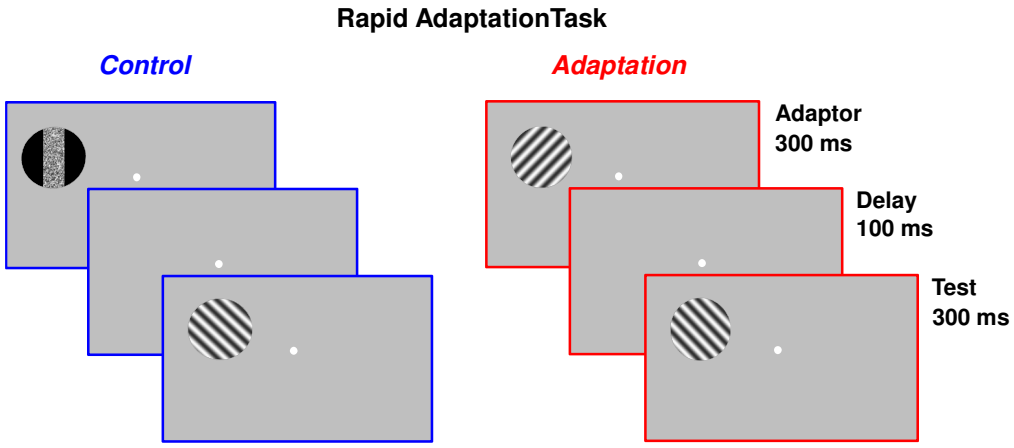

Figure 6.2. Rapid adaptation paradigm
While animals fixated a white dot at the center of a screen, an adapting stimulus was flashed for 300 ms in the center of the neurons' receptive field. After a 100 ms blank, a test stimulus of random orientation was presented for 300 ms. The adapting stimulus was either a random dot patch (control condition) or a sine-wave grating with spatial characteristics identical to those of the test orientation (adaptation condition). Each test orientation was randomly presented 50 times during control and adaptation and the different conditions were randomly interleaved. After the test phase monkeys were rewarded for maintaining fixation throughout the trial.

6.2.4 Local field potential analysis

The methods were similar to those described in chapter five. Additionally, we assessed whether LFPs are selective for orientation and whether adaptation affects LFP amplitude tuning by performing a trial-by-trial ANOVA test. Using home-made MATLAB scripts and the Chronux toolbox (Mitra and Pesaran, 1999; Jarvis and Mitra, 2001) we analyzed the LFP power density during the presentation of the test stimuli and during the inter-trial interval using sliding windows of ± 125 ms length in steps of 10 ms.

6.2.5 Cortical layer identification

The methods were identical to those described in chapter 5.

6.2.6 Spike-field coherence (SFC) as a measure of neuronal synchronization

We used multi-taper spectral analysis to compute the spike-field coherence (SFC), which measures the degree of synchronization between neurons and LFPs as a function of frequency (Thiele and Stoner, 2003; Roelfsema et al., 2004; Taylor et al., 2005; Gregoriou et al., 2009; Chalk et al., 2010). In general, the coherence between two signals (x and y) recorded at different sites is a complex quantity whose magnitude is a measure of the phase synchrony for frequency f. Coherence is an absolute value that varies between 0 and 1 (e.g., a value of 1 indicates a perfect phase relationship between the firing of the spikes to the fluctuations of the LFP). Coherence is defined as:

$$C_{yx}(f) = \frac{S_{yx}(f)}{\sqrt{S_x(f)\, S_y(f)}} \tag{6.1}$$

where and represent the auto-spectra and the cross-spectrum of the two signals and . Auto-spectra and cross-spectra are averaged across trials before the coherency calculation (Womelsdorf et al., 2006; Gregoriou et al., 2009). In an attempt to eliminate any bias from differing sample sizes, the same number of trials for each condition (adaptation and control) was used for the calculation of coherence for a given pair. Importantly, the length of time window included in each condition was also constant. Specifically, we utilized the Chronux function `coherencycpt`, which computes the multi-taper spike-field coherence for a continuous signal (LFP), and point process data (spike-train) according to an optimal family of orthogonal tapers derived from Slepian functions (Mitra and Pesaran, 1999; Pesaran et al., 2002; Womelsdorf et al., 2006; Gregoriou et al., 2009). The number of tapers was calculated according to the formula:

$$K = 2 * TW - 1 \qquad (6.2)$$

where is the highest number of tapers that can be used while preserving optimal time-frequency concentration of the data windowing available from the Slepian taper sequences, is the length of the time window in seconds, and is the half-bandwidth of the multi-taper filter. For our analysis, we applied spectral smoothing of ± 10 Hz for frequencies greater than 30 Hz and ± 4 Hz for lower frequencies. These methods have now been successfully applied to neuronal data in a number of cases (Mitra and Pesaran, 1999; Pesaran et al., 2002; Womelsdorf et al., 2006; Gregoriou et al., 2009).

While our analysis of spike-field coherence was calculated using the Chronux toolbox, we also cross-validated our results using homemade scripts in MATLAB. Briefly, we computed spike-triggered averages (STAs) by averaging the LFP signal within a window centered ± 150

ms on each elicited spike within 50-300 ms after the onset of the test stimulus. Indeed, a similar study (Wang et al., 2011) applied similar methods to study adaptation in V4. STA is normalized for spike count as it is calculated by summing all LFP segments and then dividing by the number of spikes. To quantify STA, we calculate its power spectrum (i.e., the magnitude of all frequency components of the STA as a function of frequency). SFC was computed by dividing the power spectrum of the STA to the average of all power spectra of the LFP segments that were used to obtain the STA. Both techniques yielded highly similar results.

6.2.7 Neuronal discrimination (*d'*)

As a measure of neuronal discrimination performance, we calculated the neurons' capacity (*d'*) to discriminate between orientations (Green and Swets, 1966; Macmillan and Creelman, 2005) within 22.5° of the cell's preferred orientation as the difference between the mean spike rates ($\mu_{\theta\pm22.5}$ and μ_{θ}) at the two nearby orientations divided by the root-mean-square standard deviation ($\sigma_{\theta\pm22.5}$ and σ_{θ}).

$$d' = \frac{(\mu_{\theta\pm22.5} - \mu_{\theta})}{\sqrt{\frac{\sigma^2_{\theta+22.5} + \sigma^2_{\theta}}{2}}} \tag{6.3}$$

These measures, mean firing rate and response standard deviation, were calculated from the trial-by-trial mean responses during the entire 300 ms presentation of the test stimulus in each condition (control and adaptation). Mean *d'* was calculated by averaging the *d'* values obtained for each test orientation pair around the preferred orientation (i.e. $\theta \pm 22.5°$).

6.2.8 Coefficient of variation (CV)

As a measure of neuronal precision (Softky and Koch, 1993; Mainen and Sejnowski, 1995), we calculated the variation in the neurons' interspike-interval between test orientations within

22.5° of each cells' preferred orientation. CV was computed as follows:

$$\frac{\sigma_{ISI}}{\overline{ISI}} \tag{6.4}$$

These measures, standard deviation of the ISI and mean ISI, were calculated from the trial-by-trial responses during the entire 300 ms presentation of the test stimulus in each condition (control and adaptation). Mean CV was calculated by averaging the CV values obtained for each test orientation pair around the preferred orientation, θ (i.e., θ ± 22.5°).

6.3 Results

6.3.1 Adaptation reduces neuronal variability and LFP amplitude

For each recording session, we recorded spike and LFP responses across all cortical layers during control and adaptation. The traces in **Figure 6.3** (left) show the mean LFP amplitude as a function of time produced by the stimuli evoking an increase in the response to the adaptor (45° in this example), as well as the test. **Figure 6.3** (right) shows representative spike responses recorded in the same session spanning all cortical layers. Overall, for the population of 77 cells (SG = 33, G = 24, and IG = 20), we found that adaptation significantly reduces the

mean firing rate irrespective of cortical layer (**Figure 6.4**; $P < 0.01$, Wilcoxon signed-rank test; consistent with previous results; Muller et al., 1999; Dragoi et al., 2002; Gutnisky and Dragoi, 2008).

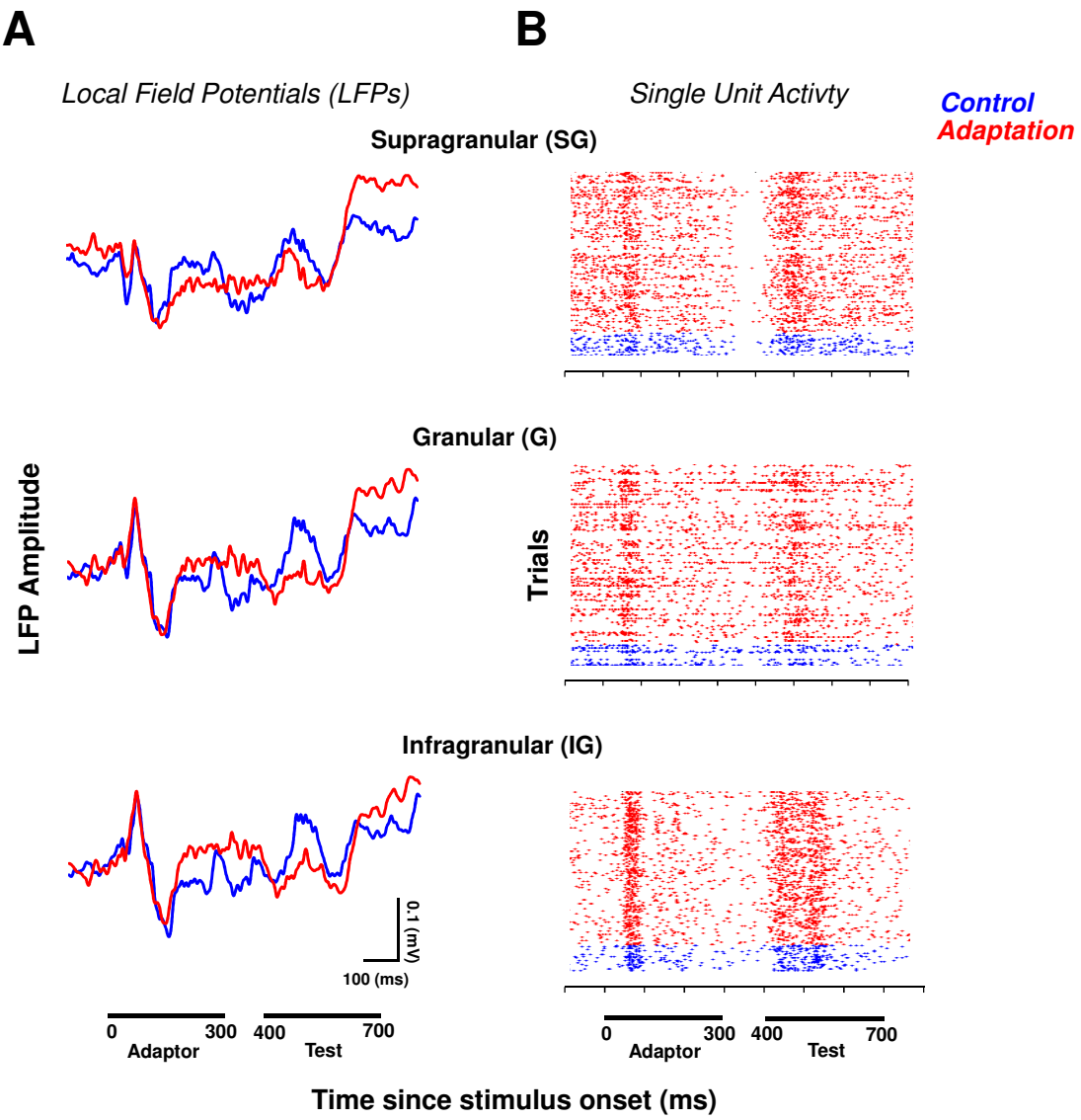

Figure 6.3. Adaptation modulates LFP and single-unit responses
(**A**) Each trace represents the average response across all trials and test orientations in each condition (a 45° adaptor). (**B**) The raster plots represent the spike times of three example V1 neurons across cortical layers responding to the adapting and test stimuli in the control (blue) and adaptation (red) conditions. For display purposes, the control and adaptation trials were grouped. Adapting (1st line) and test stimuli (2nd line).

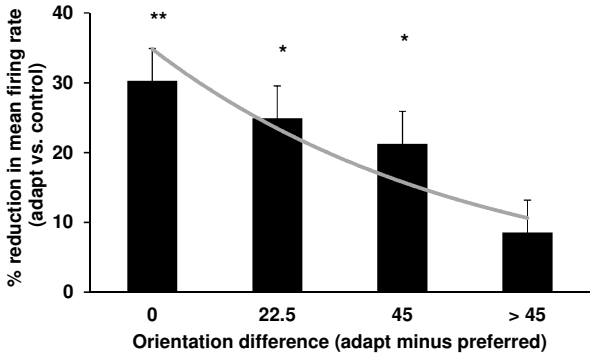

Figure 6.4. Adaptation reduces mean firing rate
Consistent with our previous adaptation experiments, for small orientation differences between the adapting stimulus and the cell's peak orientation, neurons reduce their firing rate by approximately 30% (measured at optimal orientation in the control condition). However, as the orientation difference increases, the reduction in firing rate becomes smaller (20% or less; ** $P < 0.01$, * $P < 0.05$; Wilcoxon signed-rank test).

6.3.2 Adaptation increases gamma synchronization

We examined the effect of rapid adaptation on the degree of synchronization between individual neurons and LFPs in different frequency bands by computing spike-field coherence, SFC (Fries et al., 2001; Taylor et al., 2005; Womelsdorf et al., 2006; Gregoriou et al., 2009; Chalk et al., 2010), during the presentation of the test stimulus (for the spectral analysis we eliminated the first 100 ms following test onset) for our population of 986 pairs that exhibited significant response modulation by stimulus orientation (this criterion was applied to both single-units and LFPs). To compute SFC, we used the multi-taper spectral analysis (i.e. Chronux). Since LFPs may be composed of extracellular voltage fluctuations originating from recording sites within 300 μm or less (Kruse and Eckhorn, 1996; Katzner et al., 2009), we reasoned that the effect of adaptation on neuronal synchronization would be more pronounced when the recording sites are located in close proximity. We thus computed the mean SFC by

averaging, for each recording site, the coherence values for pairs of single-units and LFPs within 300 μm of cortical space. Because of the functional significance of gamma oscillations (30-80 Hz) in visual cortex (Gray et al., 1989; Engel et al., 1991a; Womelsdorf et al., 2006; Cardin et al., 2009; Gregoriou et al., 2009; Chalk et al., 2010), the presentation of our results is focused on high-frequency synchronization.

In control trials, the presentation of the test stimulus led to pronounced synchronous activity across all cortical layers, with the most significant increase in gamma synchronization in the granular layers (**Figure 6.5** A, left). However, after adaptation, there was a significant increase in gamma synchronization specifically in the supragranular layers (**Figure 6.5** B, right). Our population analysis confirms these results – before adaptation we found spike-LFP gamma synchronization across all layers (mean ± SEM; SG, 0.08 ± 0.002; G, 0.12 ± 0.007; IG, 0.08 ± 0.006) with the largest SFC level in the granular layers (**Figure 6.6** A and **Figure 6.7** A; one-way ANOVA, $F(2, 74) = 8.75$, $P < 0.0004$; post-hoc multi-comparison, Tukey's Least Significant Difference). However, despite the high gamma synchronization in the granular layers during control, adaptation significantly increased SFC only in the supragranular layers (**Figure 6.6** B), whereas the granular and infragranular layers exhibited only a weak increase in synchronization.

6.3.3 Supragranular layers show increase in gamma synchronization

We calculated the percentage change in gamma SFC between adaptation and control (ΔSFC) across the entire frequency range and found a significant increase in synchronization for the

supragranular layer (68.91% ± 6.75%; **Figure 6.6** C and **Figure 6.7** B; one-way ANOVA, F (2, 74) = 35.24, $P < 10\text{-}10$; post-hoc multi-comparison, Tukey's Least Significant Difference). The post-adaptation increase in gamma SFC in the supragranular layers was observed only when both recording sites were stimulated with test stimuli within 45° of the cells' preferred orientation (**Figure 6.8**, $P < 0.05$, Wilcoxon signed-rank test). Non-optimal test orientations (> 45° difference between the stimulus orientation and the preferred orientation at each recording site) reduced spike rates, LFP amplitudes, and SFC in the control condition; adaptation did not result in a significant increase in gamma SFC ($P > 0.1$, Wilcoxon signed-rank test).

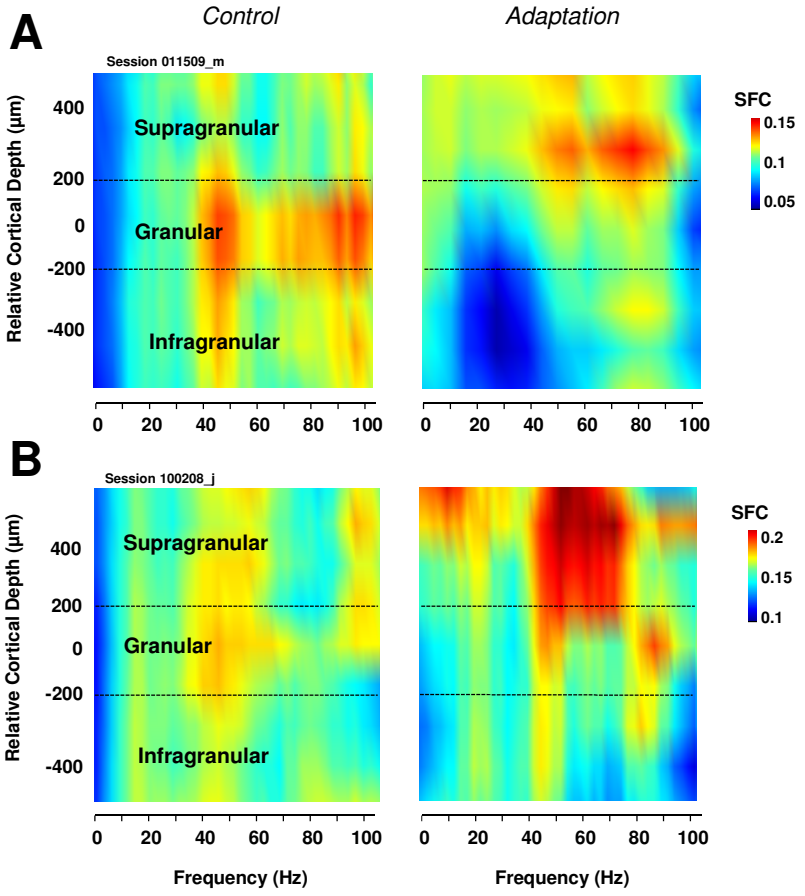

Figure 6.5. Examples of synchronization across cortical layers
(**A-B**) Represent examples from two different monkeys during the presentation of the control stimuli (left), there is an increase in gamma activity in the granular layer. Adaptation (right) increases SFC across cortical layers with the largest increase occurring in the supragranular layers. The dashed lines represent the granular layer (identified as the largest ± 200 µm).

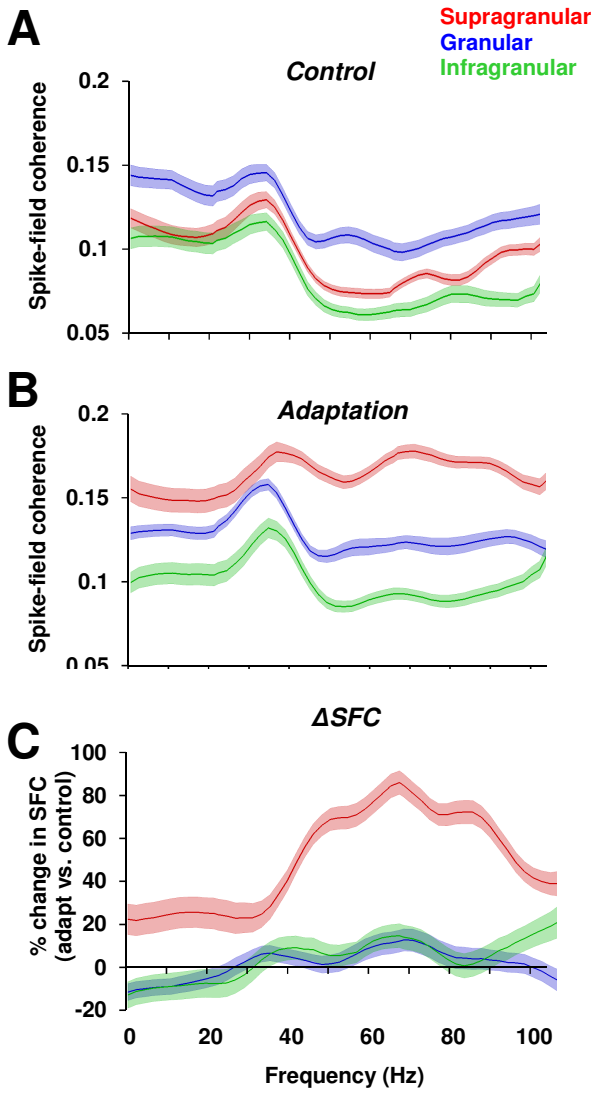

Figure 6.6. Adaptation influences synchronization
(**A**) Population analysis during the presentation of the control stimulus results in a significant increase in SFC between 30 and 80 Hz in the granular layer. (**B**) Adaptation increases SFC in the supragranular layer for all frequency bands between 0 and 80 Hz, with the largest increase in the gamma-band (30-80 Hz; shaded regions represent SEM.) (**C**) We calculated the percentage change between adaptation and control across the entire frequency range and observed a significant increase in gamma-band spike-field coherence for the supragranular layer.

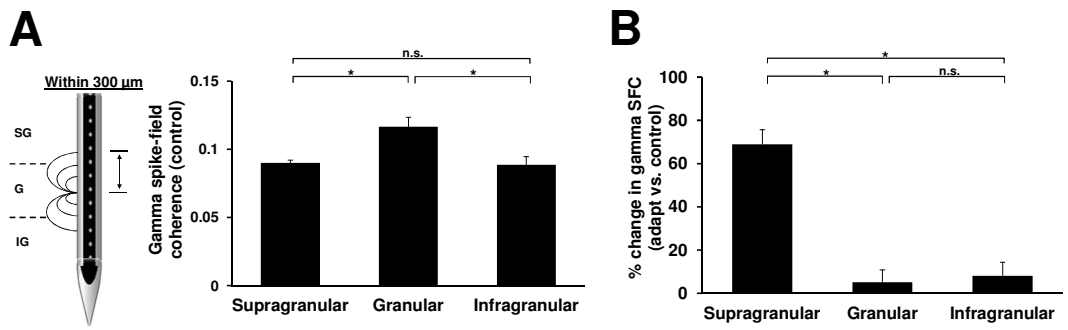

Figure 6.7. Adaptation increases gamma synchronization in supragranular layer
(**A**) 'Within 300 µm' pooling scheme – to compute SFC, we pooled the spike-field pairs within a 300 µm window around each isolated unit. Population mean gamma-band SFC (30-80 Hz) shows a significant increase in the granular layer during control. (**B**) While adaptation significantly increases the mean SFC in the supragranular layer, it does not significantly alter SFC in the granular and infragranular layers. The mean percentage change in SFC was calculated by computing the percentage change in SFC for each spike-field pair. We then averaged the calculated percentages to obtain the data shown in the figure.

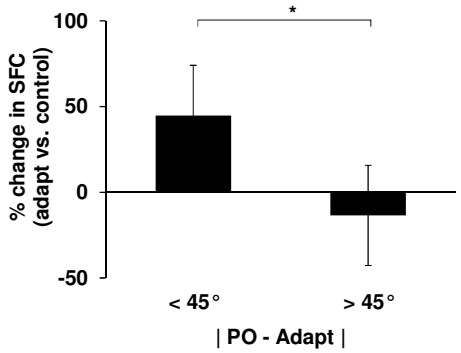

Figure 6.8. Gamma-band SFC is significant for test orientations within 45°
SFC was calculated using the 300 µm pooling scheme (cf. **Figure 6.7**). Changes in SFC after adaptation (calculated by averaging the SFC values across layers) were statistically significant only when the absolute difference between the preferred orientation of the cells and LFPs for a given penetration and the corresponding adapting stimulus ($\Delta\theta$) was less than 45° (* $P < 0.05$, Wilcoxon signed-rank test).

Noteworthy, while rapid adaptation caused an increase in gamma synchronization in the supragranular layer, we also noticed a significant increase in synchronization for lower frequencies, such as alpha (8-14 Hz) and beta (14-27 Hz) (**Figure 6.9** A, SG: 21%, $P < 0.01$;

SG: 21%, $P < 0.01$, Wilcoxon rank sum test). Overall, adaptation increased low frequency SFC across all layers, with the largest increase occurring in supragranular layers (**Figure 6.9** B).

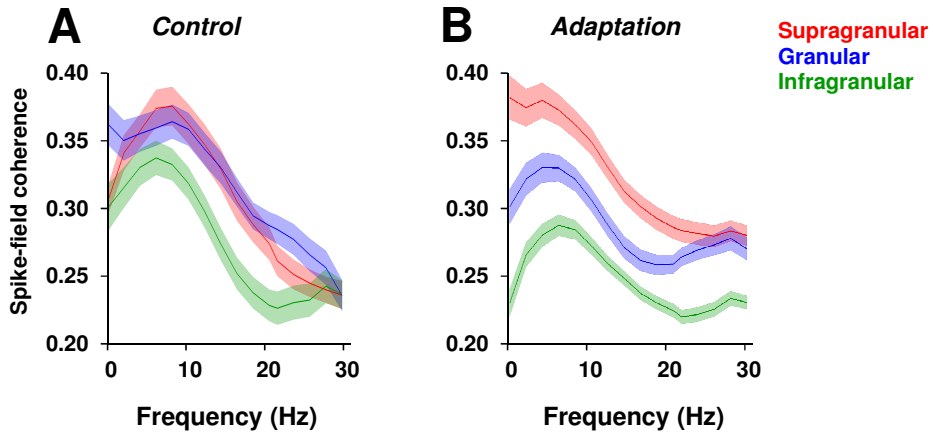

Figure 6.9. Adaptation modulates coherence < 30 Hz
Similar to Figure 6.6 for the analysis of lower frequencies, we used the multitaper method, in which we computed spike-triggered averages (STAs) by averaging the LFP signal and applying ± 4 Hz smoothing for frequencies less than 30Hz. (**A**) We observed no difference in SFC across cortical layers during the presentation of the control stimulus. (**B**) Adaptation increases SFC between 0 and 30 Hz with the largest increase occurring in supragranular and granular layers.

6.3.4 LFP area of integration influences layer-dependent synchronization

In principle, it may be possible that the 300 µm pooling of LFP inputs used for our calculation of mean spike-field coherence will have overestimated the spatial extent of the LFP inputs attributable to the same cortical layer. For instance, when recording sites are located 100 µm away from the border between two layers, the LFPs contributing to the mean spike-field coherence (for the same single-unit) would clearly originate in different layers possibly to challenge the laminar specificity of the results shown in **Figure 6.6** A and B. To control for this possibility, we recomputed spike-field coherence for each recording site by pooling only those LFPs located within the same cortical layer, irrespective of the distance between LFPs and the

single-unit site. Nonetheless, although this 'within layer' pooling scheme led to overall higher coherence values, our main results remained unchanged. That is, an increase in gamma-band SFC in the granular layer during the control condition (0.50 ± 0.02, mean ± SEM; **Figure 6.10** A; one-way ANOVA, F (2, 74) = 44.1, $P < 10^{-12}$; post-hoc multi-comparison, Tukey's Least Significant Difference). In addition we also observed consistent improvement in gamma synchronization after adaptation that was specific to the supragranular layer (**Figure 6.10** B; one-way ANOVA, F (2, 74) = 8.22, $P < 0.0006$; post-hoc multi-comparison, Tukey's Least Significant Difference).

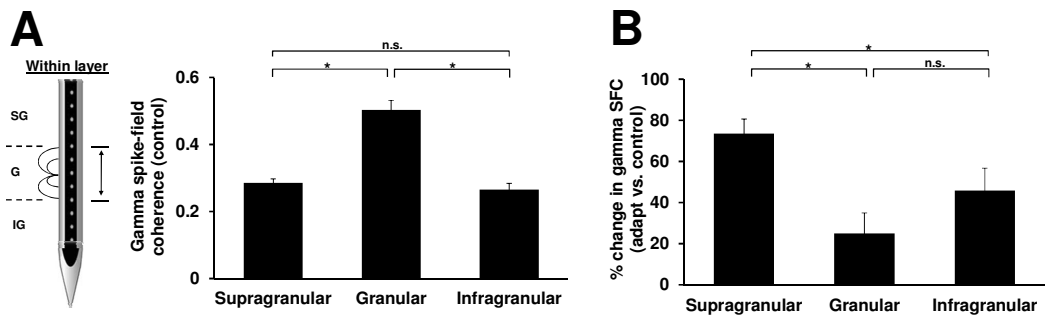

Figure 6.10. 'Within-layer' pooling scheme
Restricting the coherence analysis to those contacts within an identified layer does not alter the results shown in **Figure 6.6**. While the mean SFC in the gamma-band showed an overall increase across all layers, the main result was unchanged for this more restrictive analysis (**A**: an increase in granular SFC during control; **B**: a post-adaptation increase in synchronization in the supragranular layers).

6.3.5 Adaptation improves neuronal discrimination and spike-reliability

We further examined whether the post-adaptation increase in gamma synchronization influences neuronal performance by individual neurons. One measure of neuronal performance we explored is neuronal discriminability– (Green and Swets, 1966; Macmillan and Creelman, 2005) whether the ability of neurons in different cortical layers to discriminate small changes in

stimulus orientation is influenced by the post-adaptation change in gamma synchronization between individual cells and their local population activity. The second measure was neuronal precision, or the coefficient of variation (CV). We focused on the variation in the ISI given the importance of spike timing in our analysis of local gamma synchronization. Thus, we tested the laminar dependence in the variation of ISI timing as it relates to layer-specific post-adaptation changes in gamma synchronization.

Specifically, we addressed these issues by examining the relationships between the post-adaptation change in spike-field coherence (when recording sites were within 300 μm of each other), and either the change in neurons' capacity (*d'*) to discriminate nearby orientations (22.5° apart) or the change in the variation of the interspike-interval. Thus, we calculated the mean spike-field coherence (before and after adaptation) for the pairs of recording sites that were stimulated within 22.5° of their preferred orientations as these pairs contributed to the overall increase in gamma synchronization after adaptation shown in **Figure 6.7** B.

In agreement with previous studies (Muller et al., 1999; Dragoi et al., 2000; Gutnisky and Dragoi, 2008), we found a significant increase in *d'* after adaptation across the population of neurons ($P < 10^{-11}$; **Figure 6.11** A-C SG: $P = 5.39^{-7}$; G: $P = 3.43^{-5}$; IG: $P = 8.86^{-5}$; Wilcoxon signed-rank test). Orientation discriminability was calculated as the mean *d'* for pairs of stimuli within 22.5° of the cell's peak orientation, which were presented near the adapting orientation (within 45°). As expected, the changes in d' in each layer were accompanied by an increase in response slope (response difference at the two nearby test orientations, SG: 29.3%, $P < 10^{-7}$; G: 19.9%, $P <$ 10-4; IG: 28.3%, $P <$ 0.02, Wilcoxon signed-rank test) and a decrease in response

variance (SG: -25.8%, $P < 10^{-7}$; G: -27.7% $P < 0.002$; IG: -21.5%, $P < 0.04$, Wilcoxon signed-rank test). Importantly, the increase in discriminability after adaptation depends on cortical layer – neurons residing in supragranular layer showed the largest post-adaptation increase in d' (**Figure 6.12**, one-way ANOVA, F (2, 74) =7.66, $P < 0.0009$; post-hoc multi-comparison, Tukey's Least Significant Difference).

The second measure was neuronal precision or the CV. Under identical parameters, we calculated the CV as the standard deviation divided by the mean ISI. We focused on the variation in the ISI given the importance of spike timing in our analysis of local gamma synchronization. Thus, we tested the laminar dependence in the variation of ISI timing as it relates to layer-specific post-adaptation changes in gamma synchronization. In addition, in our analysis of the neuronal precision, we found a significant decrease in CV after adaption (mean control CV: 1.15; mean adaptation CV: 1.00) across the population of neurons (**Figure 6.13**, $P < 10^{-6}$; Wilcoxon signed-rank test). Thus, adaptation reduced the variation in ISI, which suggests a greater precision in the firing of individual neurons.

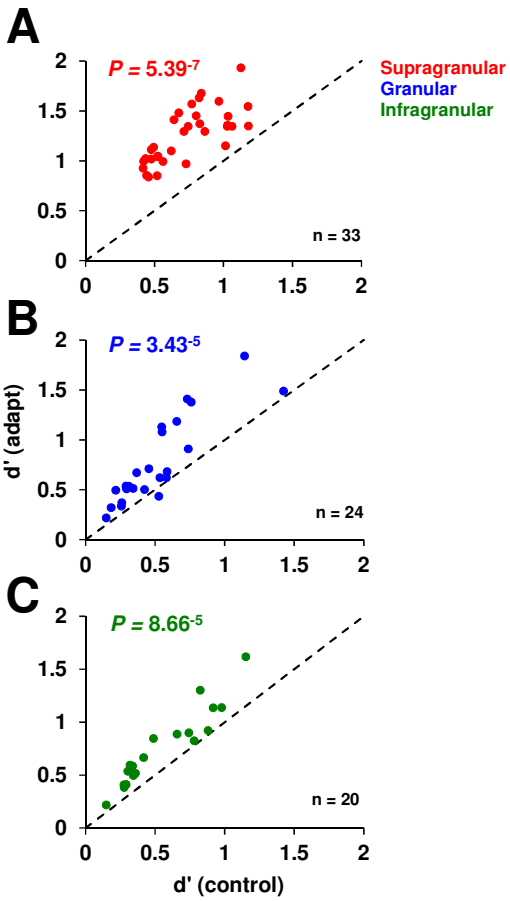

Figure 6.11. Post-adaptation changes in neuronal discrimination
(**A-C**) Scatter plots showing the effects of adaptation on neuronal discrimination performance (*d'*) at the population level across cortical layers. Each dot represents the mean *d'* during control and adaptation, while the different colors indicate the layer in which the neuron was isolated. Adaptation significantly increases orientation discriminability.

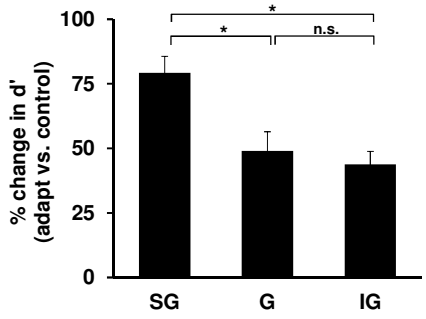

Figure 6.12. Layer-specific percentage changes in *d'*
Although adaptation significantly increases *d'* across all cortical layers, the largest occurred in the supragranular layer.

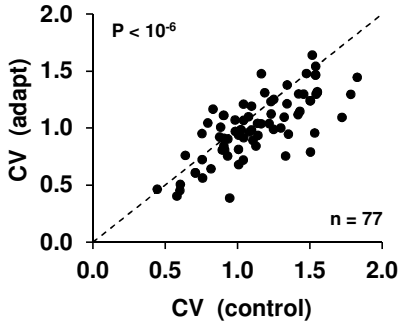

Figure 6.13. Adaptation changes spike-reliability
Scatter plot showing the effects of adaptation on neuronal precision at the population level. Each dot represents the mean CV during control and adaptation. Across the population, adaptation significantly decreases the coefficient of variation, increasing the precision of the neuron.

6.3.6 Gamma-band coherence, neuronal discrimination, and spike-reliability

We examined whether the post-adaptation increase in neuronal discriminability is correlated with changes in gamma synchronization. The increase in neuronal discriminability after adaptation has been suggested (Dragoi et al., 2002; Chelaru and Dragoi, 2008) to emerge from changes in firing rates (both suppressive and facilitatory) across the population of cells, mainly due to the depression of excitatory and inhibitory synapses originating from the neurons tuned the adapting stimulus. Thus, we explored whether the post-adaptation increase in gamma synchronization in the supragranular layers might have contributed to the larger increase in neuronal discriminability found in SG neurons after adaptation.

Given these findings, we measured the correlation between the changes in gamma-band spike-field coherence in each cortical layer and the adaptation-induced changes in neuronal discrimination performance. A significant correlation was found between the post-adaptation

change in *d'* and the corresponding change in SFC only for the recording sites in the supragranular layers (**Figure 6.14** A, r = 0.35, $P < 0.05$, Pearson correlation). In contrast, neurons in granular and infragranular layers exhibited post-adaptation changes in discriminability that were independent of the changes in gamma spike-field coherence (**Figure 6.14** B-C, G layer: r = 0.03, IG layer: r = 0.08, Pearson correlation; $P > 0.71$ for both correlation coefficients).

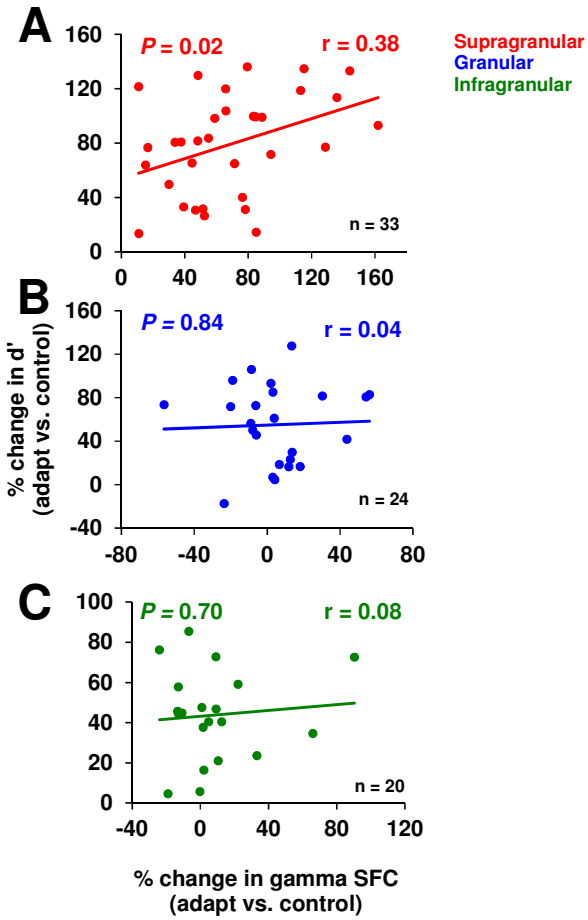

Figure 6.14. The relationship between ΔSFC in the gamma band and Δ*d'*
(**A-C**) The post-adaptation change in gamma-band SFC influences the neurons' ability to discriminate small changes in orientation. There is a significant and positive correlation between the gamma-band spike-field coherence after adaptation and the change in d' that is specific to the supragranular layers. The color lines represent the linear regression fits associated with each cortical layer.

We further computed the correlation between post-adaptation changes in the response difference at nearby orientations (response slope) and response standard deviation used to calculate d'. We found that adaptation increases spike-field coherence in the supragranular layers to enhance response slope (correlation between changes in gamma SFC and changes in response slope, r = 0.36, $P < 0.05$, Pearson correlation) and decrease response variability (correlation between changes in gamma SFC and changes in response standard deviation r = -0.34, $P < 0.05$) to enhance orientation coding by SG neurons. However, for the granular and infragranular layers, we did not find any significant correlation between post-adaptation SFC and response slope (G layer: r = -0.17, $P > 0.4$; IG layer: r = -0.13, $P > 0.58$) or response variability (G layer: r = -0.09, $P > 0.6$; IG layer: r = -0.15, $P > 0.5$, Pearson correlation).

The relationship between neuronal synchronization and the enhancement in neuronal discrimination after adaptation in the supragranular layers was specific to the gamma band. Changes in coherence in lower frequency bands, such as alpha and beta, showed no significant correlation with the post-adaptation changes in *d'* (**Figure 6.15**). We also observed that the laminar-specific relationship between the post-adaptation changes in SFC and d' was preserved when LFPs were pooled according to the 'within layer' scheme (cf. **Figure 6.10**, see **Figure 6.16** A-C). The relationship between the increase in neuronal synchronization after adaptation and the improvement in neurons' discrimination ability is consistent with recurrent models that incorporate synaptic depression to explain the decrease in postsynaptic activity and the increase in the likelihood that spikes occur near the maxima of the oscillatory part of the input after adaptation.

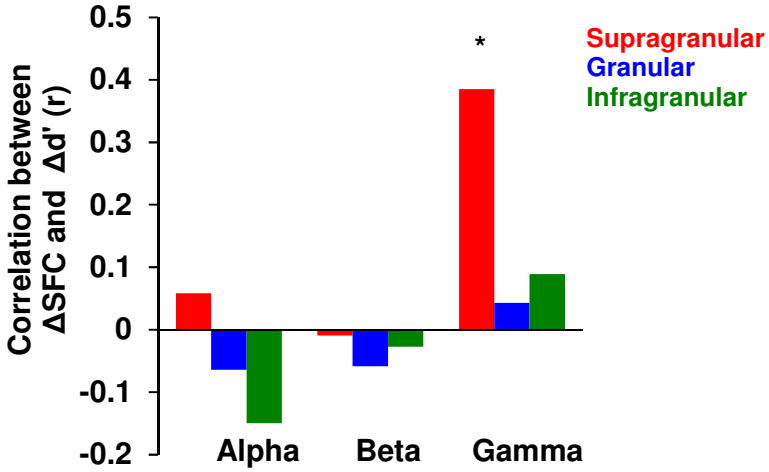

Figure 6.15. Correlation between the post-adaptation change in SFC and *d'*
The analysis of lower frequency bands (< 30 Hz) does not reveal a statistically significant correlation between the post-adaptation change in SFC and *d'*.

In addition to changes in discrimination performance after adaptation, we also measured neuronal precision by estimating the variation in the ISI by computing the CV (standard deviation/mean interspike-interval). We found that only the recording sites in the supragranular layers were associated with a significant correlation between the post-adaptation change in CV and SFC (**Figure 6.17** A, r = -0.37, $P < 0.05$, Pearson correlation). In contrast, neurons in granular and infragranular layers exhibited post-adaptation changes in precision that were independent of the changes in spike-field coherence (**Figure 6.17** B-C, G layer: r = -0.09, IG layer: r = -0.02, Pearson correlation; $P > 0.67$ for both correlation coefficients). The changes induced by adaptation are uncontaminated by fixational eye movements; we failed to find a statistically significant relationship between the horizontal/vertical saccade amplitude and frequency and stimulus condition (control vs. adaptation; $P > 0.2$, Wilcoxon signed-rank test for all comparisons).

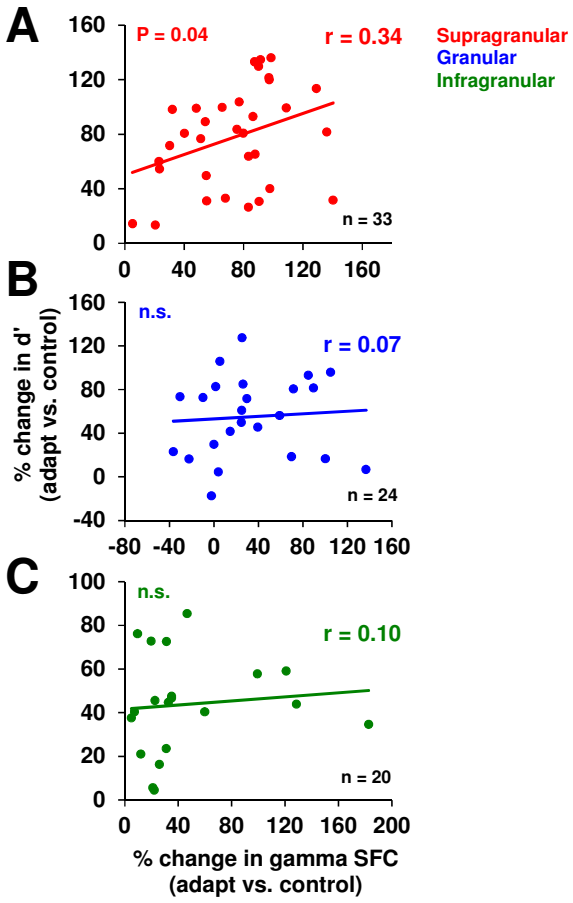

Figure 6.16. The relationship between ΔSFC and Δ*d'* – 'within layer' analysis
Same convention as in **Figure 6.14**.

6.4 Conclusions

The key result of our study is that rapid adaptation (at the time scale of visual fixation) increases the degree of spike-field coherence in the gamma-band frequency (30-80 Hz) in a layer-specific manner, and that these changes in synchronization are associated with an improved coding performance by V1 neurons. This raises the possibility that layer-specific adaptive synchronization between the spiking activity of individual neurons and their local population may be used to enhance coding schemes for sensory discrimination.

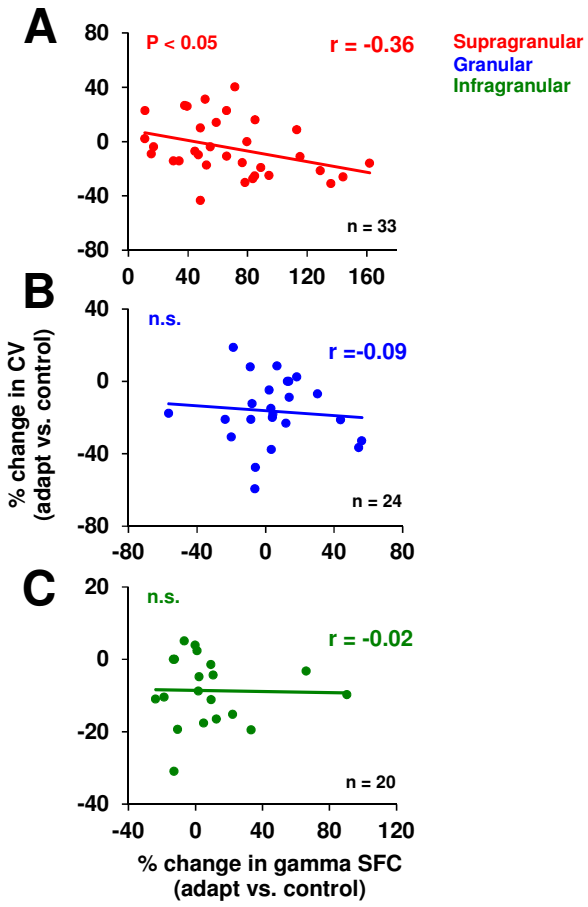

Figure 6.17. The relationship between gamma ΔSFC in the gamma band and ΔCV
The post-adaptation change in gamma-band SFC influences the variation in the ISI of the neuron. There is a significant negative correlation between the gamma-band spike-field coherence after adaptation and the change in CV that is specific to the supragranular layer. The color lines represent the linear regression fits associated with each cortical layer.

The laminar structure of the visual cortex has been known for a long time, yet whether there are differences in the way in which neuronal populations across cortical layers encode information is just beginning to be understood (Lakatos et al., 2009; Sakata and Harris, 2009). Aside from a study in anesthetized cat V1 reporting pronounced adaptive effects irrespective of cortical depth (Dragoi et al., 2000), whether adaptation influences sensory coding in a layer-specific manner has never been investigated. The fact that neurons in the supragranular layers exhibit the largest increase in gamma synchronization after adaptation and the highest

correlation with the post-adaptation improvement in feature coding has functional implications for models of cortical function. Indeed, neurons in the supragranular layers of V1 provide the main cortical input to downstream visual areas. Therefore, neurons in higher-order cortices would benefit most if cells in the supragranular layers would exhibit a large increase in stimulus coding after adaptation.

The relationship between the post-adaptation change in gamma synchronization and neuronal discriminability described here should be interpreted cautiously. The fact that a large percentage of neurons in our population exhibited an increase in d' even in the absence of a corresponding increase in gamma coherence (in the granular and infragranular layers) indicates that neuronal synchronization may play a modulatory influence on feature coding. For instance, we and others have previously shown that incorporating synaptic depression in recurrent models of cortical adaptation may be sufficient to explain the increase in neuronal discrimination performance of individual neurons and networks (Dragoi et al., 2002; Teich and Qian, 2003). However, our analysis implies that the pronounced increase in gamma SFC after adaptation in the supragranular layers might have contributed to the larger change in neuronal discriminability shown by SG neurons (consistent with the computational model proposed in Wang et al., 2011; **Figure 6.18**).

The possible relationship between gamma synchronization and neuronal performance has been indirectly suggested by attention studies in mid-level cortical areas (Fries et al., 2001; Gregoriou et al., 2009). Theoretical studies have suggested that gamma oscillations of spiking neuronal populations can enhance signal discrimination by decreasing the variance of the

responses (Masuda and Doiron, 2007), and that synchronization could enhance the response gain of neurons (Salinas and Sejnowski, 2000). In addition, recent evidence indicates that selective activation of fast-spiking interneurons enhances the gamma rhythm and controls sensory responses (Traub et al., 1996; Cardin et al., 2009; Sohal et al., 2009). This raises the possibility that an increase in local inhibition due to adaptation (Chelaru and Dragoi, 2008) could subsequently cause an increase in gamma synchronization possibly to improve neuronal discrimination performance. This inhibition-based mechanism is consistent with our finding that the relationship between the adaptation-induced changes in gamma synchronization and neuronal discriminability is more prominent in the supragranular layers of V1. Indeed, anatomical results indicate that both the density of interneurons and the distribution of GABAb receptors (known to be involved in gamma oscillations) are highest in the supragranular and granular layers of V1 (Fitzpatrick et al., 1987; Whittington et al., 1995; Eickhoff et al., 2007). While the resolution of our laminar recording technique is unable to identify unique sub layer contributions (such as 3B or 4A), our results should be viewed in terms of the major laminar circuits in V1 of macaque monkeys (See chapter 2). Future experimental and theoretical work is needed to determine precisely the mechanism underlying laminar changes in neuronal synchronization after adaptation and its relationship with neuronal performance.

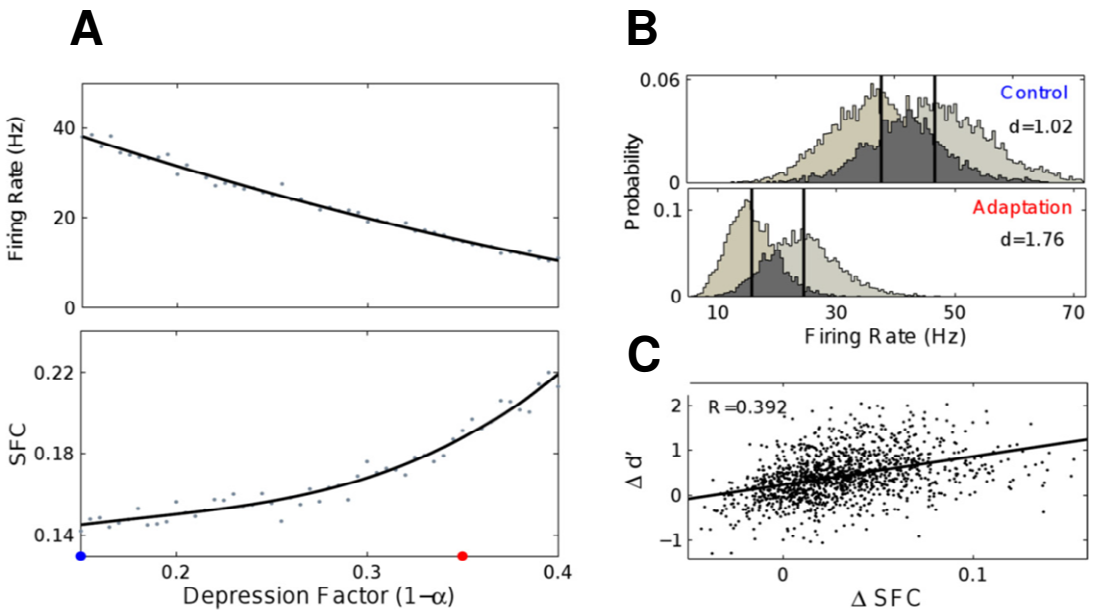

Figure 6.18. Short-term plasticity explains post-adaptation increase in SFC and *d'*
A network of 50 integrate-and-fire (IF) neurons with a 25% recurrent connection probability received input from a presynaptic population of 200 IF cells. All cells in the simulation received noisy background input with a strong spectral component at 60 Hz. Adaptation was assumed to scale the synaptic weights by a depression factor α. (**A**) Consistent with experimental data, the model network displayed decreasing response rate (top) and increasing SFC (bottom) with an increase in depression strength. (**B**) The responses to two different orientations are modeled by presenting two levels of input to the presynaptic population. Shown are the control (α = 0.85; blue dot) and adapted (α = 0.65; red dot) response distributions of responses from 50 cells to 90 presentations of the stimulus (4500 values in each distribution). Adaptation increased discriminability in the postsynaptic pool as measured by *d'*. The difference between the mean responses (vertical lines) remained high after adaptation, while the population response variance was decreased. (**C**) Change in discrimination performance (Δd') is positively correlated with the change in spike field coherence (ΔSFC). Shown are results obtained from network responses from 1000 trials with varying depression strength ($0.65 < \alpha < 1$). The line represents a regression fit. To emphasize the effect of recurrent connections, SFC was held constant in the presynaptic population in these simulations (provided by Wang et al., 2011; reprinted with permission).

“Under normal conditions the research scientist is not an innovator but a solver of puzzles, and the puzzles upon which he concentrates are just those which he believes can be both stated and solved within the existing scientific tradition.”

— Thomas Kuhn

7. RELATIONSHIP BETWEEN LAMINAR POPULATION CODING AND BEHAVIORAL PERFORMANCE

7.1 Introduction

Responses of cortical neurons are known to depend on their local network environment. As described in earlier chapters, in the primary visual cortex (V1), the input or granular layer, receives feedforward thalamocortical projections. Subsequently, neuronal impulses from the granular layer are transmitted to neurons in supragranular, or superficial, layers, which constitute the major cortical output of V1. Supragranular layers project to infragranular layers, which in turn project back to layer 4 and subcortical areas. Based on our results summarized in chapter 5, we hypothesize that neuronal populations in different cortical layers play different roles in network computation. That is, the input layer, which receives afferents from networks in hierarchically lower cortical or subcortical areas and have only local projections to other layers within the same cortical area, encode incoming stimuli optimally. In contrast, the layers that send projections to other cortical areas encode information such as to optimize information transmission and possibly as a result behavioral performance.

Population coding and its relationship to behavior are still largely unexplained, with only a handful of laboratories (including ours) attempting to address this very complex problem. Much of the work relating to behavioral performance and population coding has focused on issues of attention (Cohen and Newsome, 2008; Mitchel et al., 2009; Cohen and Maunsell, 2011). Importantly, these studies emphasize that analysis at the population level, as it relates to behavior, is important for understanding the potential mechanisms underlying attention and higher cognitive processes. In a recent study, Cohen and Maunsell, (2011)

devised a set of experiments in which they recorded from populations of neurons to approximate the amount of attentional resources (i.e. feature vs. spatial) distributed to a particular stimulus on a given trial. The main finding from this work is that feature and spatial attention have similar effects on measures of firing rate and correlations for local populations. However, spatial attention appears to be restricted to local populations, while feature attention has widespread effects across hemispheres (Cohen and Maunsell, 2011). The authors claim that simultaneously measuring populations of neurons provides a more accurate picture of the relationship between cognitive processes that affect behavior. That is, averaging responses across conditions neglects the population response and is therefore inappropriate to study cognitive mechanisms. While current research measuring population coding and behavior is focused on identifying the contribution of neurons to a given behavior, little emphasis is placed on the contribution of populations in different cortical layers.

Work from Schroeder and colleagues (Lakatos et al., 2007; Lakatos et al., 2008; Lakatos et al., 2009) has been instrumental in identifying laminar differences in population activity and behavioral responses associated with multi-modal attention. The authors performed a series of difficult experiments aimed at understanding the relationship between changes in oscillatory activity of the population response and behavioral performance on an intermodal (visual vs. auditory) selection task. In their most recent study, Lakatos et al. (2011) observed that through mechanisms of attention, networks in V1 and A1 undergo a "phase reset", irrespective of the stimulus modality, that is restricted to supragranular layers. They claim that this reset mechanism is important for controlling excitability of local populations. The main

finding from this and previous studies is that responses at the population level modulated by attention also influence the neurophysiological context and behavioral performance.

The experiments outlined in this chapter focus on population coding and the relationship to behavioral performance involving changes in the degree of synchronization via changes in the coherence between neuronal ensembles within and between cortical layers. Indeed, we have shown from the results in chapter 6 that layer-specific measures of coherence, particularly in the gamma frequency range, are important for sensory coding as measured by the improvement in neurons' ability to discriminate small changes in orientation. A logical extension from the results and conclusions presented in chapters 5 and 6 is to continue our laminar analysis of V1, but in the context of behavioral performance.

Understanding how neuronal synchronization relates to information processing among local networks is essential for understanding the relationship between efficient sensory coding and behavior. It has been proposed that one way networks of cells can efficiently process information about incoming stimuli is through changes in local oscillatory activity (measured as local field potentials, or LFPs), or synchronization (i.e. phase-locking) between spiking activity of multiple neurons and LFPs (Thiele and Stoner, 2003; Roelfsema et al., 2004; Taylor et al., 2005; Gregoriou et al., 2009). While neurophysiological investigations of synchronization have contributed to our understanding of how individual neurons and local networks process information (Gray et al., 1989; Engel et al., 1991a; Fries et al., 2001; Taylor et al., 2005; Womelsdorf et al., 2006; Cardin et al., 2009; Chalk et al., 2010), how this emerges within and between cortical layers to influence behavioral performance is still largely

unknown. Examining whether and how neuronal synchronization influences both network coding and behavioral performance is important for understanding the fundamental principles of efficient information coding by local neuronal networks.

We devised a novel set of experiments to examine how neuronal synchronization influences network processing in V1 and how it influences behavioral performance in an orientation discrimination task. These experiments use a newly developed technique in our laboratory consisting of multi-contact laminar electrodes that allow us to sample neuronal activity across all cortical layers simultaneously and assign neurons to specific cortical layers (methods summarized in chapter 5). We will test the hypothesis that individual neurons and local populations synchronize their activity in real-time to communicate information about incoming stimuli, and that the degree of synchronization modulates discrimination performance. These analyses will allow us to assess for the first time the relationship between changes in laminar cortical networks involved in stimulus processing and behavioral performance in awake-behaving primates.

7.2 Methods

All experimental procedures were performed in accordance with protocols approved by the US National Institutes of Health Guidelines for the Care and Use of Animals for Experimental Procedures.

7.2.1 Surgical procedure

The methods are similar to those described in chapter 5.

7.2.2 Electrophysiological recordings

Unique to these experiments, we used multi–contact laminar electrodes to record neuronal activity (spikes and LFPs) at multiple V1 recording sites (n = 160, 16 contacts x 10 sessions) of varying cortical depth while two non–human primates performed an orientation discrimination task (**Figure 7.1**). On average, we were able to identify 16 LFPs and 7-9 single-units per recording session. Each laminar electrode consisted of a linear array of 16 equally spaced contacts (100 µm inter-contact spacing) positioned to sample from all cortical layers simultaneously (Plextrode® U-Probe, Plexon Inc.; **Figure 5.1**). We performed laminar recordings to examine the change in the synchronization between neuronal groups in different cortical layers by calculating the coherence between neuronal ensembles. This analysis was performed by assigning the LFPs on each contact to a specific cortical layer (as previously described in chapters 5 and 6). We focused our analysis on measuring the LFP power as function of time and spike-LFP coherence when contacts of the laminar probe were identified as being in the same layer and when the contacts were in different layers.

7.2.3 Orientation discrimination task

The goal of these experiments was to assess within and between layer synchronization in the context of an orientation discrimination performance task (**Figure 7.1**). Specific to these behavioral recordings, we utilized a response bar device capable of indicating whether the monkey was holding the bar. In order to signal a difference between two stimuli, training procedures were conducted using a red-green color discrimination task in which the monkey was required to release the bar when the centrally located red square changed to green. This task served only as a way to train the monkey on the concept of 'same vs. different' in a two-alternative-forced-choice task (2-AFC). What follows is a detailed description of the main experiment. After a brief period of fixation (300 ms) animals were required to maintain fixation of a white dot at the center of a computer screen, while an oriented grating stimulus (either 45° or 135°) was flashed for 300 ms in the center of the neurons' receptive field. Stimuli were 5° circular sine wave gratings with a spatial frequency of 1.4 cycles per deg and a 50% contrast level presented binocularly. This part of the trial is referred to as the target. A delay period followed the target presentation and lasted 500 ms. After the delay, a second test grating stimulus was presented for 300 ms with stimulus features identical to those presented during the target but oriented either ± 10° or ± 20° away from target orientation (e.g. target = 45° test = 55°). The objective was for the monkeys to identify if the target stimulus orientation was the same as the orientation of test stimulus (*match*) or different (*non-match*). If the two gratings were the same, monkeys were trained to continue holding the response bar. Conversely, if the two gratings were perceived as being different, the monkey was trained to release the response bar. In all trials, monkeys were required to maintain their response (either hold or release) until

the stimulus and fixation point were removed from the screen. Correct trials were always followed by an apple juice reward and were based on identifying a *match* or identifying a *non-match.* Incorrect trials were followed by a brief 'time-out' and included those responses in which the monkey failed to identify a *match* or indicated that a *non-match* was a *match*. Trials in which the monkey broke fixation were excluded from the analysis and a criterion of 200 fixated trials (50 % *match*) was required.

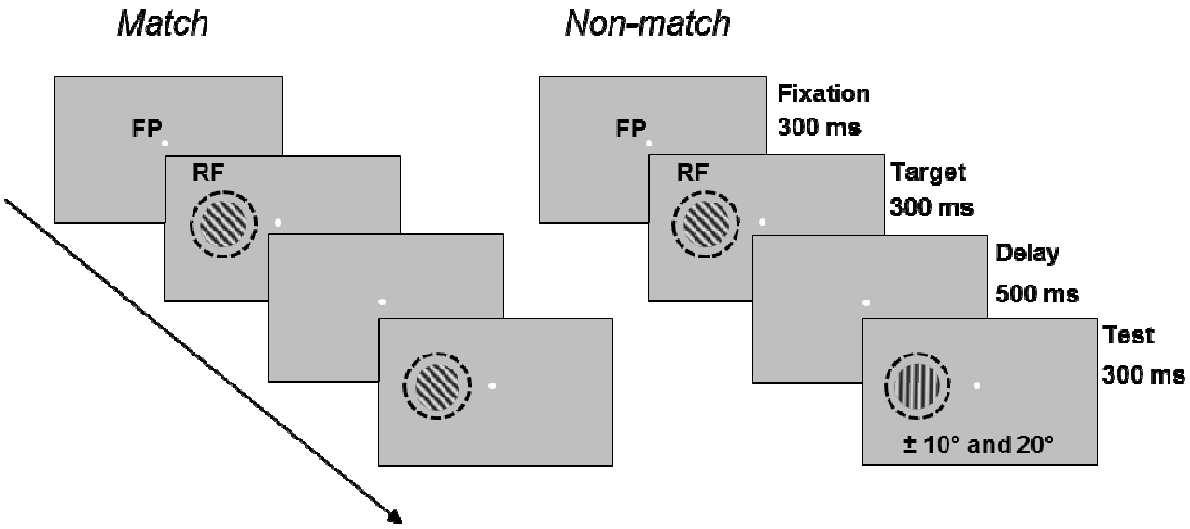

Figure 7.1. Orientation discrimination paradigm
While animals fixated a white dot at the center of a screen, an oriented stimulus was flashed for 300 ms in the center of the neurons' receptive field (target). After a 500 ms delay, a test stimulus identical to the target but oriented either ±10° or 20° was presented for 300 ms. Monkeys were required to indicate if the target and test were the same (*match*) or different (*non-match*). Across 200 trials, there was an equal probability of a trial being *match* or *non-match*. Test orientations were also randomly interleaved across trials.

7.2.4 Local field potential analysis

Low-frequency signals were pre-filtered between 0.7 to 170 Hz, further amplified, and digitized at 1 kHz as local field potentials. To correct for the time delays induced in the LFP signal by the filters in the headstage and preamplification boards, we used the software correction FPAlign provided by Plexon Inc. (http://www.plexon.com/downloads.html). LFPs were further filtered between 0.5 and 100 Hz using a fourth-order Butterworth filter. To remove line artifacts, we applied a digital notch at 60 Hz (fourth-order elliptic filter; 0.1 db peak-to-peak ripples; 40 db stopband attenuation). It is possible that artifacts from muscle activity (i.e. chewing) or other sources (i.e. line noise from the computers) will contaminate amplitude measures of the LFP. Therefore, we discarded all LFPs that had more than three standard deviations outside the mean. We estimated the LFP power density during the presentation of the target and test stimuli as well as during the delay and inter-trial interval using sliding windows of ±150 ms length in steps of 10 ms. We assessed whether LFPs are selective for orientation by measuring the tuning curve of the LFP amplitude and the LFP power spectrum. To obtain optimal spectral concentration for our spectral analysis (Mitra and Pesaran, 1999; Jarvis and Mitra, 2001; Pesaran et al., 2002; Womelsdorf et al., 2006), we used the multi-taper method by multiplying each data epoch with the taper and performing a Fourier transform (similar to those methods used in Chapter 7). The power spectral density was normalized from 0 to 1 by dividing the average power spectrum during the 300 ms fixation period before the presentation of the target stimulus (averaged across all trials in a session). This helped to balance the power spectrum between low and high frequencies within the same amplitude range (given that raw LFP power is dominate at low frequencies) and made it possible to

compare stimulus driven activity among recordings at different contacts across layers and at different brain states. We defined the average power of alpha, beta, and gamma bands according to the following frequency ranges: 8-14 Hz, 14-27 Hz, and 30-60 Hz.

7.2.5 Spike-field coherence

In order to explore synchronization between spiking activity of individual neurons and the local networks we computed spike-field coherence (SFC). Much of the analysis of coherence is similar to that described in chapter 6. Briefly, we implemented multi-taper spectral analysis to compute the SFC, which measures the degree of synchronization between neurons and LFPs as a function of frequency (Thiele and Stoner, 2003; Roelfsema et al., 2004; Taylor et al., 2005; Gregoriou et al., 2009; Chalk et al., 2010). In general, the coherence between two signals (x and y) recorded at different sites (i.e. laminar contacts) is a complex quantity whose magnitude is a measure of the phase synchrony for frequency f. Coherence is an absolute value that varies between 0 and 1 (e.g., a value of 1 indicates a perfect phase relationship between the firing of the spikes to the fluctuations of the LFP).

Previous and current research suggest LFPs represent local processing and serve as the cortical input to a given area with the resultant output represented as the spiking activity (Towe and Harding, 1970; Bartos et al., 2002). Importantly, we set out to determine how synchronization emerges between cortical layers during an orientation discrimination task. Specifically, we computed coherence between granular field potentials with spikes in supragranular layers. Coherence was also measured between field potentials in the

supragranular layer with spikes in the infragranular layer. In this way, we maintain the structure that is known about the anatomical pathways in V1 and assess functionally how synchronization between layers emerges during behavioral performance.

7.3 Results

7.3.1 Behavioral performance

The combination of behavioral tasks and electrophysiological techniques is useful because it allows one greater insight into how various properties associated with network synchronization (e.g. coherence) can potentially influence sensory coding and behavior. We assessed behavioral performance on the orientation discrimination task according to the percentage of correct (monkey W: 82.5%; monkey C: 89.9%) and incorrect trials (monkey W: 17.5%; monkey C: 10.1%). We further confirmed that across sessions (monkey W: 6; monkey C: 4) individual monkey performance was consistent between the number of *match* and *non-match* trials over the total number of correct trials. Indeed, both monkeys performed well, but did tend to have a greater percentage of *match* trials as they were more accustomed to holding the bar (**Figure 7.2**). Our subsequent analysis focused on measuring changes in LFP power and spike-field coherence across cortical layers specific to correct and incorrect trials. One interesting prediction is that discrimination in correct trials will increase the coherence only weakly when the two contacts are located in the same layer, but the increase in coherence will be more pronounced when the two contacts are located in different layers. This analysis will complement the analysis of layer-specific correlations (chapter 5) by testing whether coherence

improves efficient communication in a layer-specific manner by increasing the local synchronization between neuronal ensembles in different cortical layers possibly to influence information transmission within a cortical area.

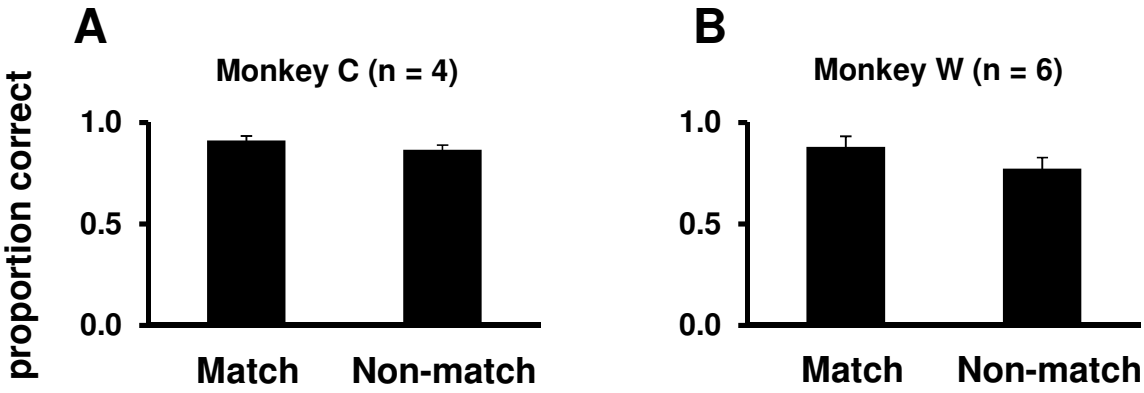

Figure 7.2. Discrimination performance
(**A-B**) We measured performance for each session in which Monkey C and W performed an orientation discrimination task. Percentage correct was calculated according to the number of correct trails in either the *match* or the *non-match* conditions. Importantly, we did not observe a significant difference between *match* and *non-match* consistent with idea that the monkeys were accurately identify changes in orientation.

7.3.2 Analysis of correct and incorrect trials

As described above we sorted all trials in a session into either correct or incorrect responses. Before measuring changes in LFP power and coherence, we first verified whether neuronal and LFP response properties are consistent across trials. For each recording session, we computed spike and LFP responses across all cortical layers discrimination and sorted trials according to correct or incorrect responses. The traces in **Figure 7.3** (left) show the mean LFP amplitude as a function of time produced by the stimuli evoking an increase in the response to the target (45° in this example), as well as the average response to the test for of all possible test orientations

(± 10° and 20°). **Figure 7.3** (right) shows representative spike responses recorded in the same session spanning all cortical layers. Overall, we conducted 10 recording sessions in which we were able to isolate 85 single-units across all cortical layers (SG: 31, G: 24, IG: 30) that exhibited significant response modulation by stimulus orientation (responses were measured for single-units throughout the test stimulus presentation). For the population of LFPs (10 sessions x 16 LFP = 160) we also observed consistent modulation in response amplitude between correct and incorrect trials. More importantly, our coherence analysis is based on the number of pairs between field potentials and single-units. For within layer coherence, we recorded 455 pairs across cortical layers (SG: 155, G: 120, IG: 180). For our between-layer analysis, we identified a total number of 305 pairs (155 for G→SG and 150 for SG→IG).

A possible confound in our analysis of correct and incorrect trials is that for some sessions (n = 3) the number of correct trials far outweighs the number of incorrect. For example, in a session consisting of 200 trials, the monkeys performance was ~ 90% correct leaving only 10% incorrect trials. For these sessions, we explored three methods to correct for this bias: (i) to compute a modified spike triggered average based on a correction factor for the difference between the number trials, (ii) to implement a statistically based bias correction utilizing the phase amplitude of the LFP, or (iii) to compute a modulation index that samples an equal number of incorrect trials from the correct trial pool (Bokil et al., 2007; Grasse and Moxon, 2010; Vinck et al., 2010). Based on my own results and the results from other members in the Dragoi laboratory each method yields highly similar results. For simplicity, we have implemented the modulation index method, which is considered a standard correction method.

For comparison purposes between sessions, our results reported in the following sections has been bias corrected and represented as both correct and incorrect or percentage change.

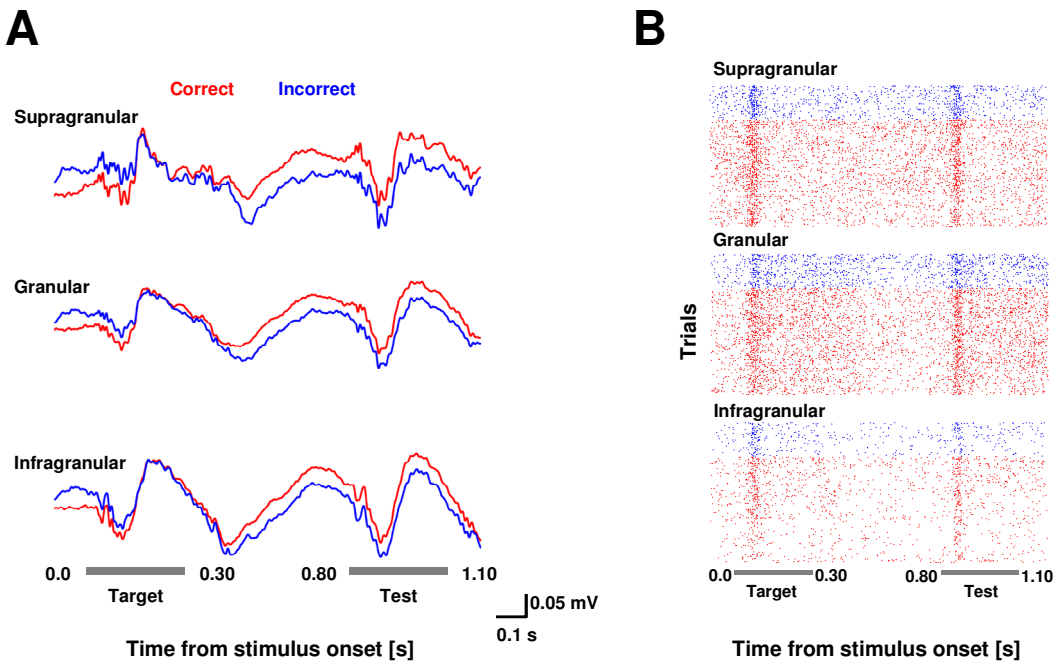

Figure 7.3. LFP and single-unit modulation in responses to target and test presentation (**A**) LFP traces represent examples of responses across cortical layers for a single penetration for correct (red) and incorrect trials (blue). LFP responses were clearly modulated during the presentation of the target (1st grey bar) and test (2nd grey bar) stimuli. Each trace represents the average response across all trials and test orientations in each condition (target = 45°). (**B**) The raster plots represent the spike times of three example V1 neurons across cortical layers responding to the target and test stimuli.

7.3.3 Spectral analysis of LFPs for correct and incorrect trials

The goal of these experiments is to examine whether and how changes in local oscillatory activity (i.e. measured as the power spectrum of the local field potential) across laminar cortical networks of V1 impacts behavioral performance. Given the known circuitry, we hypothesize that superficial layers will synchronize their activity in the gamma band which may be more important for orientation discrimination. We would expect this increase to be more consistent

during the presentation of the test stimulus for correct trials compared to incorrect. Conversely, we also expect to observe an increase in beta activity restricted deep layers. This hypothesis is motivated by the interplay between beta activity in deep layers and gamma activity in superficial layers known to underlie top-down signaling important for efficient transfer of information (Wang, 2011).

We estimated the LFP power density during the presentation of the target and test stimuli as well as during the delay using a sliding window of ±150 ms in length and an overlap step of 10 ms (**Figure 7.4**). While we expected to observe layer-specific beta and gamma modulation for correct trials, we do not report any significant difference between layers for correct or incorrect trials. This is not surprising given that the area of integration for an LFP consist of low-frequency extracellular voltage fluctuations that is believed to reflect the input to a given cortical area (within 250 to 500 μm of the recording electrode, Kruse and Eckhorn, 1996; Katzner et al., 2009). We would need to travel 3-5 contacts before we observed oscillatory activity from a distinct neuronal ensemble. Given these results, LFP power maybe insufficient in our experiment to identify laminar changes (but see Maier et al., 2011).

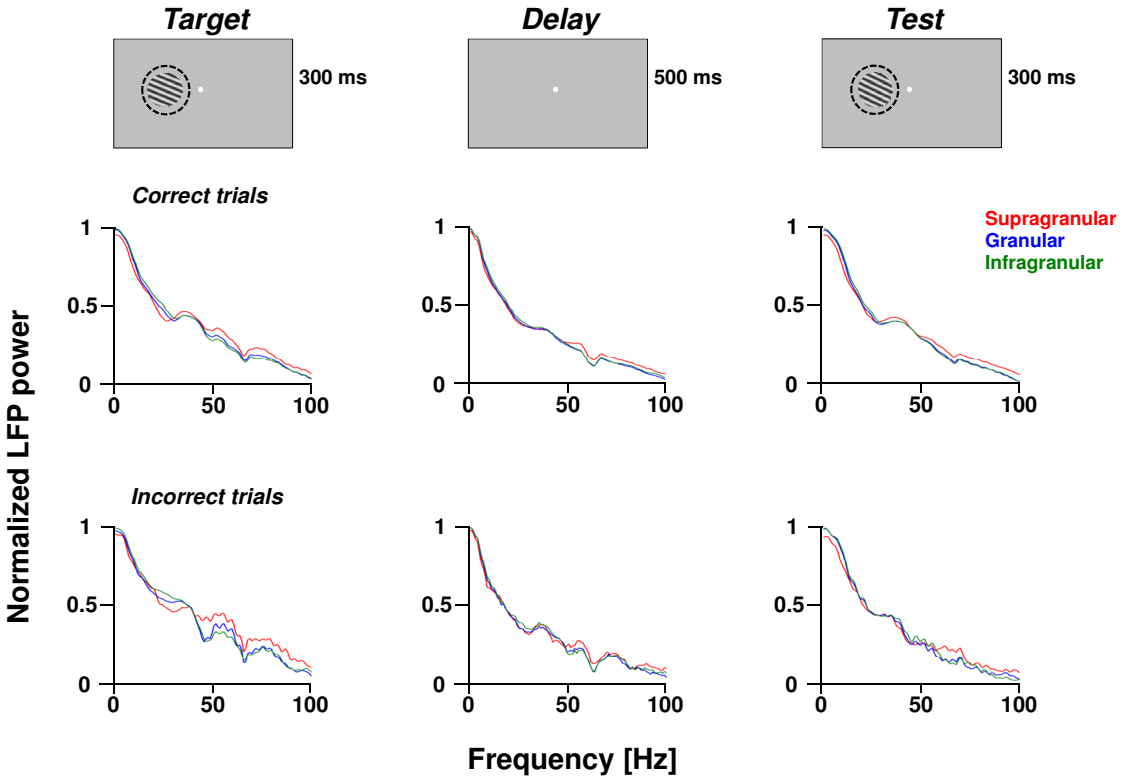

Figure 7.4. Average laminar LFP power for correct and incorrect trials
We computed the average normalized power spectrum for laminar LFPs within each cortical layer during the presentation of the target, delay, and test. We observed a slight 'bump' in the frequency range 40-50 Hz that is considered low gamma. The most consistent observation was that incorrect trials had increased variability compared to correct trials.

7.3.4 Within-layer increase in beta coherence during a discrimination task

Very little is known about how layer specific changes in neuronal synchronization influence behavioral performance. Based on the results from our LFP power spectrum analysis, we decided that a more appropriate method to examine neuronal synchronization is to measure spike-field coherence within and between specific laminar cortical networks during orientation discrimination. Consistent with recent theories of synchronization (Wang, 2011), we hypothesize that during the presentation of the test stimulus there will be an increase in gamma-band synchronization in the supragranular layers, suggesting a more efficient output network.

Conversely, neuronal synchronization in the beta band will be increased in deep layers during the presentation of the test stimulus for those trials in which the monkey correctly discriminates a change in orientation. Another predication from our study would be that while synchronization is beneficial for the efficient transfer of information within each layer, its presence during the delay period could be detrimental.

We measured spike-field coherence for pairs of field potentials and isolated single-units restricted to a given cortical layer (SG, G, or IG). We also limited our analysis to three specific time-periods: the target (300 ms), delay (500 ms), and test (300 ms) periods. We calculated the average coherence for those contacts in a given layer and time-window for all possible field potential and single-unit combinations as a function of frequency. We observed an increase in lower frequencies particularly in the beta band range (14-27 Hz) across all layers during the presentation of the target. Delay activity showed no layer or frequency specific changes. Additionally, during the presentation of the test stimulus, we also observed a consistent increase in beta activity specific to the supragranular and granular layers (**Figure 7.5**). Surprisingly, no increase in supragranular gamma-band activity was observed during the test period. While we expected to see beta band activity during the test period, we also observed increased activity during the presentation of the target. This increase in beta activity may underlie a general role of beta activity involved in broader cognitive processes. In agreement with our results, beta oscillations may also be involved in long-distance signaling along feedback pathways (Wang, 2011). While this idea is counterintuitive based on theories of network synchronization emphasizing increased activity in the gamma band related to improved behavioral performance, our study represent the first experimental evidence

investigating layer-specific changes in V1 synchronization during an orientation discrimination task.

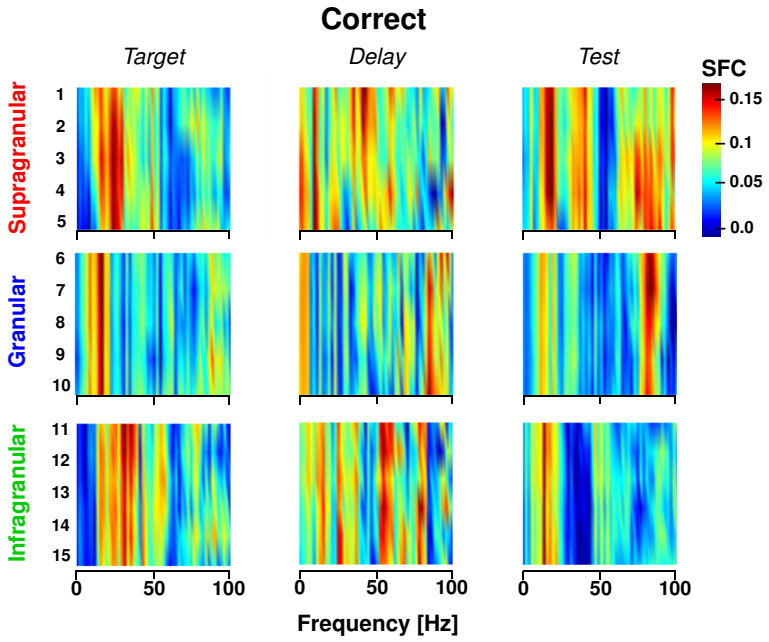

Figure 7.5. Example of within-layer spike coherence for correct trials
We measured spike-field coherence for pairs of field potentials and isolated single-units restricted to cortical layers (rows: SG, G, IG) and specific time-periods (columns: target, delay, and test). Each square represents the average coherence in a given layer and time window as a function of frequency. The numbers on the y-axis indicate the channel numbers of the LFPs assigned to a given cortical layer, based on the CSD analysis.

Analyses of incorrect trials in **Figure 7.6** yielded rather surprising results. While there was no layer or frequency specific changes during the target or delay periods, there was a supragranular layer increase in the alpha (8-14 Hz) and low beta (14-20 Hz) range during the presentation of the test stimulus. Of particular interest, incorrect trials across all periods and layers (mean SFC = 0.11), had a higher level of SFC compared to correct trials (mean SFC = 0.05). While an increase in synchronization is often interpreted as a sign of efficient network communication (Fries et al., 2001; Fries, 2005 Jensen et al., 2007), increased activity during incorrect trials suggests that it may hinder discrimination performance possibly due to the

oversaturation of the local networks. Consistent with this observation, it has recently been reported that alpha band activity (8-12 Hz) over posterior regions is increased in error trials (Busch et al. 2009; Mathewson et al. 2009). While our results are in the beta band range this may represent a general finding, in which the allocation of attentional resources alters low frequency activity in such a way that causes a higher rate of incorrect trials.

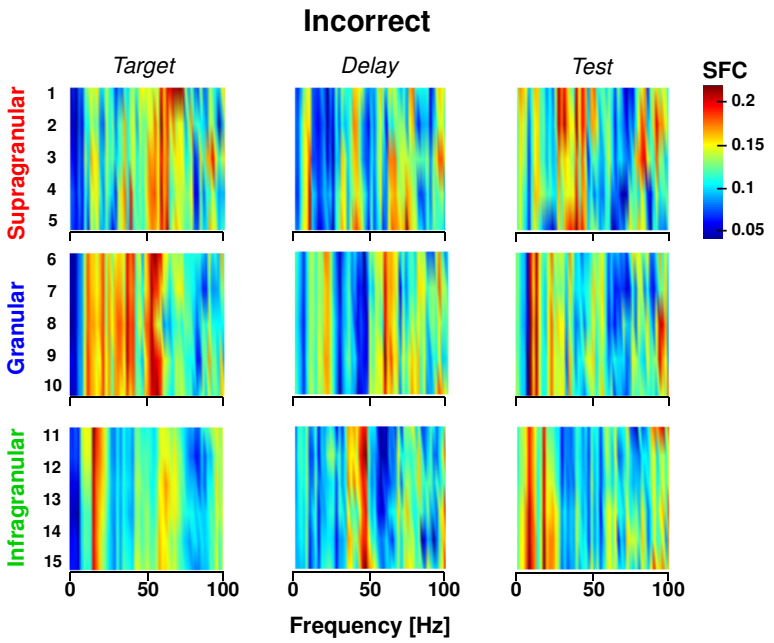

Figure 7.6. Example of within-layer spike coherence for incorrect trials
Same conventions used in **Figure 7.5,** but for incorrect trials. We observed that incorrect trials had a higher coherence level, but exhibited less layer and/or frequency specific responses.

We considered whether synchronization between field potentials and individual neurons in a given cortical layer influences orientation discrimination performance. Our analysis at the population level is summarized in **Figure 7.7** A**.** For the following results, we calculated the percentage change between incorrect and correct trials across the entire frequency range and observed significant difference between beta (14-27 Hz) and gamma (30-60 Hz) activity within

the same layer as well as significant difference for coherence across layers. We observed a significant difference between beta and gamma activity in the supragranular ($P < 0.05$, Wilcoxon rank-sum test) and granular ($P < 0.05$) layers during the target period (**Figure 7.7** B). Specifically for beta activity, we observed a significant difference between SG-G and SG-IG layers (one-way ANOVA, F (2, 24) =7.24, $P < 0.0035$; post-hoc multi-comparison, Tukey's Least Significant Difference), while the only significant difference for gamma activity was between G-IG (one-way ANOVA, F (2, 42) =4.63, $P < 0.0152$). Delay period activity remained unchanged across frequency, but we observed a significant percentage change in gamma-band coherence across all layers (one-way ANOVA, F (2, 42) =16.24, $P < 5.95\ 10^{-6}$; **Figure 7.7** B). We also observed an overall increase across all layers in the beta band during the presentation of the test (one-way ANOVA, F (2, 24) =12.73, $P < 1.70\ 10^{-4}$). Surprisingly, also during the test stimulus, gamma-band coherence was not significantly modulated across layers. ($P > 0.16$; **Figure 7.7** B). Our results are surprising – contrary to expectation, we observed that an increase in coherence, irrespective of cortical layer, impairs behavioral orientation discrimination performance. Of particular note, we did not observe any modulation in the gamma band as was expected based on our result in chapter 6. This is most likely due to changes in task demand and or attentional mechanisms. In comparison to the orientation discrimination task, we predict that our adaptation paradigm did not demand as much attentional focus. This idea is reinforced by the fact that that beta oscillations are modulated during tasks involving selective attention (Saalmann et al., 2007) as well as working memory (Tallon-B et al., 2001) and object recognition (Sehatpour et al., 2008); all cognitive processes that are being utilized during discrimination performance.

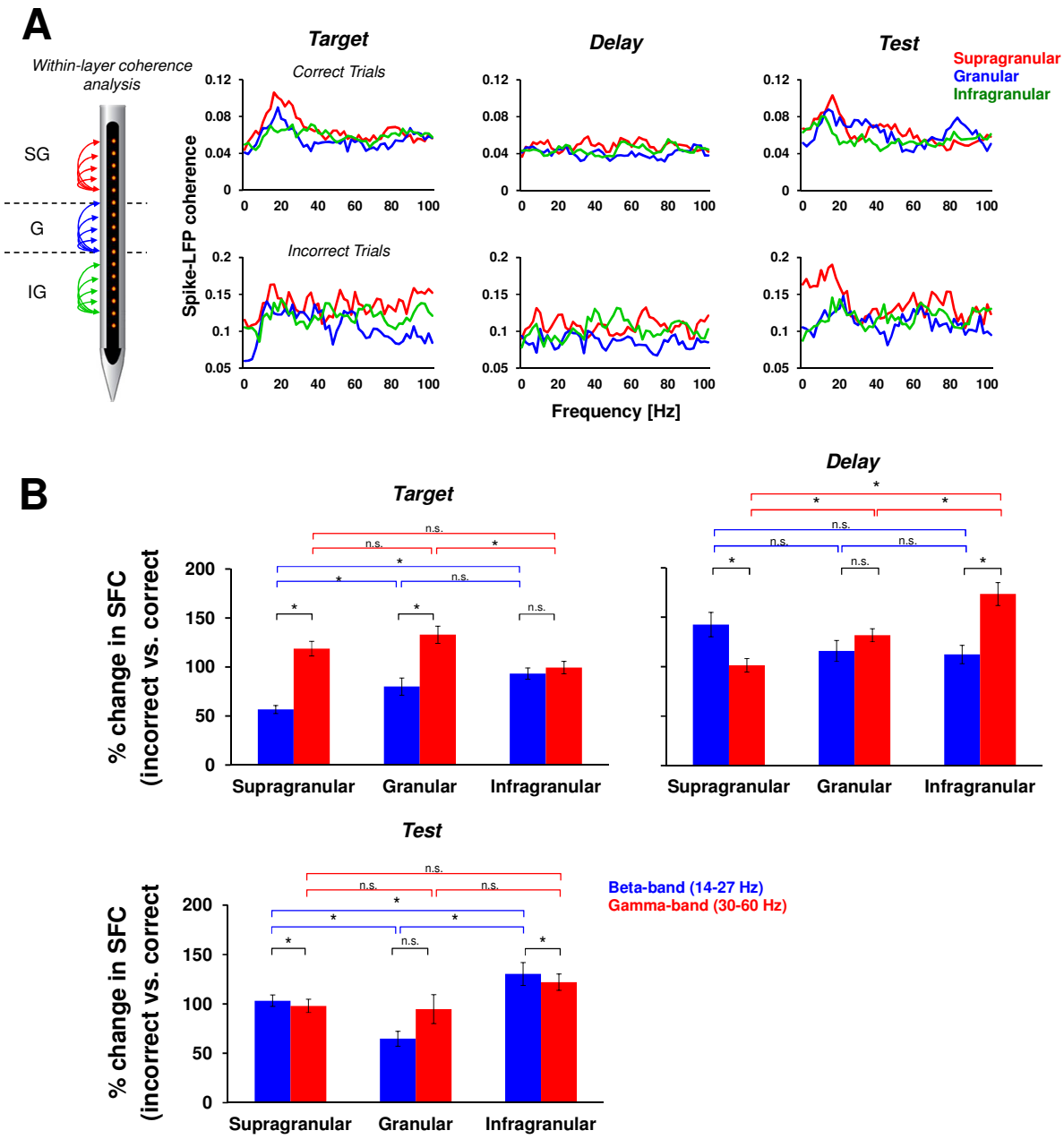

Figure 7.7. Population results for within-layer coherence analysis

(A) We calculated average SFC across sessions for correct (top row) and incorrect (bottom row) trials during three specific time-periods (columns: target, delay, and test). Each trace represents the average SFC within a given cortical layer (red- supragranular, blue- granular, green- infragranular) as a function of frequency. (**B**) We calculated the percentage change between incorrect and correct trials across the entire frequency range and observed significant difference between beta (blue) and gamma (red) activity within the same layer (black significant bars) as well as significant difference for coherence across layers (colored according to the frequency of interest).

7.3.5 Between-layer increase in beta coherence during a discrimination task

Based on extensive anatomical work (summarized in chapter 2) describing the structure of visual cortex and its laminar projects, we investigated whether and how changes in neuronal synchronization between laminar cortical networks of V1 influence behavioral performance. To reiterate, previous research has suggested that the major input to a local network manifests as the local field potential, with the spiking activity hypothesized to reflect local network output (Towe and Harding, 1970; Bartos et al., 2002). We tested the following hypotheses that neuronal synchronization in the beta and gamma bands between G→SG and SG→IG is increased during those trials in which the monkey makes a correct discrimination. Conversely, during trials in which the monkey responds incorrectly, there will be a decrease in neuronal synchronization between layers. If true, the analysis of inter-layer coherence may serve to explain better the observed differences in discrimination due to changes in laminar dependent population activity. This hypothesis is further motivated by research from two studies showing that beta activity, not gamma, is particularly important during cognitive tasks measuring inter-areal coherence (Buschman and Miller, 2007; Pesaran et al., 2008).

Similar to the within-layer analysis presented in the previous section, we now investigated whether spike-field coherence is increased between field potentials in the granular layer and spikes in supragranular. In this example, we are plotting the coherence between LFP_G and $spikes_{SG}$ for correct trials across the three time-periods of interest (**Figure 7.8**, top row). We can observe clear increases in low frequency activity in the beta-band range during the presentation of the target and test; meanwhile, the activity in the delay period remained

unchanged. For coherence between LFP_{SG} and $spikes_{IG}$ (**Figure 7.8**, bottom row) there seems to be a similar increase in low frequency activity, but to a lesser extent than G→SG.

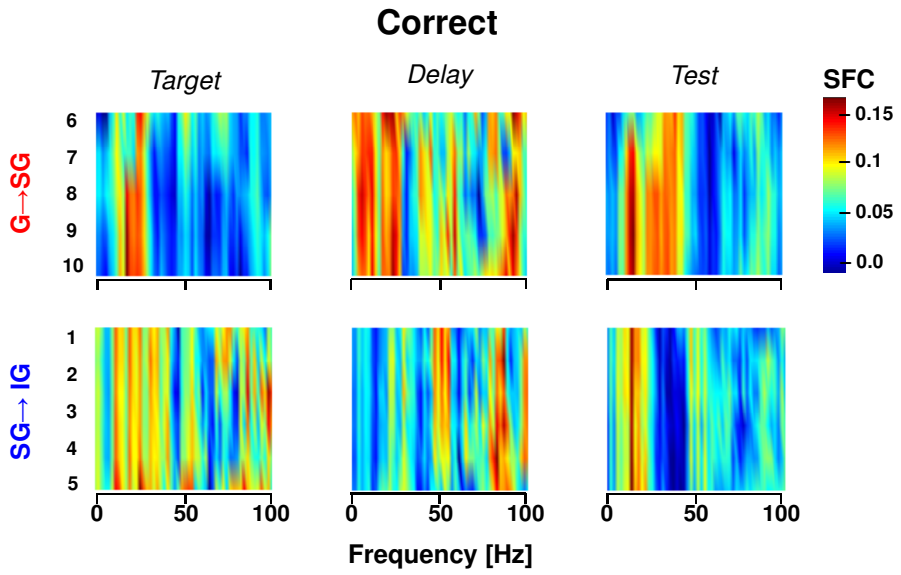

Figure 7.8. Example of between-layer spike-field coherence for correct trials
Same conventions used in **Figure 7.5**. We measured spike-field coherence for pairs of LFPs and isolated single-units between cortical layers (rows: G→SG, SG→IG) and specific time-periods (columns: target, delay, and test). Each square represents the average coherence for all pair combination between layers for a given time window as a function of frequency. The numbers on the y-axis indicate the channel numbers of the LFPs assigned to a given cortical layer, based on the CSD analysis.

For, the between-layer analysis for incorrect trials (**Figure 7.9**), we observed a consistent increase in beta activity during the presentation of the target and test stimuli. Again, we observed an overall higher level of coherence for incorrect trials (mean SFC = 0.12) compared to correct trials (mean SFC = 0.06). Possibly, these changes in coherence will be the result of differences in firing rate across trials. Further analysis of the firing rate between correct and incorrect trials failed to observe a significant difference ($P > 0.2$, Wilcoxon signed-rank test).

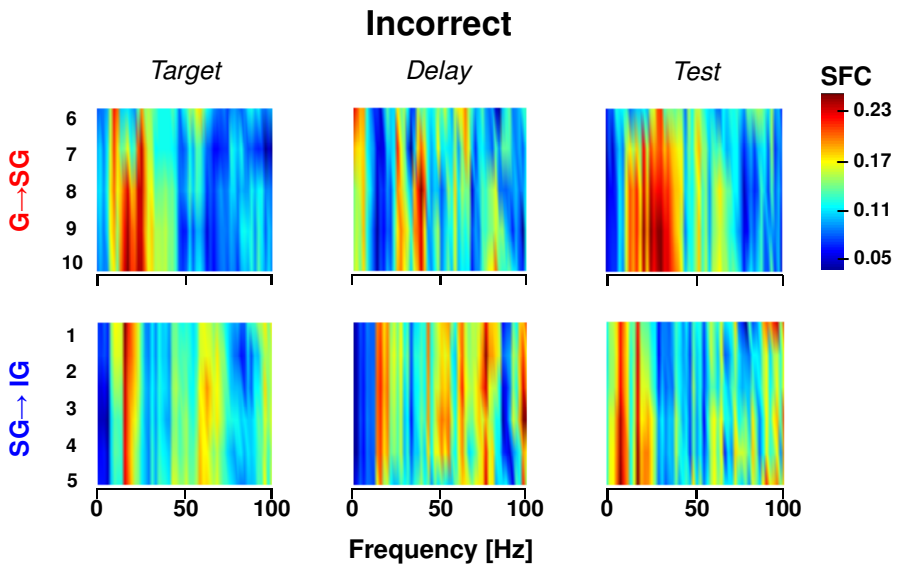

Figure 7.9. Example of between-layer spike-field coherence for incorrect trials
Same conventions used in **Figure 7.8,** but for incorrect trials.

In summary, for correct trials we observed a clear increase in beta activity for G→SG pairs during the target period (**Figure 7.10** A, top row, red traces). For incorrect trials (**Figure 7.10** A, bottom row, red traces) we observed a similar increase in beta coherence during the target, while activity in the alpha and low beta frequency was more prominent during the test. For both correct and incorrect trials, delay period activity remained unchanged across frequency. Further analysis of our between layer pairs (SG→IG; **Figure 7.10** A, top and bottom rows, blue traces) showed no specific frequency modulation during either the presentation the target or during the delay period. However, during the test period we observed an increase in coherence in the alpha/low beta range for correct trials and more beta activity for incorrect trials. Comparing the results between correct and incorrect, we observed a significant percentage change between beta and gamma activity for G→SG pairs ($P < 0.03$, Wilcoxon signed-rank test).

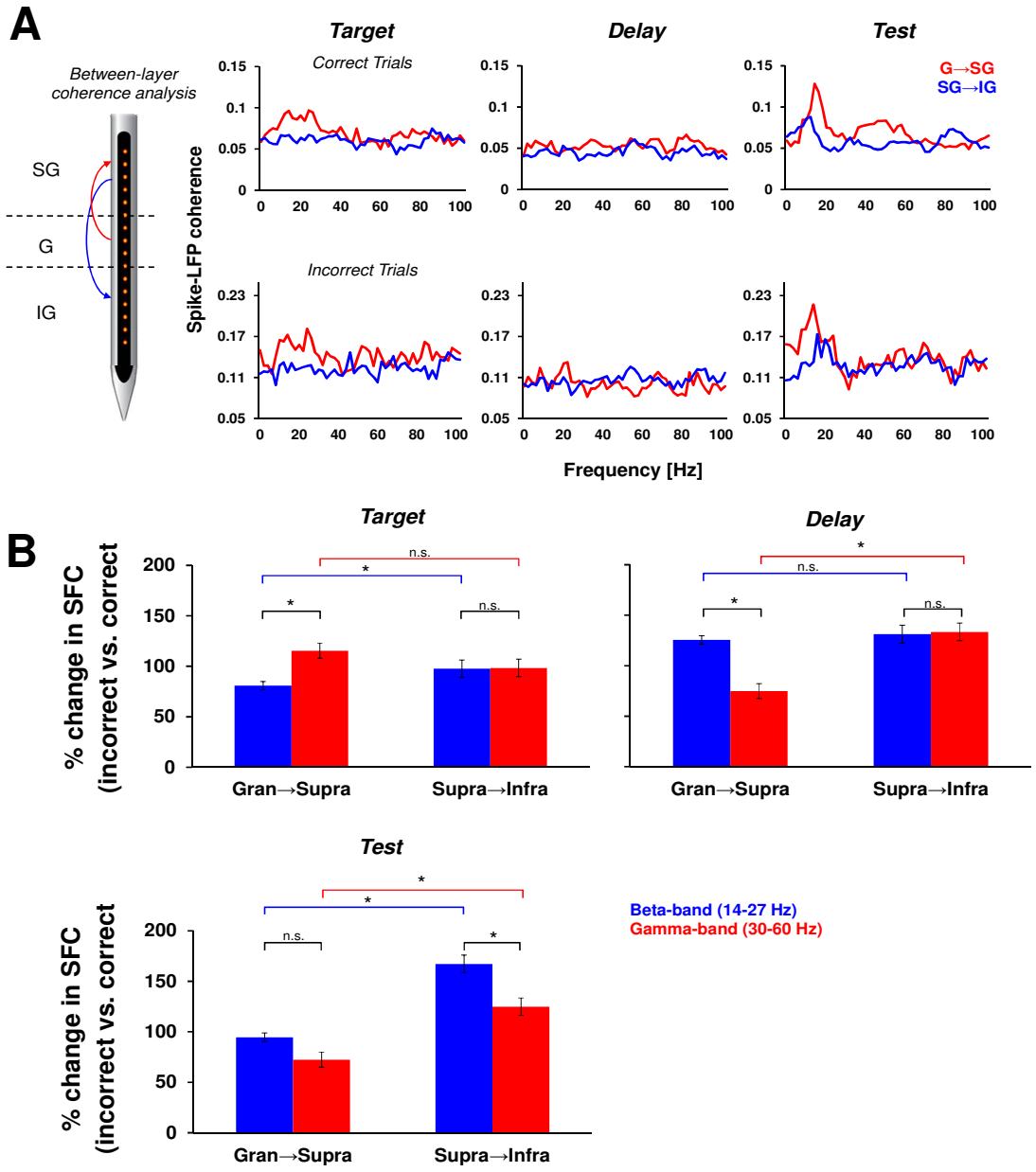

Figure 7.10. Population results for between-layer coherence analysis

(**A**) We calculated average SFC across sessions for correct (top row) and incorrect (bottom row) trials during three specific time-periods (columns: target, delay, and test). Each trace represents the average SFC between cortical layer (red, LFP_G and $spikes_{SG}$; blue, LFP_{SG} and $spikes_{IG}$) as a function of frequency. (**B**) We calculated the percentage change between incorrect and correct trials across the entire frequency range and observed significant difference between beta (blue) and gamma (red) activity within the between layer pairs (black significant bars) as well as significant difference for coherence across between layers pairs (colored according to the frequency of interest).

Specific to beta band activity, there was a significant difference between those pairs between G→SG compared to SG→IG ($P < 0.01$, Wilcoxon rank-sum test; **Figure 7.10** B). Surprisingly, for the SG pairs there was also an increased bump of activity centered on the gamma-band (30-60 Hz) during the test period ($P = 1.22\ 10^{-4}$, Wilcoxon rank-sum test; **Figure 7.10** B). One possible explanation for the increase in beta and gamma activity is the interplay between maintaining the target orientation in visual short-term memory and integrating the orientation of the test to communicate efficiently a correct discrimination. Importantly, the increase in gamma activity was only seen during the test period for correct trials.

7.4 Conclusions

Indeed, it has been proposed that one way in which networks of cells can efficiently process information about incoming stimuli is through either changes in local oscillatory activity (measured as LFPs) or synchronization (i.e. phase-locking) between the spiking activity of multiple neurons and LFPs. In this chapter, we examined whether and how neuronal synchronization influences stimulus processing and discrimination performance within and between cortical layers in V1. We devised a novel set of experiments that investigated to what extent neuronal synchronization influences network processing in V1 and how it influences discrimination performance in an orientation discrimination task. We tested the general hypothesis that individual neurons and local populations synchronize their activity in real-time to communicate information about incoming stimuli, and that the degree of synchronization modulates discrimination performance.

Surprisingly, we observed that during an orientation discrimination task laminar circuits displayed an overall decrease in synchronization for correct trials, irrespective of cortical layers. While counterintuitive to what we expected, we observed an increase in network synchronization in the beta band for those trials in which the monkey responded incorrectly. While we mainly focused our analysis on two frequency bands, beta and gamma, both known to have effects associated with task performance and stimulus modulation, we failed to identify a clear modulation in either frequency range across any the time-periods of interest (target, delay, or test). Another goal of this research was to identify key laminar difference, within and between cortical layers, in coherence related to discrimination performance.

We failed to identify a clear layer-specific modulation in either beta or gamma band for either correct or incorrect trials. This is puzzling given our previous results (summarized in chapter 6) in which we observed a clear gamma frequency and laminar dependent relationship for supragranular neurons in response to a rapid adaptation task. It is possible that some of these finding maybe due to changes in attentional mechanisms or network states. Considering our task design, we presented an equal number of *match* and *non-match* trials randomly interleaved and our SFC analysis was computed by averaging across trials for different conditions. Thus, in this way if attentional mechanisms were changing across trials than our analysis would have controlled for any variability in responses by averaging; thus, attention is not able to account for our results.

While it is commonly believed that increased synchronization is associated with improved performance and network efficiency, we have observed that synchronization in V1 is

reduced during correct orientation discrimination. Future experimental studies will need to address to what extent this desynchronized network extends to other behavioral tasks and how attention modulates network synchronization.

“It would be possible to describe everything scientifically, but it would make no sense; it would be without meaning, as if you described a Beethoven symphony as a variation of wave pressure.”

— Albert Einstein

8. GENERAL DISCUSSION

To reiterate, one of the fundamental questions in neuroscience is to understand how the encoding of sensory inputs is distributed across neuronal networks to influence sensory processing and behavioral performance. Indeed, sensory processing is a phenomenon that requires network interactions. The fact that the structure of local cortical networks is organized according to unique cortical layers raises the possibility that sensory information could be processed differently in distinct layers. In this thesis, I studied three main aspects of population coding across laminar cortical circuits in V1 with the goal of understanding how sensory information is encoded in population activity (chapter 5), how the properties of the population code adapt to changes in visual input (chapter 6), and how population coding influences behavioral performance (chapter 7).

First, I studied the structure of noise correlations in V1 laminar circuits. While significant progress has been made in our understanding of differences in response properties of neurons across cortical layers (Buffalo et al., 2011; Hansen and Dragoi, 2011; Lakatos et al., 2009; Maier et al., 2010; Maier et al., 2011), whether and how neuronal populations encode information in a laminar–dependent manner remains unclear. We found that correlations between neurons depend strongly on the local network context – whereas neurons in the granular layer showed virtually no correlated variability, neurons in supragranular and infragranular layers exhibited strong response correlations.

Our study could potentially shed light on the recent controversy in the field regarding the issue of correlated variability (Cohen and Kohn, 2011). Despite the fact that strong trial-by-

trial correlated variability has long been reported in primary visual cortex (Bair et al., 2001; Kohn and Smith, 2005; de la Rocha et al., 2007; Gutnisky and Dragoi, 2008; Smith and Kohn, 2008; Nauhaus et al., 2009), recent evidence from Ecker et al. (2010) has suggested that neuronal correlations are much lower than previously thought. Our study offers experimental evidence in support of the idea that correlations in the granular layer of V1 are an order of magnitude weaker compared to the correlations in output layers.

We found that populations of neurons in different cortical layers employ different coding strategies. By operating in a virtually uncorrelated state, cells in the granular layer (which receive afferents subcortical areas and have only local projections to other layers within V1) may encode incoming stimuli more accurately than cells in the supragranular and infragranular layers (based on the results of a model and using linear decoders). In contrast, the output layers (supragranular and infragranular), which send projections to other cortical and subcortical areas, possibly encode information less accurately by exhibiting large correlated variability.

The fact that our results suggest that response decorrelation in the granular layer may be beneficial for sensory discriminations raises the issue of whether the higher correlations in supragranular and infragranular layers are detrimental for the information that V1 transmits to other cortical areas. However, this is not likely to be the case. Whereas neuronal responses in the granular layer may be optimized for sensory discrimination, the processing of information is mostly local. In contrast, neurons in the supragranular and infragranular layers use long-range cortical projections to process afferent inputs in a context-dependent manner (Gilbert and

Wiesel, 1989; Feldmeyer et al., 2002; Briggs and Callaway, 2005). Long-range horizontal connections are essential for performing complex computations such as contour grouping (Roelfsema et al., 2004), or figure-ground segregation (Salinas and Sejnowski, 2000), which may rely on strong correlations between neurons. In addition, theoretical studies have suggested that correlated inputs are transmitted more efficiently than decorrelated inputs (van der Togt et al., 2006), thus supporting the idea that the increase in correlations in the output layers of V1 may be functionally beneficial.

Aside from a study in anesthetized cat V1 reporting pronounced adaptive effects irrespective of cortical depth (Dragoi et al., 2000), whether and how the properties of the population code adapt to changes in visual input in a layer-specific manner has never been investigated. The key result of our study (Hansen and Dragoi, 2011) is that rapid adaptation increases the degree of spike-field coherence in the gamma-band frequency (30-80 Hz) in a layer-specific manner, and that these changes in synchronization are associated with an improved coding performance by V1 neurons. This raises the possibility that layer-specific adaptive synchronization between the spiking activity of individual neurons and their local population may be used to enhance coding schemes for sensory discrimination. In addition, the fact that neurons in the supragranular layers exhibited the largest increase in gamma synchronization after adaptation and the highest correlation with the post-adaptation improvement in feature coding has functional implications for models of cortical function. Specifically, theoretical studies have suggested that gamma oscillations of spiking neuronal populations can enhance signal discrimination by decreasing the variance of the responses

(Masuda and Doiron, 2007), and that synchrony could enhance the response gain of neurons (Salinas and Sejnowski, 2000), and facilitate learning and decoding (Masquelier et al., 2009).

The possible relationship between gamma synchronization and neuronal performance has been indirectly suggested by attention studies in mid-level cortical areas (Fries et al., 2001; Gregoriou et al., 2009). Theoretical studies have suggested that gamma oscillations of spiking neuronal populations can enhance signal discrimination by decreasing the variance of the responses (Masuda and Doiron, 2007), and that synchronization could enhance the response gain of neurons (Salinas and Sejnowski, 2000). In addition, recent evidence indicates that selective activation of fast-spiking interneurons enhances the gamma rhythm and controls sensory responses (Traub et al., 1996; Cardin et al., 2009; Sohal et al., 2009). This raises the possibility that an increase in local inhibition due to adaptation (Chelaru and Dragoi, 2008) could subsequently cause an increase in gamma synchronization possibly to improve neuronal discrimination performance. This inhibition-based mechanism is consistent with our finding that the relationship between the adaptation-induced changes in gamma synchronization and neuronal discriminability is more prominent in the supragranular layers of V1. Anatomical results indicate that both the density of interneurons and the distribution of GABAb receptors (known to be involved in gamma oscillations) are highest in the supragranular and granular layers of V1 (Fitzpatrick et al., 1987; Whittington et al., 1995; Eickhoff et al., 2007).

The relationship between the post-adaptation change in gamma synchronization and neuronal discriminability described here should be interpreted cautiously. The fact that a large percentage of neurons in our population exhibited an increase in d' even in the absence of a

corresponding increase in gamma coherence (in the granular and infragranular layers) indicates that neuronal synchronization may influence feature coding. For instance, we and others have previously shown that incorporating synaptic depression in recurrent models of cortical adaptation may be sufficient to explain the increase in neuronal discrimination performance of individual neurons and networks (Dragoi et al., 2002; Teich and Qian, 2003).

The final experiments addressed in this thesis were to study network synchronization as it relates to behavioral performance. In congruence with the goal of systems neuroscience to understand the relationship of brain activity to cognitive behavior, in chapter 7 we explored the relationship between sensory coding in laminar circuits and behavioral performance. Two ways in which networks of cells can efficiently process information about incoming stimuli is either through changes in local oscillatory activity (i.e. measured as the power spectrum of the LFPs) or synchronization (i.e. measured as the phase-locking between spiking activity and LFPs). Examining whether and how neuronal synchronization influences stimulus processing and behavioral performance is important for understanding the fundamental principles of efficient information coding by local neuronal networks. We devised a set of experiments to examine how neuronal synchronization influences laminar-dependent population coding in V1 and how synchronization influences behavioral performance in an orientation discrimination task. These analyses allowed us for the first time to assess the relationship between changes in laminar cortical networks involved in stimulus processing and behavioral performance in awake-behaving monkeys.

Surprisingly, we observed that during an orientation discrimination task laminar circuits displayed an overall decrease in synchronization for correct trials, irrespective of cortical layers. While counterintuitive to what we expected, we observed an increase in network synchronization in the beta band for those trials in which the monkey responded incorrectly. While we mainly focused our analysis on two frequency bands, beta and gamma, both known to have effects associated with task performance and stimulus modulation, we failed to identify a clear modulation in either frequency range across any of the time-periods of interest (target, delay, or test).

Overall, this thesis contributes to the study of population coding, specifically how information is processed within and between cortical layers (Hansen, et al., 2011). We investigated to what extent individual neurons and networks convey visual information through measures of correlated variability and synchronization in the context of rapid adaptation and discrimination performance. Each of these projects builds on the other by studying how laminar circuits encode information in their population activity (chapter 5), how the properties of the population code adapt to changes in visual input (Hansen and Dragoi, 2011), and how population coding influences behavioral performance (chapter 7).

8.1 Open questions and future directions

While much insight into network activity has been gained from identifying and studying neuronal process across cortical layers, this represents only the first step. Information about layers has been studied to some extent in previous research (Buffalo et al., 2011; Lakatos et al.,

2008; Sun and Dan, 2009; Maier et al., 2010), but our ability to assess changes in the correlation structure and synchronization simultaneously across cortical layers represents a novel approach to study population coding that has ever been tested experimentally until now. The analysis performed in this thesis has raised several important questions and has laid the groundwork for future experiments.

The electrode technology that contributed to the development of the multi-contact laminar electrode is a relatively recent improvement over existing single electrodes. Much of the experimental focus and impetus behind multi-contact electrodes has been to maximize the number of units one can record from simultaneously, while still maintaining a high signal-to-noise ratio. The current incarnation of the laminar electrode, used throughout our experiments, is capable of recording electricity activity, both LFPs and spikes, across 16 equally spaced contacts. We have reported that our yield is on average 6-8 single-units and 14-16 LFPs. At this current configuration, we have been able to identify cortical layers as supragranular, granular, and infragranular. While this technology represents an advancement in our understanding of population coding, it lacks the precision needed to identify individual layers (e.g. differences between 2 and 3) and sublayers (e.g. 4Cα) of the visual cortex. Future work based on improving the ability to resolve single-unit activity, such as coating with carbon nanotubes, as well as improving current-source density analysis, such as subspace mapping (personal communication B. Cummings), will allow us to identify cortical layers with greater resolution.

To what extent do different cell types (excitatory or inhibitory) contribute to changes in correlations and synchronization? To examine the specific contributions of different cell types,

greater emphasis should be placed on identifying single-units and distinguishing them between fast (putative inhibitory) and regular spiking (putative excitatory) neurons. This approach requires sophisticated analysis of spike-waveform characteristics (i.e. a narrow width is typically characteristic of inhibitory cells, Cardin et al., 2009; Mitchell et al., 2007). Relevant to coherence analysis, the ability to identify specific cell types of neurons would be very informative in confirming theories that inhibitory neurons underlie local oscillations in the gamma band to influence efficient network processing (Fries et al., 2001; Fries, 2005; Jensen et al., 2007). In addition to coherence analysis between specific cell types, this information could help to construct more realistic computational models of network activity. That is, if we are able to identify the number of excitatory and inhibitory neurons contributing to a particular measure, we can then model this behavior, providing a clearer picture of the interactions between cell types as well as their laminar position. Previous work in the Dragoi laboratory has explored the distribution of excitatory and inhibitory neurons in V1, but whether there is a clear dependency on cortical layers still remains to be tested.

Our analysis of laminar correlations is the best example in this thesis of a need to further define neurons into classes (e.g. by cortical layers) and explore the various relationships (e.g. noise correlations) between classes. The results of the laminar correlation project presented in chapter 5 represent the first experimental evidence suggesting that the structure of correlations depends largely on the local network context. While the initial focus of this project was to reconcile the recent findings of Ecker et al, (2010) and Renart et al. (2010), we have since developed numerous projects extending these results exploring new aspects of negative correlations and cross-correlations.

However, the debate will continue to identify what the possible mechanism(s) is that underlies these laminar differences and what is the most appropriate method(s) needed to identify such differences. Future challenges for systems neuroscience, specifically measuring correlations, will be to identify to what extent temporal (Bair et al., 2001; Smith and Kohn, 2008) and spatial aspects (Smith and Kohn, 2008) can influence correlations. Further investigation will also explore the dependence of correlation measures on stimulus attributes (e.g. contrast and stimulus size; Kohn and Smith, 2008; Nauhaus et al., 2009) and cognitive factors (e.g. attention; Mitchell et al., 2009; Cohen and Maunsell, 2009). However, as a community we must come to an agreement that the methods employed between research groups is consistent. It may be the right time to move beyond correlations as a 'tool' to investigate cortical connectivity, and focus on other aspects of neuronal responses that will take into consideration information associated with incoming stimuli and lateral connections to produce a more accurate prediction of network responses (Pillow et al., 2008).

Analysis of synchronization between local field potentials and single-unit activity has served as the basis for our understanding of how cortical networks process and efficiently communicate stimulus information. The collective body of research exploring measures of coherence in a number of brain regions and across a variety of behavioral tasks has been instrumental in establishing a foundation for future research. The work summarized in this thesis hopefully provided the next level of understanding by exploring effects within and between layers during tasks involving both adaptation and orientation discrimination. The other main goal of this thesis was to provide insight into how a given layer processes visual information. This analysis in itself provides another foundation to continue exploring inter-

areal and layer coherence. While the results summarized in chapter 6 and 7 provide only one side of the story as to what is going on within V1, the future goal is to explore communication between visual areas (i.e. V4 and IT) in the hierarchy. Indeed, current work is focusing on this very difficult problem by carrying-out dual recordings in area V1 and V4 using laminar probes while the monkey is performing an orientation discrimination task.

9. REFERENCES

1. **Abbott LF, Dayan P** (1999) The effect of correlated variability on the accuracy of a population code. Neural Comput 11:91-101.

2. **Aertsen AM, Gerstein GL, Habib MK, Palm G** (1989) Dynamics of neuronal firing correlation: modulation of "effective connectivity". J Neurophysiol 61:900-917.

3. **Ahissar E, Vaadia E, Ahissar M, Bergman H, Arieli A, Abeles M** (1992) Dependence of cortical plasticity on correlated activity of single neurons and on behavioral context. Science 257:1412-1415.

4. **Alonso JM, Martinez LM** (1998) Functional connectivity between simple cells and complex cells in cat striate cortex. Nat Neurosci 1:395-403.

5. **Andersen P, Andersson SA** (1968) Physiological basis of the alpha rhythm: Plenum Pub Corp.

6. **Anderson J, Lampl I, Reichova I, Carandini M, Ferster D** (2000) Stimulus dependence of two-state fluctuations of membrane potential in cat visual cortex. Nat Neurosci 3:617-621.

7. **Angelucci A, Bressloff PC** (2006) Contribution of feedforward, lateral and feedback connections to the classical receptive field center and extra-classical receptive field surround of primate V1 neurons. Prog Brain Res 154:93-120.

8. **Angelucci A, Levitt JB, Walton EJ, Hupe JM, Bullier J, Lund JS** (2002) Circuits for local and global signal integration in primary visual cortex. J Neurosci 22:8633-8646.

9. **Arnal LH, Wyart V, Giraud AL** (2011) Transitions in neural oscillations reflect prediction errors generated in audiovisual speech. Nat Neurosci 14:797-801.

10. **Averbeck BB, Lee D** (2004) Coding and transmission of information by neural ensembles. Trends Neurosci 27:225-230.

11. **Averbeck BB, Romanski LM** (2006) Probabilistic encoding of vocalizations in macaque ventral lateral prefrontal cortex. J Neurosci 26:11023-11033.

12. **Bair W, Zohary E, Newsome WT** (2001) Correlated firing in macaque visual area MT: time scales and relationship to behavior. J Neurosci 21:1676-1697.

13. **Baker SN** (2007) Oscillatory interactions between sensorimotor cortex and the periphery. Curr Opin Neurobiol 17:649-655.

14. **Baker SN, Olivier E, Lemon RN** (1997) Coherent oscillations in monkey motor cortex and hand muscle EMG show task-dependent modulation. J Physiol 501 (Pt 1):225-241.

15. **Barlow HB, Foldiak P** (1989) Adaptation and decorrelation in the cortex. in The Computing Neuron. Wokingham, England: Addison-Wesley.

16. **Bartos M, Vida I, Frotscher M, Meyer A, Monyer H, Geiger JR, Jonas P** (2002) Fast synaptic inhibition promotes synchronized gamma oscillations in hippocampal interneuron networks. Proc Natl Acad Sci U S A 99:13222-13227.

17. **Bartos M, Vida I, Jonas P** (2007) Synaptic mechanisms of synchronized gamma oscillations in inhibitory interneuron networks. Nat Rev Neurosci 8:45-56.

18. **Benchenane K, Tiesinga PH, Battaglia FP** (2011) Oscillations in the prefrontal cortex: a gateway to memory and attention. Curr Opin Neurobiol 21:475-485.

19. **Berens P, Keliris GA, Ecker AS, Logothetis NK, Tolias AS** (2008) Feature selectivity of the gamma-band of the local field potential in primate primary visual cortex. Front Neurosci 2:199-207.

20. **Billings-Gagliardi S, Chan-Palay V, Palay SL** (1974) A review of lamination in area 17 of the visual cortex Macaca mulatta. J Neurocytol 3:619-629.

21. **Blakemore C, Tobin EA** (1972) Lateral inhibition between orientation detectors in the cat's visual cortex. Exp Brain Res 15:439-440.

22. **Blasdel GG, Lund JS** (1983) Termination of afferent axons in macaque striate cortex. J Neurosci 3:1389-1413.

23. **Bohland JW et al.** (2009) A proposal for a coordinated effort for the determination of brainwide neuroanatomical connectivity in model organisms at a mesoscopic scale. PLoS Comput Biol 5:e1000334.

24. **Bokil H, Purpura K, Schoffelen JM, Thomson D, Mitra P** (2007) Comparing spectra and coherences for groups of unequal size. J Neurosci Methods 159:337-345.

25. **Bollimunta A, Chen Y, Schroeder CE, Ding M** (2008) Neuronal mechanisms of cortical alpha oscillations in awake-behaving macaques. J Neurosci 28:9976-9988.

26. **Bollimunta A, Mo J, Schroeder CE, Ding M** (2011) Neuronal mechanisms and attentional modulation of corticothalamic alpha oscillations. J Neurosci 31:4935-4943.

27. **Borgers C, Kopell N** (2005) Effects of noisy drive on rhythms in networks of excitatory and inhibitory neurons. Neural Comput 17:557-608.

28. **Bosking WH, Zhang Y, Schofield B, Fitzpatrick D** (1997) Orientation selectivity and the arrangement of horizontal connections in tree shrew striate cortex. J Neurosci 17:2112-2127.

29. **Bouyer JJ, Montaron MF, Vahnee JM, Albert MP, Rougeul A** (1987) Anatomical localization of cortical beta rhythms in cat. Neuroscience 22:863-869.

30. **Boyden ES, Zhang F, Bamberg E, Nagel G, Deisseroth K** (2005) Millisecond-timescale, genetically targeted optical control of neural activity. Nat Neurosci 8:1263-1268.

31. **Brecht M, Sakmann B** (2002) Dynamic representation of whisker deflection by synaptic potentials in spiny stellate and pyramidal cells in the barrels and septa of layer 4 rat somatosensory cortex. J Physiol 543:49-70.

32. **Bremer F** (1958) Cerebral and cerebellar potentials. Physiol Rev 38:357-388.

33. **Briggs F, Callaway EM** (2005) Laminar patterns of local excitatory input to layer 5 neurons in macaque primary visual cortex. Cereb Cortex 15:479-488.

34. **Brown P** (2007) Abnormal oscillatory synchronization in the motor system leads to impaired movement. Curr Opin Neurobiol 17:656-664.

35. **Brumberg JC, Pinto DJ, Simons DJ** (1999) Cortical columnar processing in the rat whisker-to-barrel system. J Neurophysiol 82:1808-1817.

36. **Busch NA, Dubois J, VanRullen R** (2009) The phase of ongoing EEG oscillations predicts visual perception. J Neurosci 29:7869-7876.

37. **Buschman TJ, Miller EK** (2007) Top-down versus bottom-up control of attention in the prefrontal and posterior parietal cortices. Science 315:1860-1862.

38. **Buschman TJ, Miller EK** (2009) Serial, covert shifts of attention during visual search are reflected by the frontal eye fields and correlated with population oscillations. Neuron 63:386-396.

39. **Buzsaki G** (2002) Theta oscillations in the hippocampus. Neuron 33:325-340.

40. **Buzsaki G** (2006) Rhythms of the Brain. New York: Oxford University Press.

41. **Calkins DJ, Sappington RM, Hendry SH** (2005) Morphological identification of ganglion cells expressing the alpha subunit of type II calmodulin-dependent protein kinase in the macaque retina. J Comp Neurol 481:194-209.

42. **Callaway EM, Katz LC** (1993) Photostimulation using caged glutamate reveals functional circuitry in living brain slices. Proc Natl Acad Sci U S A 90:7661-7665.

43. **Callaway EM, Wiser AK** (1996) Contributions of individual layer 2-5 spiny neurons to local circuits in macaque primary visual cortex. Vis Neurosci 13:907-922.

44. **Callaway EM** (1998) Local circuits in primary visual cortex of the macaque monkey. Annu Rev Neurosci 21:47-74.

45. **Cardin JA, Carlen M, Meletis K, Knoblich U, Zhang F, Deisseroth K, Tsai LH, Moore CI** (2009) Driving fast-spiking cells induces gamma rhythm and controls sensory responses. Nature 459:663-667.

46. **Casagrande VA** (1994) A third parallel visual pathway to primate area V1. Trends Neurosci 17:305-310.

47. **Casagrande VA, Kaas JH** (1994). The afferent, intrinsic, and efferent connections of primary visual cortex in primates. In *Cerebral Cortex*, ed. A Peters, KS Rockland, 10:201–59. New York: Plenum.

48. **Casagrande VA, Norton TT** (1991) Lateral geniculate nucleus: a reviewof its physiology and function. In Vision and Visual Dysfunction: The Neural Basis of Visual Function, ed. AG Leventhal, 4:41–84. New York: Macmillan.

49. **Castro-Alamancos MA** (2004) Dynamics of sensory thalamocortical synaptic networks during information processing states. Prog Neurobiol 74:213-247.

50. **Chalk M, Herrero JL, Gieselmann MA, Delicato LS, Gotthardt S, Thiele A** (2010) Attention reduces stimulus-driven gamma frequency oscillations and spike field coherence in V1. Neuron 66:114-125.

51. **Chatterjee S, Callaway EM** (2003) Parallel colour-opponent pathways to primary visual cortex. Nature 426:668-671.

52. **Chelaru MI, Dragoi V** (2008) Asymmetric synaptic depression in cortical networks. Cereb Cortex 18:771-788.

53. **Chen Y, Geisler WS, Seidemann E** (2008) Optimal temporal decoding of neural population responses in a reaction-time visual detection task. J Neurophysiol 99:1366-1379.

54. **Cohen MR, Newsome WT** (2008) Context-dependent changes in functional circuitry in visual area MT. Neuron 60:162-173.

55. **Cohen MR, Maunsell JH** (2009) Attention improves performance primarily by reducing interneuronal correlations. Nat Neurosci 12:1594-1600.

56. **Cohen MR, Kohn A** (2011) Measuring and interpreting neuronal correlations. Nat Neurosci 14:811-819.

57. **Conley M, Fitzpatrick D** (1989) Morphology of retinogeniculate axons in the macaque. Vis Neurosci 2:287-296.

58. **Connors BW, Amitai Y** (1997) Making waves in the neocortex. Neuron 18:347-349.

59. **Constantinidis C, Goldman-Rakic PS** (2002) Correlated discharges among putative pyramidal neurons and interneurons in the primate prefrontal cortex. J Neurophysiol 88:3487-3497.

60. **Coplan JD, Lydiard RB** (1998) Brain circuits in panic disorder. Biol Psychiatry 44:1264-1276.

61. **Crochet S, Petersen CC** (2006) Correlating whisker behavior with membrane potential in barrel cortex of awake mice. Nat Neurosci 9:608-610.

62. **Csicsvari J, Henze DA, Jamieson B, Harris KD, Sirota A, Bartho P, Wise KD, Buzsaki G** (2003) Massively parallel recording of unit and local field potentials with silicon-based electrodes. J Neurophysiol 90:1314-1323.

63. **Cunningham MO, Whittington MA, Bibbig A, Roopun A, LeBeau FEN, Vogt A, Monyer H, Buhl EH, Traub RD** (2004) A role for fast rhythmic bursting neurons in cortical gamma oscillations in vitro. Proceedings of the National Academy of Sciences of the United States of America 101:7152-7157.

64. **Dacey DM, Lee BB** (1994) The 'blue-on' opponent pathway in primate retina originates from a distinct bistratified ganglion cell type. Nature 367:731-735.

65. **da Silva FH, van Lierop TH, Schrijer CF, van Leeuwen WS** (1973a) Organization of thalamic and cortical alpha rhythms: spectra and coherences. Electroencephalogr Clin Neurophysiol 35:627-639.

66. **da Silva FH, van Lierop TH, Schrijer CF, van Leeuwen WS** (1973b) Essential differences between alpha rhythms and barbiturate spindles: spectra and thalamo-cortical coherences. Electroencephalogr Clin Neurophysiol 35:641-645.

67. **de la Rocha J, Doiron B, Shea-Brown E, Josic K, Reyes A** (2007) Correlation between neural spike trains increases with firing rate. Nature 448:802-806.

68. **de Lange FP, Jensen O, Bauer M, Toni I** (2008) Interactions between posterior gamma and frontal alpha/beta oscillations during imagined actions. Front Hum Neurosci 2:7.

69. **Destexhe A, Contreras D** (2006) Neuronal computations with stochastic network states. Science 314:85-90.

70. **Ding M, Chen Y, Bressler SL** (2006) Granger Causality: Basic Theory and Application to Neuroscience. In: Handbook of Time Series Analysis, pp 437-460: Wiley-VCH Verlag GmbH & Co. KGaA.

71. **Dong H, Wang Q, Valkova K, Gonchar Y, Burkhalter A** (2004) Experience-dependent development of feedforward and feedback circuits between lower and higher areas of mouse visual cortex. Vision Res 44:3389-3400.

72. **Dong Y, Mihalas S, Qiu F, von der Heydt R, Niebur E** (2008) Synchrony and the binding problem in macaque visual cortex. J Vis 8:30 31-16.

73. **Donner TH, Siegel M** (2011) A framework for local cortical oscillation patterns. Trends Cogn Sci 15:191-199.

74. **Dragoi V, Sharma J, Sur M** (2000) Adaptation-induced plasticity of orientation tuning in adult visual cortex. Neuron 28:287-298.

75. **Dragoi V, Rivadulla C, Sur M** (2001) Foci of orientation plasticity in visual cortex. Nature 411:80-86.

76. **Dragoi V, Sharma J, Miller EK, Sur M** (2002) Dynamics of neuronal sensitivity in visual cortex and local feature discrimination. Nat Neurosci 5:883-891.

77. **Duzel E, Penny WD, Burgess N** (2010) Brain oscillations and memory. Curr Opin Neurobiol 20:143-149.

78. **Ecker AS, Berens P, Keliris GA, Bethge M, Logothetis NK, Tolias AS** (2010) Decorrelated neuronal firing in cortical microcircuits. Science 327:584-587.

79. **Eickhoff SB, Rottschy C, Zilles K** (2007) Laminar distribution and co-distribution of neurotransmitter receptors in early human visual cortex. Brain Struct Funct 212:255-267.

80. **Elston GN** (2002) Cortical heterogeneity: implications for visual processing and polysensory integration. J Neurocytol 31:317-335.

81. **Elston GN** (2003) Cortex, cognition and the cell: new insights into the pyramidal neuron and prefrontal function. Cereb Cortex 13:1124-1138.

82. **Engel A, Konig P, Kreiter A, Singer W** (1991a) Interhemispheric synchronization of oscillatory neuronal responses in cat visual cortex. Science 252:1177-1179.

83. **Engel AK, Fries P** (2011) Beta-band oscillations--signalling the status quo? Curr Opin Neurobiol 20:156-165.

84. **Engel AK, Konig P, Singer W** (1991b) Direct physiological evidence for scene segmentation by temporal coding. Proc Natl Acad Sci U S A 88:9136-9140.

85. **Engel AK, Fries P, Singer W** (2001) Dynamic predictions: oscillations and synchrony in top-down processing. Nat Rev Neurosci 2:704-716.

86. **Engel AK, Konig P, Kreiter AK, Singer W** (1991c) Interhemispheric synchronization of oscillatory neuronal responses in cat visual cortex. Science 252:1177-1179.

87. **Feldmeyer D, Lubke J, Silver RA, Sakmann B** (2002) Synaptic connections between layer 4 spiny neurone-layer 2/3 pyramidal cell pairs in juvenile rat barrel cortex: physiology and anatomy of interlaminar signalling within a cortical column. J Physiol 538:803-822.

88. **Fell J, Axmacher N** (2011) The role of phase synchronization in memory processes. Nat Rev Neurosci 12:105-118.

89. **Felleman DJ, Van Essen DC** (1991) Distributed hierarchical processing in the primate cerebral cortex. Cereb Cortex 1:1-47.

90. **Felsen G, Shen YS, Yao H, Spor G, Li C, Dan Y** (2002) Dynamic modification of cortical orientation tuning mediated by recurrent connections. Neuron 36:945-954.

91. **Federer F, Ichida JM, Jeffs J, Schiessl I, McLoughlin N, Angelucci A** (2009) Four Projection Streams from Primate V1 to the Cytochrome Oxidase Stripes of V2. The Journal of Neuroscience 29:15455-15471.

92. **Ferster D** (1986) Orientation selectivity of synaptic potentials in neurons of cat primary visual cortex. J Neurosci 6:1284-1301.

93. **Fitzpatrick D, Lund JS, Schmechel DE, Towles AC** (1987) Distribution of GABAergic neurons and axon terminals in the macaque striate cortex. J Comp Neurol 264:73-91.

94. **Freiwald WA, Kreiter AK, Singer W** (1995) Stimulus dependent intercolumnar synchronization of single-unit responses in cat area 17. Neuroreport 6:2348-2352.

95. **Frien A, Eckhorn R, Bauer R, Woelbern T, Gabriel A** (2000) Fast oscillations display sharper orientation tuning than slower components of the same recordings in striate cortex of the awake monkey. Eur J Neurosci 12:1453-1465.

96. **Fries P** (2005) A mechanism for cognitive dynamics: neuronal communication through neuronal coherence. Trends Cogn Sci 9:474-480.

97. **Fries P** (2009) Neuronal gamma-band synchronization as a fundamental process in cortical computation. Annu Rev Neurosci 32:209-224.

98. **Fries P, Nikolic D, Singer W** (2007) The gamma cycle. Trends Neurosci 30:309-316.

99. **Fries P, Reynolds JH, Rorie AE, Desimone R** (2001) Modulation of oscillatory neuronal synchronization by selective visual attention. Science 291:1560-1563.

100. **Fries P, Womelsdorf T, Oostenveld R, Desimone R** (2008) The effects of visual stimulation and selective visual attention on rhythmic neuronal synchronization in macaque area V4. J Neurosci 28:4823-4835.

101. **Georgopoulos AP, Schwartz AB, Kettner RE** (1986) Neuronal population coding of movement direction. Science 233:1416-1419.

102. **Geweke J** (1984) Measures of Conditional Linear Dependence and Feedback Between Time Series. Journal of the American Statistical Association 79:907-915.

103. **Gilbert CD, Wiesel TN** (1979) Morphology and intracortical projections of functionally characterised neurones in the cat visual cortex. Nature 280:120-125.

104. **Gilbert CD, Wiesel TN** (1983) Clustered intrinsic connections in cat visual cortex. J Neurosci 3:1116-1133.

105. **Gilbert CD, Wiesel TN** (1989) Columnar specificity of intrinsic horizontal and corticocortical connections in cat visual cortex. J Neurosci 9:2432-2442.

106. **Gilbertson T, Lalo E, Doyle L, Di Lazzaro V, Cioni B, Brown P** (2005) Existing motor state is favored at the expense of new movement during 13-35 Hz oscillatory synchrony in the human corticospinal system. J Neurosci 25:7771-7779.

107. **Goense JB, Logothetis NK** (2008) Neurophysiology of the BOLD fMRI signal in awake monkeys. Curr Biol 18:631-640.

108. **Granger CWJ** (1969) Investigating Causal Relations by Econometric Models and Cross-spectral Methods. Econometrica 37:424-438.

109. **Grasse DW, Moxon KA** (2010) Correcting the bias of spike field coherence estimators due to a finite number of spikes. J Neurophysiol 104:548-558.

110. **Gray CM** (1994) Synchronous oscillations in neuronal systems: mechanisms and functions. J Comput Neurosci 1:11-38.

111. **Gray CM, Singer W** (1989) Stimulus-specific neuronal oscillations in orientation columns of cat visual cortex. Proc Natl Acad Sci U S A 86:1698-1702.

112. **Gray CM, Konig P, Engel AK, Singer W** (1989) Oscillatory responses in cat visual cortex exhibit inter-columnar synchronization which reflects global stimulus properties. Nature 338:334-337.

113. **Gray CM, Maldonado PE, Wilson M, McNaughton B** (1995) Tetrodes markedly improve the reliability and yield of multiple single-unit isolation from multi-unit recordings in cat striate cortex. J Neurosci Methods 63:43-54.

114. **Green DM, Swets JA** (1966) Signal detection and psychophysics New York: Wiley.

115. **Gregoriou GG, Gotts SJ, Zhou H, Desimone R** (2009) High-frequency, long-range coupling between prefrontal and visual cortex during attention. Science 324:1207-1210.

116. **Greschner M, Shlens J, Bakolitsa C, Field GD, Gauthier JL, Jepson LH, Sher A, Litke AM, Chichilnisky EJ** (2011) Correlated firing among major ganglion cell types in primate retina. J Physiol 589:75-86.

117. **Gutnisky DA, Dragoi V** (2008) Adaptive coding of visual information in neural populations. Nature 452:220-224.

118. **Haider B, Duque A, Hasenstaub AR, McCormick DA** (2006) Neocortical network activity in vivo is generated through a dynamic balance of excitation and inhibition. J Neurosci 26:4535-4545.

119. **Hansen BJ and Dragoi V**. (2011) Adaptation-induced synchronization in laminar cortical circuits. Proc Natl Acad Sci U S A 108:10720-10725.

120. **Hansen BJ, Eagleman S, and Dragoi V.** (2011). Examining Local Network Processing using Multi-contact Laminar Electrode Recording. JoVE. 55 http://www.jove.com/details.php?id=2806.

121. **Hasenstaub A, Shu Y, Haider B, Kraushaar U, Duque A, McCormick DA** (2005) Inhibitory postsynaptic potentials carry synchronized frequency information in active cortical networks. Neuron 47:423-435.

122. **Hendry SH, Yoshioka T** (1994) A neurochemically distinct third channel in the macaque dorsal lateral geniculate nucleus. Science 264:575-577.

123. **Henrie JA, Shapley R** (2005) LFP power spectra in V1 cortex: the graded effect of stimulus contrast. J Neurophysiol 94:479-490.

124. **Hirsch JA, Martinez LM, Pillai C, Alonso JM, Wang Q, Sommer FT** (2003) Functionally distinct inhibitory neurons at the first stage of visual cortical processing. Nat Neurosci 6:1300-1308.

125. **Hirsch JA, Martinez LM** (2006) Laminar processing in the visual cortical column. Curr Opin Neurobiol 16:377-384.

126. **Hirsch JA, Martinez LM, Alonso JM, Desai K, Pillai C, Pierre C** (2002) Synaptic physiology of the flow of information in the cat's visual cortex in vivo. J Physiol 540:335-350.

127. **Huang X, Lisberger SG** (2009) Noise correlations in cortical area MT and their potential impact on trial-by-trial variation in the direction and speed of smooth-pursuit eye movements. J Neurophysiol 101:3012-3030.

128. **Hubel DH, Wiesel TN** (1972) Laminar and columnar distribution of geniculo-cortical fibers in the macaque monkey. J Comp Neurol 146:421-450.

129. **Hughes SW, Crunelli V** (2005) Thalamic mechanisms of EEG alpha rhythms and their pathological implications. Neuroscientist 11:357-372.

130. **Iversen JR, Repp BH, Patel AD** (2009) Top-down control of rhythm perception modulates early auditory responses. Ann N Y Acad Sci 1169:58-73.

131. **Jarvis MR, Mitra PP** (2001) Sampling properties of the spectrum and coherency of sequences of action potentials. Neural Comput 13:717-749.

132. **Jasper H, Penfield W** (1949) Electrocorticograms in man: Effect of voluntary movement upon the electrical activity of the precentral gyrus. European Archives of Psychiatry and Clinical Neuroscience 183:163-174.

133. **Jefferys JG, Traub RD, Whittington MA** (1996) Neuronal networks for induced '40 Hz' rhythms. Trends Neurosci 19:202-208.

134. **Jensen O, Mazaheri A** (2010) Shaping functional architecture by oscillatory alpha activity: gating by inhibition. Front Hum Neurosci 4:186.

135. **Jensen O, Kaiser J, Lachaux JP** (2007) Human gamma-frequency oscillations associated with attention and memory. Trends Neurosci 30:317-324.

136. **Jones SR, Pinto DJ, Kaper TJ, Kopell N** (2000) Alpha-frequency rhythms desynchronize over long cortical distances: a modeling study. J Comput Neurosci 9:271-291

137. **Johnston, D and Wu, SM** (1995). Foundations of Cellular Neurophysiology, MIT Press.

138. **Kamondi A, Acsady L, Wang XJ, Buzsaki G** (1998) Theta oscillations in somata and dendrites of hippocampal pyramidal cells in vivo: activity-dependent phase-precession of action potentials. Hippocampus 8:244-261.

139. **Karameh FN, Dahleh MA, Brown EN, Massaquoi SG** (2006) Modeling the contribution of lamina 5 neuronal and network dynamics to low frequency EEG phenomena. Biol Cybern 95:289-310.

140. **Katzner S, Nauhaus I, Benucci A, Bonin V, Ringach DL, Carandini M** (2009) Local origin of field potentials in visual cortex. Neuron 61:35-41.

141. **Kelly SP, Lalor EC, Reilly RB, Foxe JJ** (2006) Increases in alpha oscillatory power reflect an active retinotopic mechanism for distracter suppression during sustained visuospatial attention. J Neurophysiol 95:3844-3851.

142. **Kennedy H, Bullier J, Dehay C** (1985) Cytochrome oxidase activity in the striate cortex and lateral geniculate nucleus of the newborn and adult macaque monkey. Exp Brain Res 61:204-209.

143. **Klostermann F, Nikulin VV, Kuhn AA, Marzinzik F, Wahl M, Pogosyan A, Kupsch A, Schneider GH, Brown P, Curio G** (2007) Task-related differential dynamics of EEG alpha- and beta-band synchronization in cortico-basal motor structures. Eur J Neurosci 25:1604-1615.

144. **Kohn A, Smith MA** (2005) Stimulus dependence of neuronal correlation in primary visual cortex of the macaque. J Neurosci 25:3661-3673.

145. **Kraskov A, Quiroga RQ, Reddy L, Fried I, Koch C** (2007) Local field potentials and spikes in the human medial temporal lobe are selective to image category. J Cogn Neurosci 19:479-492.

146. **Kreiman G, Hung CP, Kraskov A, Quiroga RQ, Poggio T, DiCarlo JJ** (2006) Object selectivity of local field potentials and spikes in the macaque inferior temporal cortex. Neuron 49:433-445.

147. **Kruse W, Eckhorn R** (1996) Inhibition of sustained gamma oscillations (35-80 Hz) by fast transient responses in cat visual cortex. Proc Natl Acad Sci U S A 93:6112-6117.

148. **Lakatos P, Chen CM, O'Connell MN, Mills A, Schroeder CE** (2007) Neuronal oscillations and multisensory interaction in primary auditory cortex. Neuron 53:279-292.

149. **Lakatos P, Karmos G, Mehta AD, Ulbert I, Schroeder CE** (2008) Entrainment of neuronal oscillations as a mechanism of attentional selection. Science 320:110-113.

150. **Lakatos P, O'Connell MN, Barczak A, Mills A, Javitt DC, Schroeder CE** (2009) The leading sense: supramodal control of neurophysiological context by attention. Neuron 64:419-430.

151. **Lee D, Port NL, Kruse W, Georgopoulos AP** (1998) Variability and correlated noise in the discharge of neurons in motor and parietal areas of the primate cortex. J Neurosci 18:1161-1170.

152. **Levitt JB, Yoshioka T, Lund JS** (1994) Intrinsic cortical connections in macaque visual area V2: evidence for interaction between different functional streams. J Comp Neurol 342:551-570.

153. **Lima B, Singer W, Chen NH, Neuenschwander S** (2008) Synchronization dynamics in response to plaid stimuli in monkey V1. Cereb Cortex 20:1556-1573.

154. **Livingstone MS, Hubel DH** (1984) Anatomy and physiology of a color system in the primate visual cortex. J Neurosci 4:309-356.

155. **Logothetis NK** (2003) The underpinnings of the BOLD functional magnetic resonance imaging signal. J Neurosci 23:3963-3971.

156. **Lopes da Silva F** (1991) Neural mechanisms underlying brain waves: from neural membranes to networks. Electroencephalogr Clin Neurophysiol 79:81-93.

157. **Lopes da Silva FH, Vos JE, Mooibroek J, Van Rotterdam A** (1980) Relative contributions of intracortical and thalamo-cortical processes in the generation of alpha rhythms, revealed by partial coherence analysis. Electroencephalogr Clin Neurophysiol 50:449-456.

158. **Macmillan NA, Creelman CD** (2005) Detection Theory: A User's Guide, 2nd Edition. Mahwah: Lawrence Erlbaum Associates.

159. **Maier A, Aura CJ, Leopold DA** (2011) Infragranular sources of sustained local field potential responses in macaque primary visual cortex. J Neurosci 31:1971-1980.

160. **Maier A, Adams GK, Aura C, Leopold DA** (2010) Distinct superficial and deep laminar domains of activity in the visual cortex during rest and stimulation. Front Syst Neurosci 4.

161. **Mainen ZF, Sejnowski TJ** (1995) Reliability of spike timing in neocortical neurons. Science 268:1503-1506.

162. **Malach R, Amir Y, Harel M, Grinvald A** (1993) Relationship between intrinsic connections and functional architecture revealed by optical imaging and in vivo targeted biocytin injections in primate striate cortex. Proc Natl Acad Sci U S A 90:10469-10473.

163. **Martin KAC** (1984) Neuronal circuits in cat striate cortex. In Cerebral Cortex, ed. EG Jones, A Peters, 2:241–84. New York: Plenum.

164. **Martinez LM, Alonso JM** (2001) Construction of complex receptive fields in cat primary visual cortex. Neuron 32:515-525.

165. **Martinez LM, Alonso JM, Reid RC, Hirsch JA** (2002) Laminar processing of stimulus orientation in cat visual cortex. J Physiol 540:321-333.

166. **Martinez LM, Wang Q, Reid RC, Pillai C, Alonso JM, Sommer FT, Hirsch JA** (2005) Receptive field structure varies with layer in the primary visual cortex. Nat Neurosci 8:372-379.

167. **Masquelier T, Hugues E, Deco G, Thorpe SJ** (2009) Oscillations, phase-of-firing coding, and spike timing-dependent plasticity: an efficient learning scheme. J Neurosci 29:13484-13493.

168. **Masuda N, Doiron B** (2007) Gamma oscillations of spiking neural populations enhance signal discrimination. PLoS Comput Biol 3:e236.

169. **Mathewson KE, Gratton G, Fabiani M, Beck DM, Ro T** (2009) To see or not to see: prestimulus alpha phase predicts visual awareness. J Neurosci 29:2725-2732.

170. **Maunsell JH, Nealey TA, DePriest DD** (1990) Magnocellular and parvocellular contributions to responses in the middle temporal visual area (MT) of the macaque monkey. J Neurosci 10:3323-3334.

171. **Miltner WH, Braun C, Arnold M, Witte H, Taub E** (1999) Coherence of gamma-band EEG activity as a basis for associative learning. Nature 397:434-436.

172. **Mitchell JF, Sundberg KA, Reynolds JH** (2007) Differential attention-dependent response modulation across cell classes in macaque visual area V4. Neuron 55:131-141.

173. **Mitchell JF, Sundberg KA, Reynolds JH** (2009) Spatial attention decorrelates intrinsic activity fluctuations in macaque area V4. Neuron 63:879-888.

174. **Mitra PP, Pesaran B** (1999) Analysis of dynamic brain imaging data. Biophys J 76:691-708.

175. **Mitzdorf U** (1985) Current source-density method and application in cat cerebral cortex: investigation of evoked potentials and EEG phenomena. Physiol Rev 65:37-100.

176. **Mitzdorf U, Singer W** (1979) Excitatory synaptic ensemble properties in the visual cortex of the macaque monkey: a current source density analysis of electrically evoked potentials. J Comp Neurol 187:71-83.

177. **Muller JR, Metha AB, Krauskopf J, Lennie P** (1999) Rapid adaptation in visual cortex to the structure of images. Science 285:1405-1408.

178. **Nassi JJ, Callaway EM** (2006) Multiple circuits relaying primate parallel visual pathways to the middle temporal area. J Neurosci 26:12789-12798.

179. **Nassi JJ, Callaway EM** (2007) Specialized circuits from primary visual cortex to V2 and area MT. Neuron 55:799-808.

180. **Nassi JJ, Callaway EM** (2009) Parallel processing strategies of the primate visual system. Nat Rev Neurosci 10:360-372.

181. **Nassi JJ, Lyon DC, Callaway EM** (2006) The parvocellular LGN provides a robust disynaptic input to the visual motion area MT. Neuron 50:319-327.

182. **Nauhaus I, Busse L, Carandini M, Ringach DL** (2009) Stimulus contrast modulates functional connectivity in visual cortex. Nat Neurosci 12:70-76.

183. **Nelson JI, Frost BJ** (1978) Orientation-selective inhibition from beyond the classic visual receptive field. Brain Res 139:359-365.

184. **Nicolelis MA** (1999) Methods for neural ensemble recordings Boca Raton: CRC Press.

185. **O'Kusky J, Colonnier M** (1982) A laminar analysis of the number of neurons, glia, and synapses in the adult cortex (area 17) of adult macaque monkeys. J Comp Neurol 210:278-290.

186. **Palanca BJ, DeAngelis GC** (2005) Does neuronal synchrony underlie visual feature grouping? Neuron 46:333-346.

187. **Palmer C, Cheng SY, Seidemann E** (2007) Linking neuronal and behavioral performance in a reaction-time visual detection task. J Neurosci 27:8122-8137.

188. **Palva S, Palva JM** (2007) New vistas for alpha-frequency band oscillations. Trends Neurosci 30:150-158.

189. **Paradiso MA** (1988) A theory for the use of visual orientation information which exploits the columnar structure of striate cortex. Biol Cybern 58:35-49.

190. **Pesaran B, Nelson MJ, Andersen RA** (2008) Free choice activates a decision circuit between frontal and parietal cortex. Nature 453:406-409.

191. **Pesaran B, Pezaris JS, Sahani M, Mitra PP, Andersen RA** (2002) Temporal structure in neuronal activity during working memory in macaque parietal cortex. Nat Neurosci 5:805-811.

192. **Pettersen KH, Devor A, Ulbert I, Dale AM, Einevoll GT** (2006) Current-source density estimation based on inversion of electrostatic forward solution: effects of finite extent of neuronal activity and conductivity discontinuities. J Neurosci Methods 154:116-133.

193. **Pfurtscheller G, Stancak A, Jr., Neuper C** (1996) Post-movement beta synchronization. A correlate of an idling motor area? Electroencephalogr Clin Neurophysiol 98:281-293.

194. **Pillow JW, Shlens J, Paninski L, Sher A, Litke AM, Chichilnisky EJ, Simoncelli EP** (2008) Spatio-temporal correlations and visual signalling in a complete neuronal population. Nature 454:995-999.

195. **Pogosyan A, Gaynor LD, Eusebio A, Brown P** (2009) Boosting cortical activity at Beta-band frequencies slows movement in humans. Curr Biol 19:1637-1641.

196. **Poort J, Roelfsema PR** (2009) Noise correlations have little influence on the coding of selective attention in area V1. Cereb Cortex 19:543-553.

197. **Poulet JF, Petersen CC** (2008) Internal brain state regulates membrane potential synchrony in barrel cortex of behaving mice. Nature 454:881-885.

198. **Puchalla JL, Schneidman E, Harris RA, Berry MJ** (2005) Redundancy in the population code of the retina. Neuron 46:493-504.

199. **Ramon y Cajal S** (1899) Comparative study of the sensory areas of the human cortex.

200. **Ray WJ, Cole HW** (1985) EEG alpha activity reflects attentional demands, and beta activity reflects emotional and cognitive processes. Science 228:750-752.

201. **Read HL, Winer JA, Schreiner CE** (2001) Modular organization of intrinsic connections associated with spectral tuning in cat auditory cortex. Proc Natl Acad Sci U S A 98:8042-8047.

202. **Reid RC, Alonso JM** (1995) Specificity of monosynaptic connections from thalamus to visual cortex. Nature 378:281-284.

203. **Renart A, de la Rocha J, Bartho P, Hollender L, Parga N, Reyes A, Harris KD** (2010) The asynchronous state in cortical circuits. Science 327:587-590.

204. **Rinberg D, Bialek W, Davidowitz H, Tishby N (2003)** Spike sorting in the frequency domain with overlap detection. Arxiv preprint physics/0306056.

205. **Ringach DL, Hawken MJ, Shapley R** (1997) Dynamics of orientation tuning in macaque primary visual cortex. Nature 387:281-284.

206. **Ringach DL, Shapley RM, Hawken MJ** (2002) Orientation Selectivity in Macaque V1: Diversity and Laminar Dependence. The Journal of Neuroscience 22:5639-5651.

207. **Roelfsema PR, Lamme VA, Spekreijse H** (2004) Synchrony and covariation of firing rates in the primary visual cortex during contour grouping. Nat Neurosci 7:982-991.

208. **Roerig B, Chen B** (2002) Relationships of local inhibitory and excitatory circuits to orientation preference maps in ferret visual cortex. Cereb Cortex 12:187-198.

209. **Roerig B, Chen B, Kao JP** (2003) Different inhibitory synaptic input patterns in excitatory and inhibitory layer 4 neurons of ferret visual cortex. Cereb Cortex 13:350-363.

210. **Rols G, Tallon-Baudry C, Girard P, Bertrand O, Bullier J** (2001) Cortical mapping of gamma oscillations in areas V1 and V4 of the macaque monkey. Vis Neurosci 18:527-540.

211. **Romo R, Hernandez A, Zainos A, Salinas E** (2003) Correlated neuronal discharges that increase coding efficiency during perceptual discrimination. Neuron 38:649-657.

212. **Rutishauser U, Ross IB, Mamelak AN, Schuman EM** (2010) Human memory strength is predicted by theta-frequency phase-locking of single neurons. Nature 464:903-907.

213. **Saalmann YB, Pigarev IN, Vidyasagar TR** (2007) Neural mechanisms of visual attention: how top-down feedback highlights relevant locations. Science 316:1612-1615.

214. **Sakata S, Harris KD** (2009) Laminar structure of spontaneous and sensory-evoked population activity in auditory cortex. Neuron 64:404-418.

215. **Salin PA, Bullier J** (1995) Corticocortical connections in the visual system: structure and function. Physiol Rev 75:107-154.

216. **Salinas E, Sejnowski TJ** (2000) Impact of correlated synaptic input on output firing rate and variability in simple neuronal models. J Neurosci 20:6193-6209.

217. **Sanes JN, Donoghue JP** (1993) Oscillations in local field potentials of the primate motor cortex during voluntary movement. Proc Natl Acad Sci U S A 90:4470-4474.

218. **Schneidman E, Berry MJ, Segev R, Bialek W** (2006) Weak pairwise correlations imply strongly correlated network states in a neural population. Nature 440:1007-1012.

219. **Schoffelen JM, Oostenveld R, Fries P** (2005) Neuronal coherence as a mechanism of effective corticospinal interaction. Science 308:111-113.

220. **Schroeder CE, Mehta AD, Givre SJ** (1998) A spatiotemporal profile of visual system activation revealed by current source density analysis in the awake macaque. Cereb Cortex 8:575-592.

221. **Schroeder CE, Tenke CE, Givre SJ, Arezzo JC, Vaughan HG, Jr.** (1991) Striate cortical contribution to the surface-recorded pattern-reversal VEP in the alert monkey. Vision Res 31:1143-1157.

222. **Schwark HD, Jones EG** (1989) The distribution of intrinsic cortical axons in area 3b of cat primary somatosensory cortex. Exp Brain Res 78:501-513.

223. **Sehatpour P, Molholm S, Schwartz TH, Mahoney JR, Mehta AD, Javitt DC, Stanton PK, Foxe JJ** (2008) A human intracranial study of long-range oscillatory coherence across a frontal-occipital-hippocampal brain network during visual object processing. Proc Natl Acad Sci U S A 105:4399-4404.

224. **Series P, Latham PE, Pouget A** (2004) Tuning curve sharpening for orientation selectivity: coding efficiency and the impact of correlations. Nat Neurosci 7:1129-1135.

225. **Shadlen MN, Newsome WT** (1998) The variable discharge of cortical neurons: implications for connectivity, computation, and information coding. J Neurosci 18:3870-3896.

226. **Shapley R, Lennie P** (1985) Spatial frequency analysis in the visual system. Annu Rev Neurosci 8:547-583.

227. **Shipp S, Zeki S** (1989) The Organization of Connections between Areas V5 and V1 in Macaque Monkey Visual Cortex. Eur J Neurosci 1:309-332.

228. **Shmuel A, Korman M, Sterkin A, Harel M, Ullman S, Malach R, Grinvald A** (2005) Retinotopic axis specificity and selective clustering of feedback projections from V2 to V1 in the owl monkey. J Neurosci 25:2117-2131.

229. **Shushruth S, Mangapathy P, Ichida JM, Bressloff PC, Schwabe L, Angelucci A** (2012) Strong recurrent networks compute the orientation tuning of surround modulation in the primate primary visual cortex. J Neurosci 32:308-321.

230. **Siegel M, Engel AK, Donner TH** (2011) Cortical network dynamics of perceptual decision-making in the human brain. Front Hum Neurosci 5:21.

231. **Siegel M, Donner TH, Oostenveld R, Fries P, Engel AK** (2008) Neuronal synchronization along the dorsal visual pathway reflects the focus of spatial attention. Neuron 60:709-719.

232. **Sincich LC, Horton JC** (2002) Divided by cytochrome oxidase: a map of the projections from V1 to V2 in macaques. Science 295:1734-1737.

233. **Sincich LC, Horton JC** (2005) The circuitry of V1 and V2: integration of color, form, and motion. Annu Rev Neurosci 28:303-326.

234. **Singer W** (1996) Neurophysiology: the changing face of inhibition. Curr Biol 6:395-397.

235. **Smith MA, Kohn A** (2008) Spatial and temporal scales of neuronal correlation in primary visual cortex. J Neurosci 28:12591-12603.

236. **Softky WR, Koch C** (1993) The highly irregular firing of cortical cells is inconsistent with temporal integration of random EPSPs. J Neurosci 13:334-350.

237. **Sohal VS, Zhang F, Yizhar O, Deisseroth K** (2009) Parvalbumin neurons and gamma rhythms enhance cortical circuit performance. Nature 459:698-702.

238. **Somers DC, Nelson SB, Sur M** (1995) An emergent model of orientation selectivity in cat visual cortical simple cells. J Neurosci 15:5448-5465.

239. **Sompolinsky H, Yoon H, Kang K, Shamir M** (2001) Population coding in neuronal systems with correlated noise. Phys Rev E Stat Nonlin Soft Matter Phys 64:051904.

240. **Steriade M** (2001) Impact of network activities on neuronal properties in corticothalamic systems. J Neurophysiol 86:1-39.

241. **Steriade M, Gloor P, Llinas RR, Lopes de Silva FH, Mesulam MM** (1990) Report of IFCN Committee on Basic Mechanisms. Basic mechanisms of cerebral rhythmic activities. Electroencephalogr Clin Neurophysiol 76:481-508.

242. **Sun W, Dan Y** (2009) Layer-specific network oscillation and spatiotemporal receptive field in the visual cortex. Proc Natl Acad Sci U S A 106:17986-17991.

243. **Swadlow HA** (2003) Fast-spike interneurons and feedforward inhibition in awake sensory neocortex. Cereb Cortex 13:25-32.

244. **Swann JW, Smith KL, Lee CL** (2001) Neuronal activity and the establishment of normal and epileptic circuits during brain development. Int Rev Neurobiol 45:89-118.

245. **Swann N, Tandon N, Canolty R, Ellmore TM, McEvoy LK, Dreyer S, DiSano M, Aron AR** (2009) Intracranial EEG reveals a time- and frequency-specific role for the right inferior frontal gyrus and primary motor cortex in stopping initiated responses. J Neurosci 29:12675-12685.

246. **Tallon-Baudry C, Bertrand O, Fischer C** (2001) Oscillatory synchrony between human extrastriate areas during visual short-term memory maintenance. J Neurosci 21:RC177.

247. **Taylor K, Mandon S, Freiwald WA, Kreiter AK** (2005) Coherent oscillatory activity in monkey area v4 predicts successful allocation of attention. Cereb Cortex 15:1424-1437.

248. **Teich AF, Qian N** (2003) Learning and adaptation in a recurrent model of V1 orientation selectivity. J Neurophysiol 89:2086-2100.

249. **Telfeian AE, Connors BW** (2003) Widely integrative properties of layer 5 pyramidal cells support a role for processing of extralaminar synaptic inputs in rat neocortex. Neurosci Lett 343:121-124.

250. **Thiele A, Stoner G** (2003) Neuronal synchrony does not correlate with motion coherence in cortical area MT. Nature 421:366-370.

251. **Thut G, Nietzel A, Brandt SA, Pascual-Leone A** (2006) Alpha-band electroencephalographic activity over occipital cortex indexes visuospatial attention bias and predicts visual target detection. J Neurosci 26:9494-9502.

252. **Tiesinga P, Fellous JM, Sejnowski TJ** (2008) Regulation of spike timing in visual cortical circuits. Nat Rev Neurosci 9:97-107.

253. **Towe AL, Harding GW** (1970) Extracellular microelectrode sampling bias. Exp Neurol 29:366-381.

254. **Traub RD, Whittington MA, Stanford IM, Jefferys JG** (1996) A mechanism for generation of long-range synchronous fast oscillations in the cortex. Nature 383:621-624.

255. **Ts'o DY, Gilbert CD, Wiesel TN** (1986) Relationships between horizontal interactions and functional architecture in cat striate cortex as revealed by cross-correlation analysis. J Neurosci 6:1160-1170.

256. **Tsodyks M, Kenet T, Grinvald A, Arieli A** (1999) Linking spontaneous activity of single cortical neurons and the underlying functional architecture. Science 286:1943-1946.

257. **Usrey WM, Fitzpatrick D** (1996) Specificity in the axonal connections of layer VI neurons in tree shrew striate cortex: evidence for distinct granular and supragranular systems. J Neurosci 16:1203-1218.

258. **Vaadia E, Haalman I, Abeles M, Bergman H, Prut Y, Slovin H, Aertsen A** (1995) Dynamics of neuronal interactions in monkey cortex in relation to behavioural events. Nature 373:515-518.

259. **Van Essen DC, DeYoe EA** (1994). Concurrent processing in the primate visual cortex. In The Cognitive Neurosciences, ed. MS Gazzaniga, pp. 383–400. Cambridge, MA: MIT Press.

260. **Van Essen DC, Newsome WT, Maunsell JH, Bixby JL** (1986) The projections from striate cortex (V1) to areas V2 and V3 in the macaque monkey: asymmetries, areal boundaries, and patchy connections. J Comp Neurol 244:451-480.

261. **van der Togt C, Kalitzin S, Spekreijse H, Lamme VA, Super H** (2006) Synchrony dynamics in monkey V1 predict success in visual detection. Cereb Cortex 16:136-148.

262. **van Vreeswijk C, Sompolinsky H** (1996) Chaos in neuronal networks with balanced excitatory and inhibitory activity. Science 274:1724-1726.

263. **van Wingerden M, Vinck M, Lankelma JV, Pennartz CM** (2010) Learning-associated gamma-band phase-locking of action-outcome selective neurons in orbitofrontal cortex. J Neurosci 30:10025-10038.

264. **Vida I, Bartos M, Jonas P** (2006) Shunting inhibition improves robustness of gamma oscillations in hippocampal interneuron networks by homogenizing firing rates. Neuron 49:107-117.

265. **Vinck M, van Wingerden M, Womelsdorf T, Fries P, Pennartz** CM (2010) The pairwise phase consistency: a bias-free measure of rhythmic neuronal synchronization. Neuroimage 51:112-122.

266. **Wang XJ** (2011) Neurophysiological and computational principles of cortical rhythms in cognition. Physiol Rev 90:1195-1268.

267. **Wang Y, Iliescu BF, Ma J, Josic K, Dragoi V** (2011) Adaptive changes in neuronal synchronization in macaque v4. J Neurosci 31:13204-13213.

268. **White JA, Chow CC, Ritt J, Soto-Trevino C, Kopell N** (1998) Synchronization and oscillatory dynamics in heterogeneous, mutually inhibited neurons. J Comput Neurosci 5:5-16.

269. **Whittington MA, Traub RD, Jefferys JG** (1995) Synchronized oscillations in interneuron networks driven by metabotropic glutamate receptor activation. Nature 373:612-615.

270. **Wiser AK, Callaway EM** (1996) Contributions of individual layer 6 pyramidal neurons to local circuitry in macaque primary visual cortex. J Neurosci 16:2724-2739.

271. **Womelsdorf T, Fries P** (2007) The role of neuronal synchronization in selective attention. Curr Opin Neurobiol 17:154-160.

272. **Womelsdorf T, Fries P, Mitra PP, Desimone R** (2006) Gamma-band synchronization in visual cortex predicts speed of change detection. Nature 439:733-736.

273. **Womelsdorf T, Vinck M, Leung LS, Everling S** (2010) Selective theta-synchronization of choice-relevant information subserves goal-directed behavior. Front Hum Neurosci 4:210.

274. **Womelsdorf T, Schoffelen JM, Oostenveld R, Singer W, Desimone R, Engel AK, Fries P** (2007) Modulation of neuronal interactions through neuronal synchronization. Science 316:1609-1612.

275. **Worden MS, Foxe JJ, Wang N, Simpson GV** (2000) Anticipatory biasing of visuospatial attention indexed by retinotopically specific alpha-band electroencephalography increases over occipital cortex. J Neurosci 20:RC63.

276. **Xing D, Yeh CI, Shapley RM** (2009) Spatial spread of the local field potential and its laminar variation in visual cortex. J Neurosci 29:11540-11549.

277. **Yabuta NH, Callaway EM** (1998) Cytochrome-oxidase blobs and intrinsic horizontal connections of layer 2/3 pyramidal neurons in primate V1. Vis Neurosci 15:1007-1027.

278. **Yao H, Dan Y** (2001) Stimulus timing-dependent plasticity in cortical processing of orientation. Neuron 32:315-323.

279. **Yeh CI, Xing D, Williams PE, Shapley RM** (2009) Stimulus ensemble and cortical layer determine V1 spatial receptive fields. Proc Natl Acad Sci U S A 106:14652-14657.

280. **Yoshioka T, Levitt JB, Lund JS** (1992) Intrinsic lattice connections of macaque monkey visual cortical area V4. J Neurosci 12:2785-2802.

281. **Yu J, Ferster D** (2010) Membrane potential synchrony in primary visual cortex during sensory stimulation. Neuron 68:1187-1201.

282. **Zhang F, Wang LP, Brauner M, Liewald JF, Kay K, Watzke N, Wood PG, Bamberg E, Nagel G, Gottschalk A, Deisseroth K** (2007) Multimodal fast optical interrogation of neural circuitry. Nature 446:633-639.

283. **Zohary E, Shadlen MN, Newsome WT** (1994) Correlated neuronal discharge rate and its implications for psychophysical performance. Nature 370:140-143.

10. VITA

Bryan J. Hansen was born in Albany, New York on January 31st, 1984, the son of Kori Hansen. After graduating from Plano Senior High School, Plano, Texas in 2002, he entered Baylor University in Waco, Texas. Bryan received the degree of Bachelor of Science with a major in Neuroscience in May 2006. In August 2006, he entered the Ph.D. program in Neuroscience at the University of Texas Health Science Center at Houston Medical School and the Graduate School of Biomedical Sciences in Houston, Texas.